POLITECNICO DI MILANO

Faculty of industrial engineering

Master of energyengineering

Modelling On/Off–Design performance of a concentrated solar power
plant using supercritical carbon dioxide as working fluid

Advisor: Prof. Stefano CAMPANARI

Coadvisor: Prof. Paolo SILVA

Master thesis of:

Mehdi Aminyavari 764109

Academic year of 2013/2014

ACKNOWLEDGEMENT

Firstly, I would like to thank my supervisors, Prof. Stefano Campanari and Prof. Paolo Silva, for their advices and useful guidance through the writing of this thesis and also I would like to thank Prof. Fabio Rinaldi and PhD student Behzad Najafi for their helpful suggestion and co-operation.

I also want to dedicate this thesis as a gift to my devoted parents for their support through my whole life.

SUMMARY

Solar power is the conversion of sunlight into electricity, either directly using photovoltaic (PV), or indirectly using concentrated solar power (CSP) and thermodynamic cycles. Nowadays, solar tower and parabolic trough power plants represent one of the most interesting opportunities in the field of energy production through renewable sources. Concentrated solar power systems use lenses or mirrors and tracking systems to focus a large area of sunlight into a small beam, generating heat for a thermodynamic cycle; instead Photovoltaic directly convert light (either without or with optical concentration) into electric current using the photoelectric effect.

Commercial concentrated solar power plants were first developed in the 1980s. Nowadays the largest solar power plant in the world is the 354 MW SEGS CSP installation located in the Mojave Desert of California. Other large CSP plants include the Solnova Solar Power Station (150 MW) and the Andasol solar power station (150 MW), both in Spain. These plants are generally based on parabolic trough receivers, while others are using solar towers (for instance the PS10 and PS20 plant near Seville in Spain, taken as a reference in this work). Oppositely, the over 250 MW Agua Caliente Solar Project in the United States, and the 221 MW Charanka Solar Park in India, are the world's largest photovoltaic power stations. In 2012, an estimated $93.0 TW_h$ was generated from solar power, about 0.41% of all electricity generation. This was a 58% increase over 2011.

However, despite these announce, performance prediction of this kind of plants is still difficult, mainly due to the uncertainties on solar field whose description is often only experimental. Most of the models available from previous studies employ a very general description, aimed at analyzing the plant economic feasibility, but most are neglecting a detailed thermodynamic modeling of plant components. Even though recently some more detailed study have been carried out on thermodynamic modeling of CSP plants, only few of them deals with solar tower plants and a fraction is dedicated to one of the most promising configuration for future development of this technology, which relies on a power cycle working with supercritical carbon dioxide (sCO_2).

It is worth noting that, due to the random and somewhat unpredictable nature of the primary energy source exploited by the power plant these facilities are subjected to extremely variable working conditions. For these reasons, a model for the prediction of solar plant energy balances and performances for different ambient conditions and solar radiations is developed in this work with the aim to better understand the plant behavior, improve performances and optimize the plant working conditions. The model focuses on the operating conditions of the receiver of the solar tower, assuming a given geometry (based on the cavity of the PS20 plant in Spain) and

investigating the use of supercritical CO2 as working fluid for a closed gas cycle. An on-design analysis is developed to make an assessment of selected plant configurations, while off-design simulation, that illustrates the system response to radiation conditions other than nominal, can help system management maybe anticipating external condition variation.

The developed model demonstrates its functionality during the design process in different ways. On one hand it allows to calculate the performance of the plant at rated conditions, developing a sensitivity analysis of the parameters involved. On the other hand, various off-design conditions can be studied and, consequently, based on that it would be possible to carry out a long term –for instance yearly- thermodynamic and, in the future, economical analysis. Finally, it allows detecting undesirable operating conditions of one or more components that could affect plant reliability, as for the case of receiver, which is investigated here to predict whether the pipes temperature exceeds the material constraints or not.

The code is implemented in MATLAB and works in two modes, on-design and off-design. A detailed finite element model on receiver has been developed and the power block has been studied to define the thermodynamic properties at inlet / outlet of each component and the required heat exchange areas. The solar field has not been analyzed in this thesis and its detailed description is left to separate works; here we use a reliable representation of the radiation distribution on the receiver, taken from available data corresponding to the PS10 plant in Spain. Anyhow for future works it will be possible to develop software being able to study also the heliostat field parameters and their effect on the power plant operation.

As mentioned, this model performs initially an on-design analysis, based on input specifications defined by the user like overall power output or compressor pressure ratio, as well as more specific parameters regarding either the power block or the receiver(compressor and turbine efficiency, piping size), which can be modified to study their effect on plant performance and sizing. The model then calculates the heat and mass balance of both power block and receiver at rated operation.

Then, the off-design analysis is carried out focusing on thermal input variations at the tower, which is in practice introduced by a modified radiation map on the panels of the receiver, based on some results of the on-design program such as CO_2 mass flow rate and heat exchanger size. As a result, new stable working conditions will be calculated depending on the heat input and on the pressure settings in the gas cycle.

Key words: Concentrating solar power plant; Solar receiver; Supercritical Carbon dioxide; Renewable energy; Thermodynamic model; On-design; Off-design.

ABSTRACT

La ricerca nel campo delle centrali solari a concentrazione di vari tipi,, in particolare, quelle di tipo solare termodinamico basate su ricevitore centrale a torre, ha registrato un grande miglioramento negli ultimi dieci anni, raggiungendo il pieno esercizio commerciale con l'impianto PS10 in Spagna. A dispetto di precedenti impianti dimostrativi di prova che hanno sperimentato tipologie innovative di ricevitori e diversi layout del ciclo termodinamico, questa prima centrale commerciale ha adottato un ricevitore con semplice produzione di vapore saturo destinato ad un ciclo termodinamico con turbina a vapore, con limitazioni evidenti sull'efficienza , al fine di ottenere l'affidabilità degli impianti.

Tuttavia, secondo l'esperienza acquisita, per raggiungere un costo competitivo dell'elettricità prodotta, i costi di capitale e di manutenzione devono essere ridotti e l'efficienza del ciclo termodinamico deve essere notevolmente aumentata. Per raggiungere questi obiettivi, la modifica del ciclo termodinamico è considerata indispensabile, passando all'utilizzo di vapore surriscaldato o di CO_2supercritica come fluido di lavoro. In questo lavoro, viene proposto l'impiego di cicli a CO2 supercritica per questa applicazione, valutando le possibili condizioni di lavoro del ricevitore e l'efficienza complessiva del ciclo termodinamico ad esso connesso.

Si considera in particolare il caso di un ciclo 'combinato' che comprende unciclo a gastoppinga CO2 e un ciclo bottoming del tipo OrganicRankineCycle (ORC). I risultati preliminari indicano che questo ciclo èpromettente per impianti CSP a torre, avendo la possibilità di competere in termini di efficienza con altre tecnologie convenzionali, ed utilizzando turbomacchine e scambiatori di calore di dimensioni molto compatte.

TABLE OF CONTENTS

FIGURE INDEX

x

TABLE INDEX

x

1 INTRODUCTION

Solar power has been harnessed by humans since ancient times. The technology that has been used to harness solar energy has been evolving since then. Since the use of the oculus at the Parthenon in Rome day lighting techniques have been used by ancient architects. Natural light has been dominant method in the history of lighting.

During the industrial revolution the use of coal had increased steadily and has shifted from wood and other kinds of biomass to fossil fuels. In the 1860's there was the expectation that coal would soon be exhausted as a power source so there was research conducted into solar power. However during the early part of the 20th century the development and research of solar power slowed and stopped because of the increasing availability and cost effectiveness of coal and petroleum at that time.

In 1973 during the oil embargo and the 1979 energy crisis there was a review and reorganization of energy policies around the world and especially in the industrialized countries. This brought new life to solar power research and development of solar power technologies.

The technologies used in harnessing solar power are on the verge of rapid growth and development in the 21st century. Architects and engineers are increasingly aware of the advantages of building in passive solar power into their designs. The cost of solar water heaters is becoming increasingly competitive with more conventional water heaters in certain areas. Photovoltaic technology is slowly becoming a cheap way of generating electricity.

There are many advantages worth considering when it comes to solar energy and everything that it offers. There are many advantages that solar energy has over oil energy. Not only does solar energy benefit our pocketbook, but it also benefits the environment as well. However, there are two sides to everything, and here is a list of solar power disadvantages to accompany the list of advantages.

Advantages:

- Solar energy is a completely renewable resource. This means that even when we cannot make use of the sun's power because of nighttime or cloudy and stormy days, we can always rely on the sun showing up the very next day as a

constant and consistent power source unlike fossil fuels which is what most people currently use to power their homes is not a renewable resource. This means that as soon as the oil is gone, it is gone forever and we will no longer have power or energy.

- Solar cells make absolutely no noise at all. They do not make a single peep while extracting useful energy from the sun. On the other hand, the giant machines utilized for pumping oil are extremely noisy and therefore very impractical.
- Solar energy creates absolutely no pollution. This is perhaps the most important advantage that makes solar energy so much more practical than oil. Oil burning releases harmful greenhouses gases, carcinogens and carbon dioxide into our precious air.
- Very little maintenance is required to keep solar cells running. There are no moving parts in a solar cell, which makes it impossible to really hurt them. Solar cells tend to last a good long time with only an annual cleaning to worry about.
- Solar powered panels and products are typically extremely easy to install. Wires, cords and power sources are not needed at all, making this an easy prospect to employ.
- Solar power technology is improving consistently over time, as people begin to understand all of the benefits offered by this incredible technology. As our oil reserves decline, it is important for us to turn to alternative sources for energy.
- Solar panels and solar lighting may seem quite expensive when first purchase it, but in the long run you will find yourself saving quite a great deal of money. After all, it does not cost anything to harness the power of the sun.

Disadvantages:

- The Solar Cells and Solar Panels that are needed to harness solar energy tend to be very expensive when you first purchase them.
- Solar power cannot be harnessed during a storm, on a cloudy day or at night. This limits how much power can be saved for future days. Some days you may still need to rely on oil to power your home.

Of course the mentioned problems can be overcome. In spite of difficulties put up by some utilities for grid connected photovoltaic systems there will be increased use of these technologies and solar power will be increasingly crucial in ending our addiction to fossil fuels and fighting the threat of global warming and assuring a future based on renewable and clean energy.

One of the most known technologies in this concern is Concentrated Solar Power (CSP) and even though it is revolutionary within the field of renewable energy there is nothing new about the idea of concentrating solar power. The first mentioning of the use of concentrating solar power derives from ancient Greece, where Archimedes

in **214-212 BC**, as a defensive tactic, used bronze shields to concentrate the sun's rays onto invading Roman ships which, according to the myth, caught on fire.

The first operational concentrated solar power plant was built in Sant'llario, Italy in **1968** by Professor Giovanni Francia. This plant has architectural similarities to modern plants with its central receiver surrounded by a field of solar collectors. In **1982** the U.S. Department of Energy, along with an industry consortium began operating Solar One, a 10MW central-receiver demonstration project. The project established the feasibility of power tower systems. Four years later, in **1986**, the world's largest solar thermal facility, located in Kramer Junction, California, was commissioned. The solar field contained rows of mirrors that concentrated the sun's energy onto a system of pipes circulating a heat transfer fluid. The heat transfer fluid was used to produce steam, which powered a conventional turbine to produce electricity[1]. As it can be seen in Figure 1-1, since 2008 the amount of CSP installed in the world is rapidly increasing.
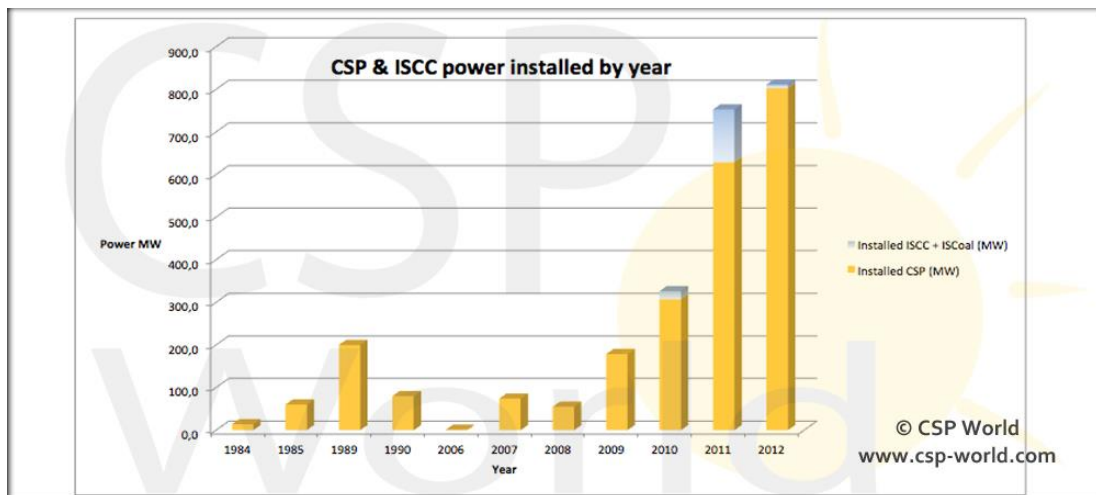
Figure 1-1 CSP and ISCC power installed in the world by year[2]

The major radiative contribution is present in the "Sun Belt". This area extends from latitudes35°N to35° S and receives thousands of times the global energy requested, as it can be seen in Figure 1-2.
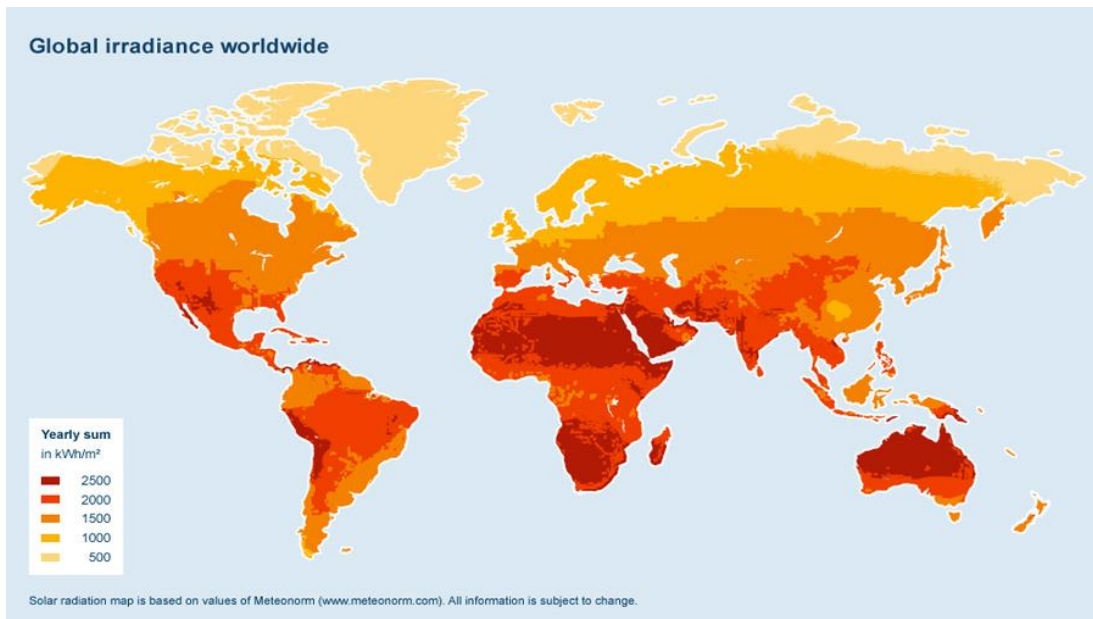
Figure 1-2 World solar radiation map

As the picture demonstrates, the amount of irradiance in northern Africa, southern Middle East and Australia is so high. In this sense, growth in the amount of installed PV capacity in Australia for example has been dramatic with a 10-fold increase between 2009 and 2011 and by the end of 2012 they had over 2,412 MW of installed photovoltaic which would contribute 1.1 percent of Australia's electrical energy. It is also worth to note that STELA declared that the electricity consumption of Europe would be satisfied if the solar energy irradiating an area equal to just 0.4% of the Sahara desert were used, or 2% for the world energy demand[3].

2SOLAR ENERGY

2.1 Solar radiation

The sun is a star that behaves as a black body at the temperature of 5777 K. inside its core several fusion reactions supply the energy that the sun emits, the most important of which is the process where hydrogen combines to form helium. This energy is then transferred from the interior to the external surface by a succession of radiative and convective processes.

The sun irradiates to universe$3.8 \times 10^{14} TW$, but due to the high distance of $1.495 \times 10^{11} m$ and the dimentions of the two bodies, only $172500\ TW$ are intercepted by the earth. This amount of energy is defined by the "solar constant", $G_{sc} = 1367\ \text{W/m}^2$, which represent the mean value of thermal received, outside the atmosphere, per unit area normal to the propagation direction. The irradiance falling on the earth's atmosphere changes over a year by about 6.6% due to the variation in the earth/sun distance. Solar activity variations cause irradiance changes of up to 1%. For Solar Simulators, it is convenient to describe the irradiance of the simulator in "suns." One "sun" is equivalent to irradiance of one solar constant. Nevertheless, the effective radiation received from the sun can vary from this value due to the following aspect:

1) Periodic variation of intrinsic solar radiation related sunspot activities (less than $\pm 1.5\%$)

2) Variation of earth-sun distance in the range of $\pm 3\%$

Regarding the spectral distribution, most of the solar radiation is concentrated on wavelengths ranging from 0.15 to 4 μm, where three spectrums are found; visible-between 0.4 to 0.74 μm, ultraviolet less than to 4 μm, and infrared above to 0.74 μm. In practice, this spectral distribution is modified due to:

1) Atmospheric scattering by air molecules, water and dust

2) Atmospheric absorption by $O_3, H_2O\ and\ CO_2$
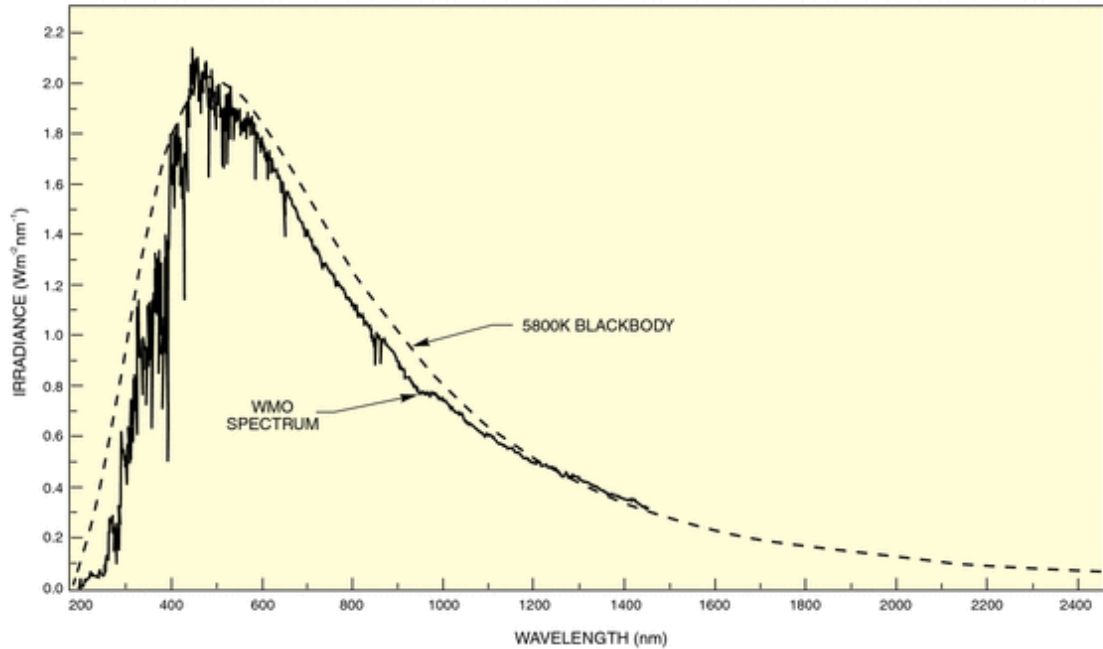
Figure 2-1Spectrum of the radiation outside the earth's atmosphere compared to spectrum of a 5800 K blackbody.

2.1.1 Scattering

Scattering of radiation is caused by interactions with air molecules, water, and dust. The degree to which scattering occurs is a function of the number of particles trough which the radiation must pass and the size of the particles relative to the wavelength λ, three different kinds of scattering are identified with respect to this latter aspect:

1) Rayleigh scattering: it involves very small molecules (almost 10% of λ : N_2 and O_2) that deflect radiation in every direction. The effect is directly proportional to the atmosphere thickness and inversely proportional to the 4th power of λ, what means that it is significant only for λ<0.6 μm.
2) Mie scattering: it involves larger particles (almost 10% - 1000% of λ) like water vapor molecules and airborne particles (dust, salt crystal, smoke). As the previous case, it is inverse proportion to λ and directly proportional to the atmosphere thickness.
3) Non selective scattering: it involves larger airborne particles like water drops and ice crystals that re-emit a widespread white light. It depends on the concentration

and the extension of aerosol and it does not depend on λ. For this reason, it is very variable with the atmospheric condition and cannot be easily forecasted.
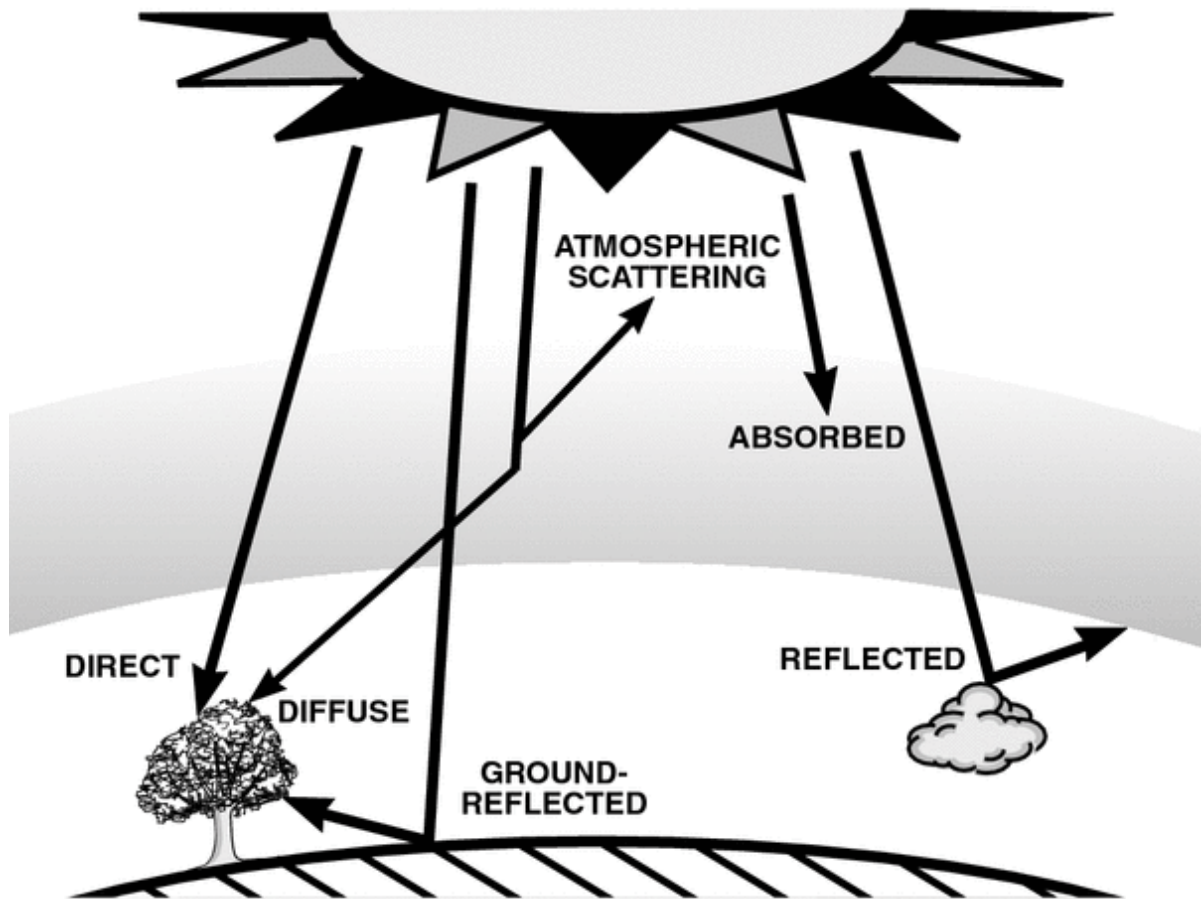
Figure 2-2 The total global radiation on the ground has direct, scattered and reflective components.

2.1.2 Absorption

Absorption of radiation is due to the presence of certain molecules found in the atmosphere, mainly O_3, CO_2, H_2O, N_2O and CH_4 that re-emit radiation in the infrared band. Every molecules has its own characteristic absorption band like, for instance, O_3 which absorbs radiation with λ<0.29 μm, thus protecting the earth from UV radiation. The water molecules have different absorptivity at 1, 1.14 and 1.18 μm, while 2.5 μm the combined effect with CO_2 makes the atmosphere opaque to infrared radiation (Figure 2-3).
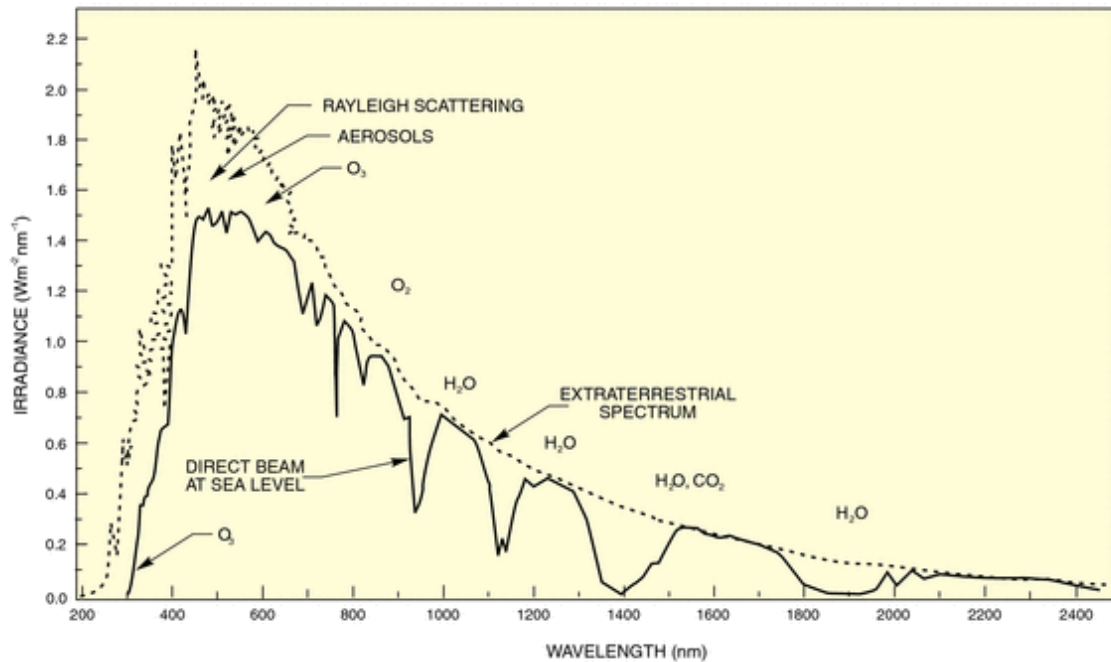
Figure 2-3incident solar spectrum at sea level on a clear day. The dotted curve shows the extra terrestrial spectrum.

The ground level spectrum also depends on how far the sun's radiation must pass through the atmosphere. Elevation is one factor. Denver has a mile (1.6 km) less atmosphere above it than does Washington, and the impact of the time of year on solar angle is important, but the most significant changes are due to the earth's rotation (Figure 2-4). At any location, the length of the path the radiation must take to reach ground level changes as the day progresses. So not only are there the obvious intensity changes in ground solar radiation level during the day, going to zero at night, but the spectrum of the radiation changes through each day because of the changing absorption and scattering path length.

With the sun overhead, direct radiation that reaches the ground passes straight through the entire atmosphere, all of the air mass, overhead. We call this radiation "Air Mass 1 Direct" (AM 1D) radiation, and for standardization purposes we use a sea level reference site. The global radiation with the sun overhead is similarly called "Air Mass 1 Global" (AM 1G) radiation. Because it passes through no air mass, the extra-terrestrial spectrum is called the "Air Mass 0" spectrum.

The atmospheric path for any zenith angle is simply described relative to the overhead air mass (Figure 2-4). The actual path length can correspond to air masses of less than 1 (high altitude sites) to very high air mass values just before sunset. Our Oriel Solar Simulators use filters to duplicate spectra corresponding to air masses of 0, 1, 1.5 and 2, the values on which most comparative test work is based.

$$AM \simeq P/P_O = \sec\theta_z$$
$$\theta_z - \text{ZENITH ANGLE}$$

ZENITH

AM 2.0
60.1°

AM 1.5
48.2°

AM 0

ATMOSPHERE   AM 1.0
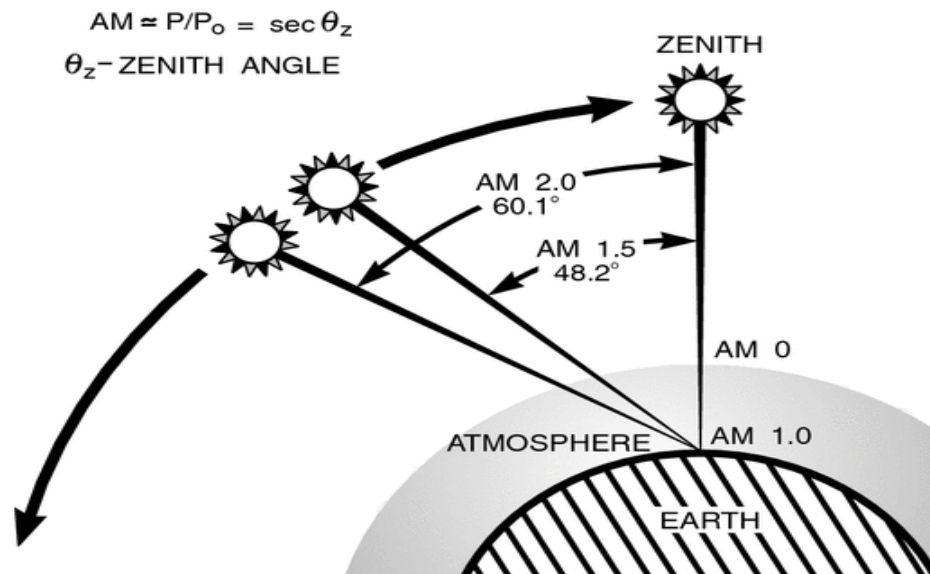
EARTH

Figure 2-4The path length in units of Air Mass, changes with the zenith angle.

Solar radiation reaching the earth's surface varies significantly with location, atmospheric conditions including cloud cover, aerosol content, and ozone layer condition, and time of day, earth/sun distance, solar rotation and activity. Since the solar spectra depend on so many variables, standard spectra have been developed to provide a basis for theoretical evaluation of the effects of solar radiation and as a basis for simulator design. These standard spectra start from a simplified (i.e. lower resolution) version of the measured extra-terrestrial spectra, and use sophisticated models for the effects of the atmosphere to calculate terrestrial spectra.

The most widely used standard spectra are those published by The Committee International ed' Eclaraige (CIE), the world authority on radiometric and photometric nomenclature and standards. The American Society for Testing and Materials (ASTM) publish three spectra - the AM 0, AM 1.5 Direct and AM 1.5 Global for a 37° tilted surface. The conditions for the AM 1.5 spectra were chosen by ASTM "because they are representative of average conditions in the 48 contiguous states of the United States". Figure 2-5 shows typical differences in standard direct and global spectra. These curves are from the data in ASTM Standards, E 891 and E 892 for AM 1.5, a turbidity of 0.27 and a tilt of 37° facing the sun and a ground albedo of 0.2.
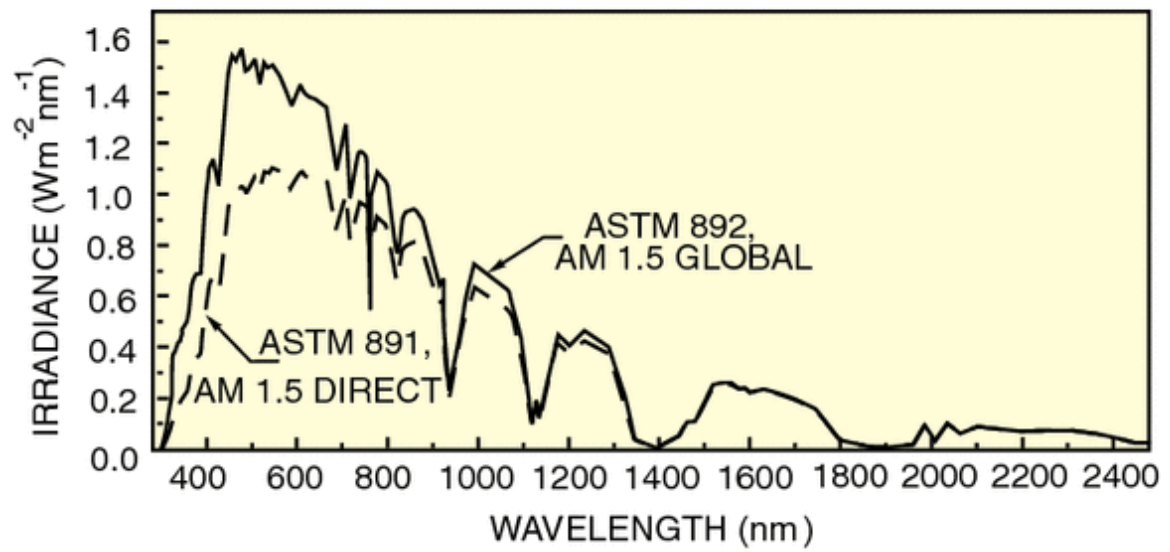
Figure 2-5Standard spectra for AM 1.5. The direct spectrum is from ASTM E891 and global ASTM E892.

3 CONCENTRATING SOLAR POWER PLANTS

Concentrating solar power plants use a technology based on the conversion of the direct component of solar radiation into high temperature thermal energy and then into electricity, heat or mechanical work. To obtain a higher level of energy per unit area, concentrators (mirrors or lens) are used.

Solar radiation received by a collection surface, A_c is redirected onto an absorption surface, A_{abc}. The ratio between these two surfaces is one of the most representative indicators of the system and is called "concentration ratio", C_r. The collection system receives and concentrates the solar radiation on an absorber where solar radiation is converted into thermal energy (normally increasing the enthalpy of a fluid that later is used in a conventional power plant).

Concentrating solar power plants allow to exploit more efficiently the solar radiation, with respect to non-concentrating systems, because of the higher temperatures reached by the working fluid. In fact, according to Stefan Boltzmann law (infrared radiation emitted by the pipes is proportional to the 4th power of absolute temperature), the efficiency of the receiver decreases with increasing operating temperature but, for a specific operative temperature, this efficiency is higher for higher concentration ratios (Figure 3-1) as long as receiver emissivity is reduced for the wavelength corresponding to its operating temperature. Therefore, the total efficiency always shows an optimum that depends on temperature and C_r.
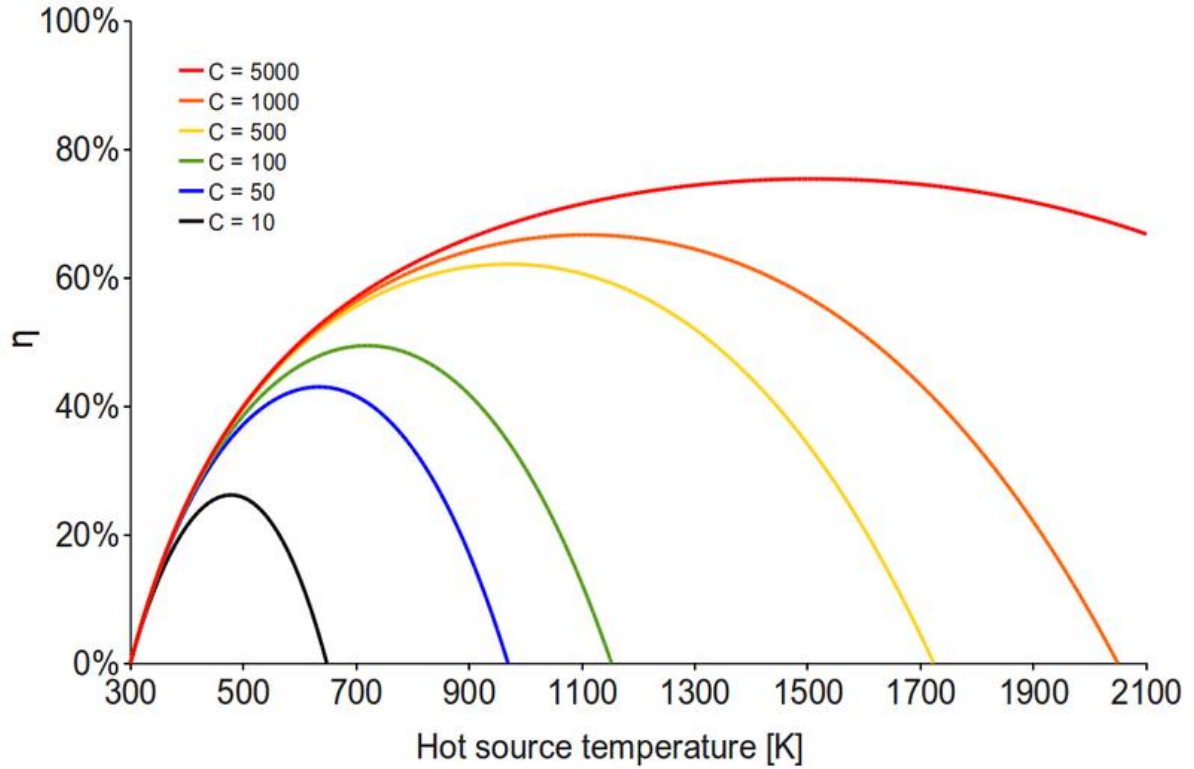
Figure 3-1Cr influence on cycle efficiency[4]

In practice, the concentration ratio has limiting values for a geometrical reason. From the Earth, the Sun subtends an angle of 32' that corresponds to a semi-angle θ_s of 4.653×10^{-3} rad. Therefore, the direct component of the solar radiation does not consist of perfectly parallel beams but it is distributed in a cone that will not reach a receiver of small dimensions completely. For a 3D concentrator (solar tower) the limit is:

$$C_{r,3D} = \frac{1}{(sin\,\theta_s)^2} = 46189 \tag{3-1}$$

For a 2D concentrator (Parabolic trough):

$$C_{r,2D} = \frac{1}{sin\,\theta_s} = 215 \tag{3-2}$$

The actual values of concentration ratio are distant from the values above, showing good development perspectives.

A thermal solar power plant consists of a number of subsystems: collector/concentrator, receiver/absorber, power converter, heat storage and, probably, conventional burner/boiler. The collection system concentrates and re-directs the solar radiation towards the absorber where radiation is transformed into thermal energy used to power the cycle.

A heat storage system or a conventional fossil fuel boiler is needed to provide energy to the power cycle when solar radiation is not available, permitting the plant to produce electricity according to the demand. This is a great benefit for the electric system in terms of stability but reduces the overall efficiency of the system for each kWh produced from fossil fuels (this comment does not apply to the operation with heat storage systems).

Presently, there are four principal technologies of CSP plants:

1) *Parabolic trough*: these plants concentrate solar radiation on a focus line, where the absorber is located; by mean of parabolic mirrors (i.e. linear collectors/concentrators are used). Nowadays, it is the most developed and widespread technology.

2) *Parabolic dish*: these plants focus all the solar radiation collected by a dish onto a single point where a receiver captures the concentrated energy and transforms it into heat (i.e. bi-dimensional collectors are used). Most of the times, the receiver is incorporated into a Stirling engine.

3) *Fresnel reflector*: these plants are similar to the parabolic trough systems but instead of parabolic mirrors, a series of long, narrow, flat mirrors are used.

4) *Solar tower*: these plants, by means of a heliostat field, concentrate solar radiation on a point where an absorber is located. This point is actually an "area" that is located at the top of a high tower.

3.1 Parabolictrough

The parabolic trough technology is, among all the solar thermal power systems, the one that has reached the highest level of commercial maturity. The presence of 9 SEGS plants in the Mojave Desert (USA) for a total power of 354 MW_e has helped a strong development of the technology producing, until now, more than $13TW_h$. In Europe, this technology has been carried out recently thanks to Andasol I and II plants (100 MW), in the province of Granada, which went online in March 2009.

Figure 3-2Andasol I and II parabolic trough power plants

These plants use linear parabolic concentrators that track the Sun, rotating on a single axis, and focus the radiation on a receiver tube that runs along the focal line, hence transferring heat to a thermal fluid that flows inside the trough. This fluid is then used as thermal input in a steam generator as in traditional plants.

The concentrator consists of:
- A *steel structure* that keeps the correct position of the mirrors even under wind or other atmospheric loads.
- A *reflecting surface* that is a common glass mirror with proper curvature and low iron content to improve its transmittance.

Parabolic collectors usually have an aperture of about 6 m, a concentrating ratio of 61-80 (e.g. SEGS) and a length of 100-150 m, with the aim of reducing the cost of the tracking mechanism and the losses at the end of the collector.   The absorbing pipe is a key element in parabolic trough plants. For temperatures less than 300°C, the absorber could be made of stainless steel coated with cobalt or chromium; instead, for the temperature level reached actually, vacuum tubes are preferred. These absorbers are made by an internal stainless steel pipe with a proper selective coating and an external glass pipe, separated by a vacuum annulus (approximately 0.013 Pa). The selective coating has a high absorptivity (> 90%) for the short

wavelength typical of solar radiation and a low emissivity (< 30%) in the infrared spectrum that is the typical band in which the absorber re-emits to atmosphere.

Regarding what flows inside the pipe, several working fluids can be used in parabolic trough plants:
−Synthetic oils
−Mineral oils
−Molten salts
−Water
−Ionic liquids
−Air or other gases

If the temperatures desired are moderate (< 200°C), demineralised water might be the best choice but, nowadays, the main working fluid is synthetic oil (e.g. Therminol ® VP-1) thanks to its low vapour pressure, that allows working at modest pressure and with economic materials reaching 390°C. Currently under development is the usage of molten salts mixtures ($NaNO_3\_KNO$) that can reach temperature of about 550°C, improving cycle efficiency but showing some technological problems:

1) High solidification temperature (142°C – 238°C, depending on salt composition). For this reason, the mixture must be kept fluid during start-ups by pre-heating the pipes and during the night by a system that makes the fluid flows continuously.
2) High corrosiveness that makes it necessary to use more expensive pipes and components

Direct seam generation is likely to be the next step in parabolic trough evolution. The problems with it are linked to the fact that a phase change must take place inside the pipes that the very high pressure requested. This kind of technology has been studied in the DISS project at the "Plataforma Solar de Almeria" producing superheated steam at 400°C/100 bars.
Regarding the performance of this technology, different types of losses are identified in these plants:
   − *Shadow losses*: between a parabolic mirror and another.
   − *Losses for no interception*: due to single axis rotation
   − *Optical losses*: reflectivity of parabolic concentrator, interception factor (Not all the radiation reflected by the mirror reach the absorber), transmittance of the glass, absorbance of selective coating.
   − *Thermal losses*: conductive, convective and radiative losses of the absorber.

Because of the losses indicated, the thermal efficiency of this kind of plants is in the range 60-80% and the overall efficiency from collector to grid is around 15%.

To increase the working hours and then the dispatch-able current, commercial plants utilizing parabolic trough are of the hybrid type, using fossil fuels for night hour's operation.

Another important aspect of these plants is the storage system that consists of two tanks: a hot tank that receives the hot fluid from the solar field and a cold tank. The first one is filled during hours of peak insulation and then emptied when solar radiation is not sufficient to produce steam. The hot fluid, flowing through a heat exchanger produces steam and is then stored in the cold tank. For the storage system molten salts are normally used, taking advantage of the fact that they do not have environmental impact, are safe and cost less than synthetic oil.
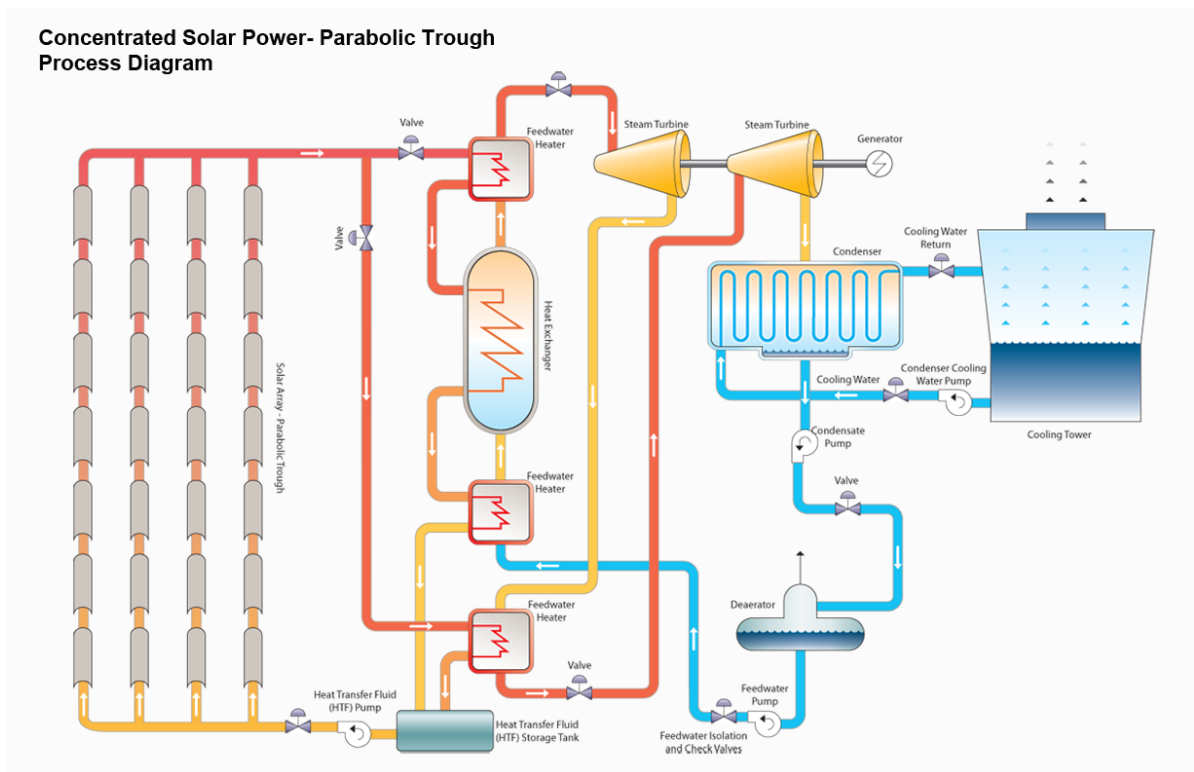
Figure 3-3Schematic of parabolic trough power plant

3.2 Parabolicdish

A solar parabolic dish system is composed by:
- A large *parabolic dish* that tracks the Sun by a rotational movement along two orthogonal axes and concentrates the solar radiation on a receiver set at the focal point.
- A *thermal engine* placed at the top of the receiver that uses a working fluid heated by the concentrated radiation.

Parabolic dishes are characterized by a high efficiency, modularity and autonomy but until now reliability problems, related to the receiver/engine block working at very high temperature, and high costs have obstructed their entry in power generation market.

The parabolic dish can be made by discrete elements (facets) that approximate the geometry of a parabolic or by a continuous metallic membrane that approximates the ideal geometry. With this particular geometry, it is possible to reach a concentration ratio C_r of almost 3000, what means very high temperature on the absorber and, therefore, increased solar to electric energy conversion efficiency of circa 31.25%. Thus, a 10 m in diameter dish is able to supply $30kW_e$ in presence of a solar flux of $1000\ W/m^2$[5].

Regarding the receiver, this component has two functions: absorbing the solar radiation reflected by the concentrator and transferring this energy to the working fluid of a thermal engine associated. Usually, the receivers used in parabolic dishes are of the cavity type in order to reduce radiative and convective losses.
Until now, two kinds of receiver have been used:
1) *Pipes receiver*: the absorber consists of several pipes in which the working fluid of the engine flows. The high temperatures of these absorbers (800°C) make it difficult to use selective coatings due to the great overlap between absorbed and emitted radiation.
2) *Reflux receiver (heat pipe)*: these receivers use a liquid metal (usually Sodium) that evaporates at the absorbing surface and condenses on the pipes inside which the working fluid flows. With this solution really high heat transfer coefficient can be obtained ($800W/cm^2$) and the metal condensation allows a more uniform heating of the working fluid.

The power system is a thermal engine, most of the times a Stirling reciprocating engine or a Brayton cycle gas turbine.

In Stirling engines, the working fluid is usually Hydrogen or Helium that is alternately cooled, compressed until $20MPa$, heated until 700°C and then expanded to start the cycle again. Normally, sodium is adopted as intermediate fluid for these engines. Brayton engines, instead, use air as working fluid with a maximum pressure

of $0.25 MPa$ and a turbine inlet temperature of 850°C. This kind of applications, thanks to the high working fluid temperature, can reach an efficiency of 2527%. In these systems, the receiver is a volumetric absorber where solar concentrated radiation passes through a quartz window and is absorbed by a honeycomb-like system that provides a high exchange surface.
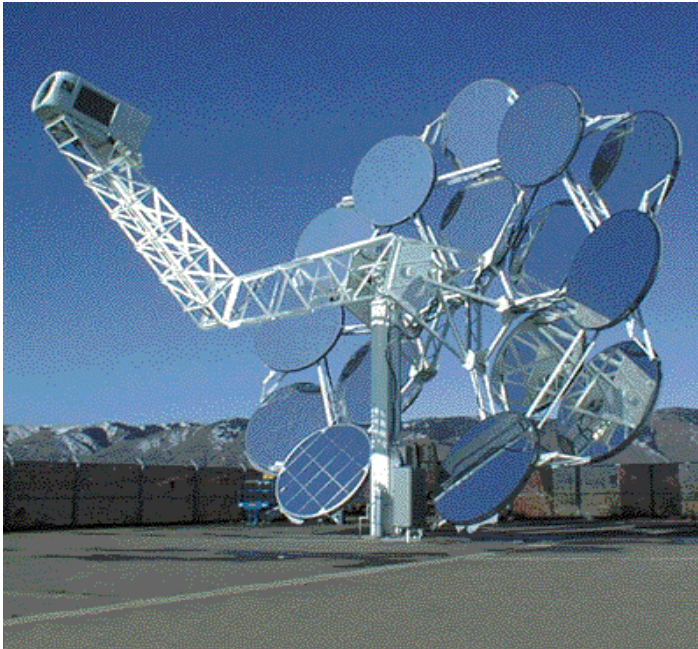
Figure 3-4Circular parabolic dishes with Sterling engine

Figure 3-5Parabolic dish field

3.3 Concentrating linear Fresnelreflector

A linear Fresnel collector is a type of concentrating solar power system that, instead of using parabolic reflectors (as the parabolic trough), employs flat mirrors simulating a continuous surface to collect and concentrate solar energy, therefore reducing construction problems and costs.

The systemconsists of:

- *Long parallel rows of mirrors*that can rotate around their longitudinal axis and concentrate solar radiation on a linear receiver that is suspended at a certain height above the mirror plane. Geometry of this type allows disposing two or more receivers in parallel in order to have a single receiver shared by a number of mirrors, optimizing the land use and minimizing mirror blocks.
- *The absorbing pipe*that is, essentially, the same used in parabolic trough systems, even if it works at lower temperature because of the lower achievable concentration ratio (in the order of 20).

Good exploitation of land, lightness, simplicity of construction and low cost are promoting a fast development of this technology, even if low capacity of concentration and therefore low working temperatures limit its efficiency. One of the plants currently in operation (since March 2009) is the Fresnel plant 1.4 MW PE1 of Novatec Biosol, located in Murcia (South of Spain). This plant is characterized by an absorber tube positioned in the focal line at 7.4 m above the ground where water evaporates directly into saturated steam at 270°C and at a pressure of 55 bar.

Figure 3-6Concentrating linear Fresnel plant

3.4   Solar powertower

The last technology described is the *solar power tower* that will be largely explained in the following parts of this work. These plants use mirrors called *heliostats* that track the sun by a two axes rotational movement, concentrating the sunlight onto a receiver that is normally placed at the top of a tower. In the receiver, the concentrated solar radiation is converted into thermal energy by means of a transport fluid.

Solar towers concentrate solar radiation in three dimensions (in a point, theoretically) and for this reason they can reach high concentrating ratios and therefore working temperatures (1000°C in the future). The main components of a tower plant are:
  1) The heliostats field
  2) The tower
  3) The receiver
  4) The power block

The *heliostat field* is the most characteristic component of this kind of plants and constitutes about 50% of the total cost [6]. Eachheliostatisformed by:

- Reflective surface, for example glass mirrors with optical characteristics similar to parabolic trough or reflective surface containing polymeric film with high reflectivity that has the inconvenient of a reduced useful life.
- Supporting structure.
- Tracking system.
- Control system.

The heliostat distribution on the ground meets technical-economical criteria that take into account:

- Shadows created amongst neighbor heliostats.
- Radiation block by the heliostat that is placed ahead.
- Tower height.
- Land costs.

This optimization process brings to a "heliostat field" that can be:

- *North field* (South for the southern hemisphere): used for high latitude (as Europe); for example, in Spain, both power towers at Sanlucar la Mayor, PS10 and PS20, have heliostat fields of this type.
- *Circular field*: used in low latitude where the sun stays high most of the day; for example the heliostat field that operated at the Solar Two plant in Barstow, USA.
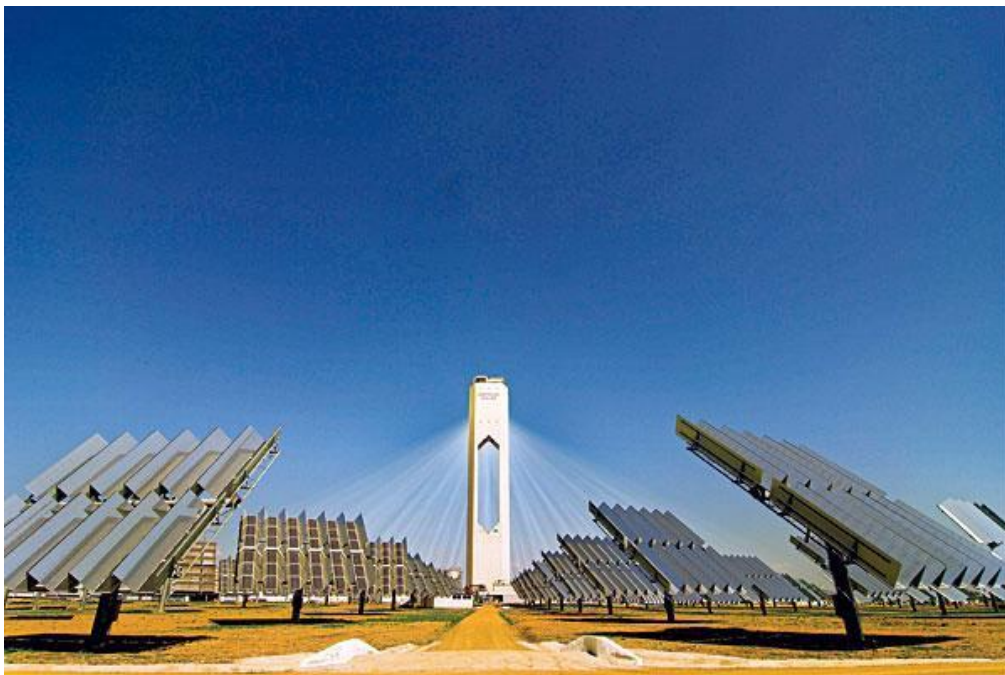
Figure 3-7Concentrated solar tower in Seville, PS10.

The *tower*, whether made of metal or concrete, has the function of supporting the receiver that must be placed at a certain height above the heliostat field, in order to reduce shadows and blocks losses.

Figure 3-8Heliostat field of PS10 and PS20 in Seville, Spain

The *receiver*, instead, is the device where the concentrated solar radiation is converted into thermal energy. During the short story of central receiver technology very different types have been proposed, designed, tested and built[7].

- From a geometrical point of view there are two configurations: cavity receivers (as CESA 1, SOLGAS, and PS10) and external receivers. The external ones can be again classified in: flat (SSPS-ASR, Phoebus TSA), cylindrical (Solar One, Solar Two) and semi-cylindrical (first PS10 version).
- For the heat transfer mechanism: direct and indirect absorption receivers. Another differentiation is among: tubular (Solar One, Solar Two, CESA-1, ASR, GAST), plate and volumetric (atmospheric or pressurized).
- For the working fluid: steam-water with either superheating or boiling (Solar One, CESA-1) or only with boiling (PS10, SOLGAS, Colon Solar, STEOR); air (Phoebus-TSA, GAST); molten salts (Solar Two); molten sodium (SSPS ASR).

The use of gases is quite interesting because the high concentrating ratio (~ 2000) allows this technology to reach very high working temperatures which would not be exploited by classic steam cycles. In this case, a volumetric receiver pressurized at 1.5MPa can increase the gas temperature up to 800°C (with metallic absorber) or

1200°C (with ceramic absorber). Therefore, this technology is suitable to be incorporated into a combined gas and steam cycle where the air leaving the compressor is sent to the receiver, heated there and then expanded in the turbine. Another option of the receiver layout is positioning it at the base of the tower, after a hyperbolic reflector necessary to conduct the radiation down to the receiver: this allows obtaining a better optical efficiency, a more stable distribution of heat flux and a simpler plant (all the devices are placed at ground level).

The principal energy processes (losses) that occur in a solar tower power plant are:

1. Collection losses.
   a. Geometrical losses: they are a function of the solar field geometry (relative position of plant elements and the Sun): cosine factor (reduction of visible area due to the inclination of the heliostat with respect to the sunbeam direction), shadow losses, blockage losses.
   b. Optical losses: reflectivity losses.
2. Solar radiation transmission through the atmosphere due absorption and dispersion processes.
3. Losses in the transportation of concentrated energy from collectors to receiver.
4. Losses in the photo-thermic conversion:
   a. Radiative losses.
   b. Convective losses.
   c. Conduction losses.

These effects will be taken into account in the next chapters, when dealing with the modelling of a solar tower receiver.

4 SUPERCRITICAL FLUID

4.1 History of SupercriticalFluids

The use of supercritical fluids in different processes is not new and has not been invented by humans. Mother Nature has been processing minerals in aqueous solutions at near or above the critical point of water for billions of years[8]. Only in the late 1800s, scientists started to use this natural process, called hydrothermal processing in their labs for creating various crystals. During the last $50 - 60$ years, this process (operating parameters - water pressures from 20 to $200\,MPa$ and temperatures from 300 to 500 ℃) has been widely used in the industrial production of high-quality single crystals (mainly gem stones) such as quartz, sapphire, titanium oxide, tourmaline, zircon and others.

First works devoted to the problem of heat transfer at supercritical pressures started as early as the 1930s. Schmidt and his associates investigated free-convection heat transfer of fluids at the near-critical point with the application to a new effective cooling system for turbine blades in jet engines. They found that the free convection heat transfer coefficient at the near-critical state was quite high, and decided to use this advantage in single-phase thermosyphons with an intermediate working fluid at the near-critical point[9].

In the 1950s, the idea of using supercritical water appeared to be rather attractive for thermal power industry. The objective was increasing the total thermal efficiency of coal-fired power plants. At supercritical pressures there is no liquid-vapour phase transition; therefore, there is no such phenomenon as Critical Heat Flux (CHF) or dry out. Only within a certain range of parameters a deteriorated heat transfer may occur. Work in this area was mainly performed in the former USSR and in the USA in the 1950s – 1980s[10]. In general, the total thermal efficiency of modern thermal power plants with subcritical parameters steam generators is about $36 - 38\%$, but reaches $45 - 50\%$ with supercritical parameters, i.e., with a "steam" pressure of 23.5 $- 26\,MPa$ and inlet turbine temperature of 535 – 580 ℃ thermal efficiency is about

45% and even higher at ultra-supercritical parameters ($25 - 35MPa$ and $600 - 700°C$).

Use of supercritical water in power-plant steam generators is the largest application of a fluid at supercritical pressures in industry. However, other areas exist in which supercritical fluids are used or will be implemented in the near future[11]:

- using supercritical carbon-dioxide Brayton cycle for Generation IV Sodium Fast Reactors (SFRs), Lead-cooled Fast Reactors (LFRs) (Figure 4-1) and High Temperature helium-cooled thermal Reactors (HTRs);
- using supercritical carbon dioxide for cooling printed circuits;
- using near-critical helium to cool coils of superconducting electromagnets, superconducting electronics and power-transmission equipment;
- using supercritical hydrogen as a fuel for chemical and nuclear rockets;
- using supercritical methane as a coolant and fuel for supersonic transport;
- using liquid hydrocarbon coolants and fuels at supercritical pressures in cooling jackets of liquid rocket engines and in fuel channels of air-breathing engines;
- using supercritical carbon dioxide as a refrigerant in air-conditioning and refrigerating systems;
- using a supercritical organic fluid in ORC cycles, for instance applied to the transformation of geothermal energy into electricity;
- using Supercritical Water Oxidation (SCWO) technology for treatment of industrial and military wastes;
- using carbon dioxide in the Supercritical Fluid Leaching (SFL) method for removal of uranium from radioactive solid wastes and in decontamination of surfaces; and
- Using supercritical fluids in chemical and pharmaceutical industries in such processes as supercritical fluid extraction, supercritical fluid chromatography, polymer processing and others.

The most widely used supercritical fluids are water and after that carbon dioxide, helium and refrigerants[11]. Usually, carbon dioxide and refrigerants are considered as modelling fluids instead of water due to significantly lower critical pressures and temperatures, which decrease complexity and costs of thermal hydraulic experiments. Therefore, knowledge of thermo-physical properties specifics at critical and supercritical pressures is very important for safe and efficient use of fluids in various industries.
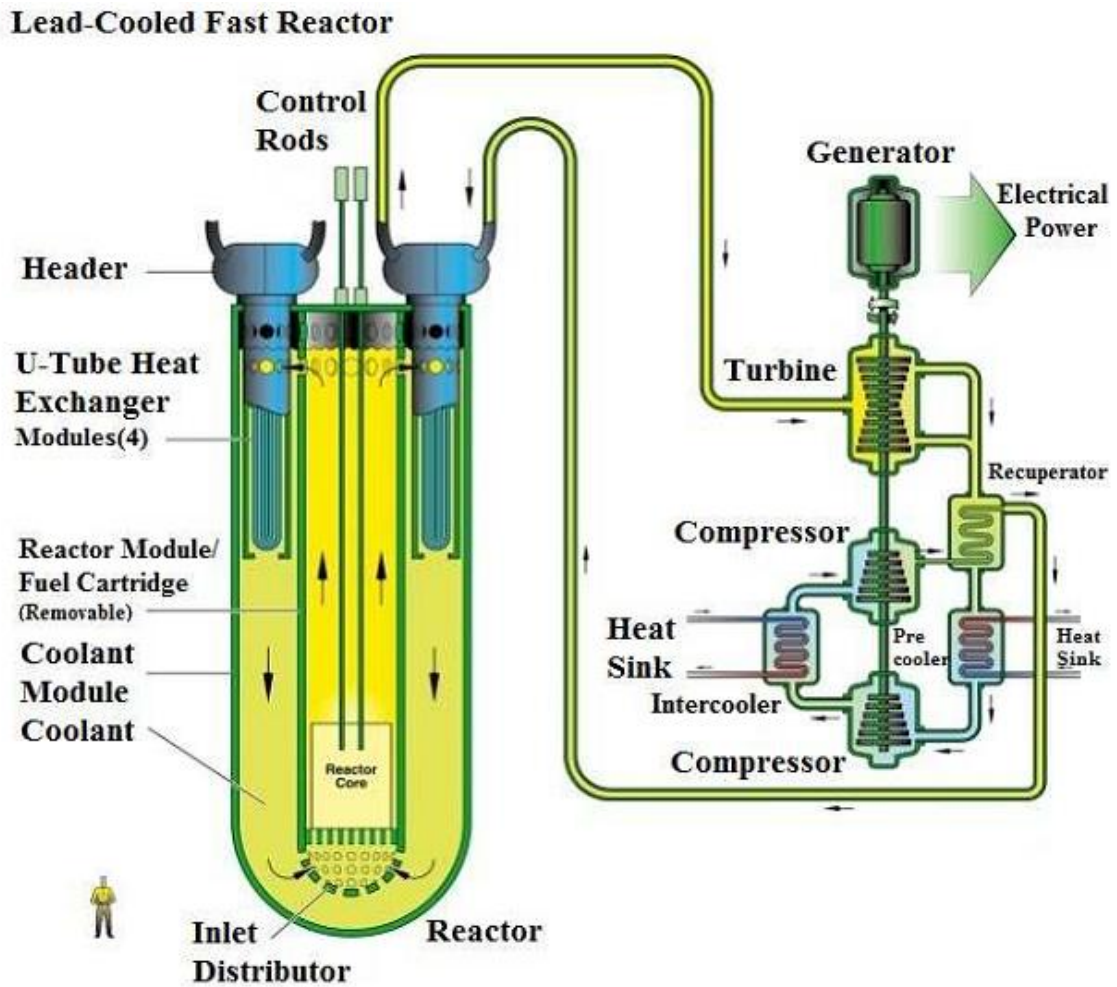
Figure 4-1Lead-cooled Fast Reactor with supercritical carbon dioxide Brayton cycle (courtesy of DOE USA).

4.2 Principles of Supercritical Fluids (SCFs)

A supercritical fluid (SCF) is any compound at a temperature and pressure above the critical point. Above the critical temperature(T_c) the pure gaseous component cannot be liquefied regardless of the pressure applied. The critical pressure (P_c) is the vapor pressure of the gas at the critical temperature. In the supercritical environment only one phase exists.
The fluid, as it is termed, is neither a gas nor a liquid. This phase retains a solvent power approximating liquids as well as the transport properties common to gases.

By increasing the pressure of the gas above the critical point (Figure 4-2), it is possible to give liquid-like densities and solvating strengths. Near the critical point, the density of the gas will increase rapidly with increasing pressure. Here, the solubility of many compounds is several orders of magnitude greater than predicted from the classical thermodynamics of ideal gases. As the average distance between molecules decreases, non-ideal gas behaviour will begin to govern the interactions between the solvent and the sample accounting for a tremendous enhancement in solubility. In supercritical region, solvating strength is a direct function of density, which in turns is dependent on system pressure (at constant temperature). Solvating strengths can be fine-tuned by adjusting the pressure and/or temperature, using the solvent anywhere in the range of ideal gas to nearly pure liquid. Because of the non-compressibility of liquids, this phenomenon is unique to supercritical fluids.

It is even possible, by adding small quantities of co-solvent, to custom design a supercritical fluid for a specific application.
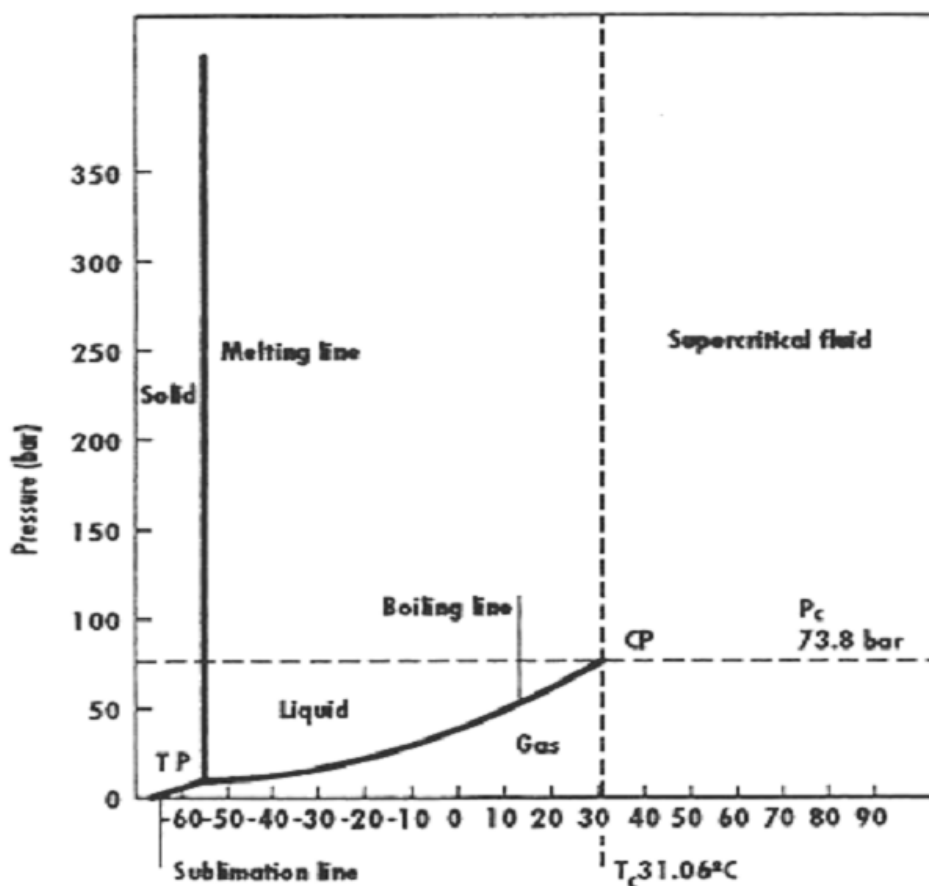
Figure 4-2Phase (pressure-temperature) diagram forCO2: CP=criticalpoint, TP=triple point, P_c= critical pressure, T_c= critical temperature.

4.2.1 Properties of SupercriticalCO2

Pure carbon dioxide exhibits triple point behaviour dependent on the temperature and pressure, as shown in Figure 4-2.

Table 4-1General properties – carbon dioxide

Chemical formula	CO_2
Molecularstructure	O=C=O
Molecularweight	44.011 kg/kmol
Molecular volume (normalconditions)	22.263 m^3/kmol
Critical temperature	31 °C
Critical pressure	73.83 bar
Critical density	466 kg/m^3
Sublimationpoint	−78.9 °C @ 0.981 bar
Triple point	−56.6 °C @ 5.18 bar

The triple point (at a pressure 5.11 bar and temperature of −56.7℃) is defined as the temperature and pressure where three phases (gas, liquid and solid) can exist simultaneously in thermodynamic equilibrium. The solid-gas phase boundary is called the sublimation line, as a solid changing state directly into a gas is called sublimation. Physically, this boundary implies that the gas and solid can co-exist and transform back and forth without the presence of liquid as an intermediate phase.

Above the critical point (73.8 bar and 31.1℃), the liquid and gas phases cannot exist as separate phases, and liquid phase carbon dioxide develops supercritical properties, where it has some characteristics of a gas and others of a liquid.

In the event of an uncontrolled release of carbon dioxide (e.g. damage to a pipe containing liquid carbon dioxide), a portion of the escaping fluid will quickly expand to carbon dioxide gas. The temperature of the released carbon dioxide gas will fall rapidly due to the pressure drop (Joule-Thompson effect – see later description), causing some of the released carbon dioxide to form carbon dioxide snow. As a result of the low temperature of the carbon dioxide, the surrounding air will also be cooled down, which will cause the water vapor in the air to condense locally, which will look like a thick fog. This will continue (to a greater or lesser extent) as long as there is cold carbon dioxide present (e.g. subliming 'snow').

A phase diagram, as shown inFigure 4-2, is a common way to represent the various phases of a substance and the conditions under which each phase exists. However, it

tells us little regarding how the changes of state for carbon dioxide occur during a transient. The carbon dioxide pressure-enthalpy diagram (P-h), shown in Figure 4-3or temperature- entropy (T-s) diagrams shown in Figure 4-4 provide insight to the phase changes.
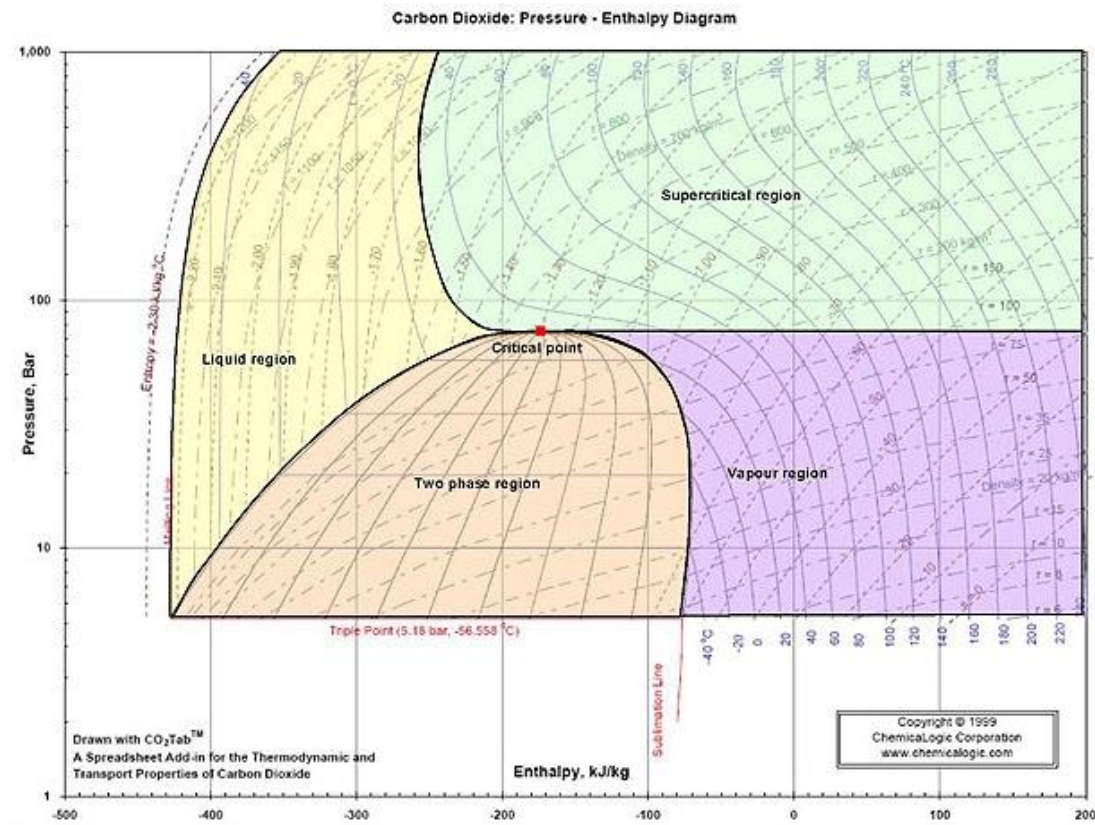
Figure 4-3P-H diagram of Carbon dioxide
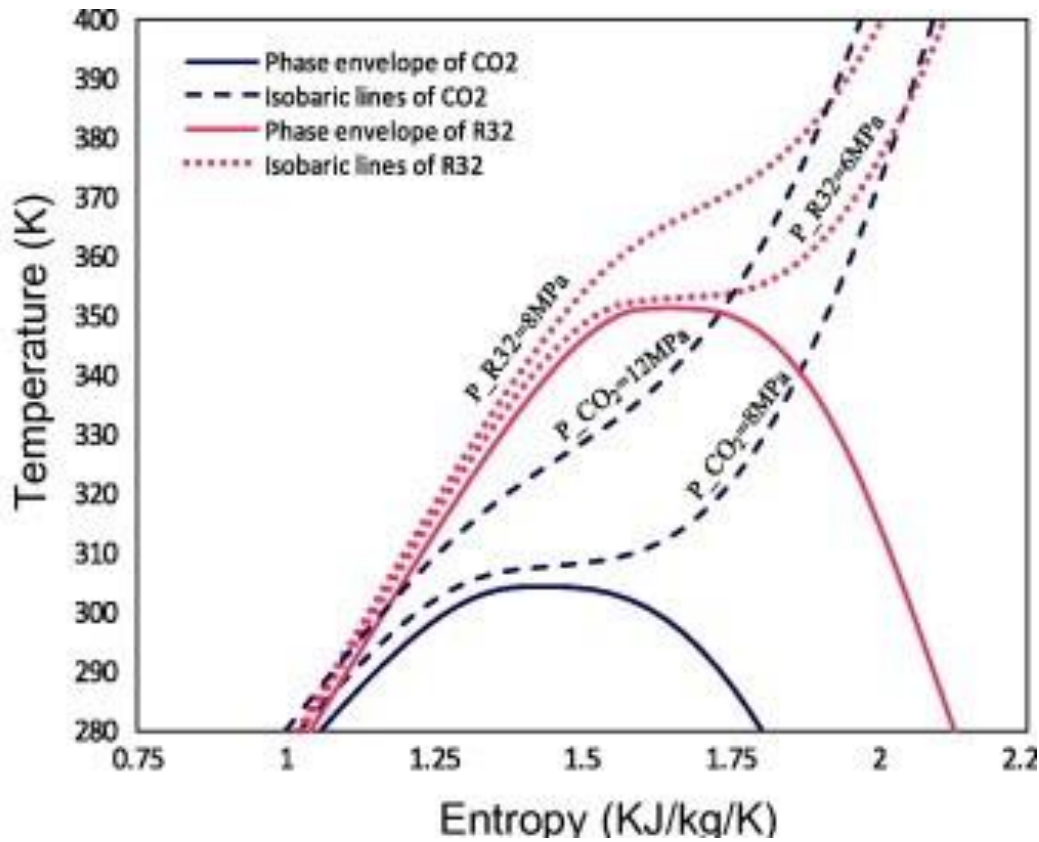
Figure 4-4T-S diagram of Carbon dioxide

Error! Reference source not found. illustrate the thermal capacity, density, thermal conductivity and viscosity of carbon dioxide around critical temperature. As it can be seen, passing through critical temperature, the density will dramatically decrease while thermal capacity shows a very sharp peak which will be considered as a discontinuity since it will go back down to its original value afterward.

Generally thermal conductivity and viscosity will follow the same trend as density but for the case of thermal conductivity, as it can be seen, the corresponding value for critical temperature will rise a bit and then goes down again.
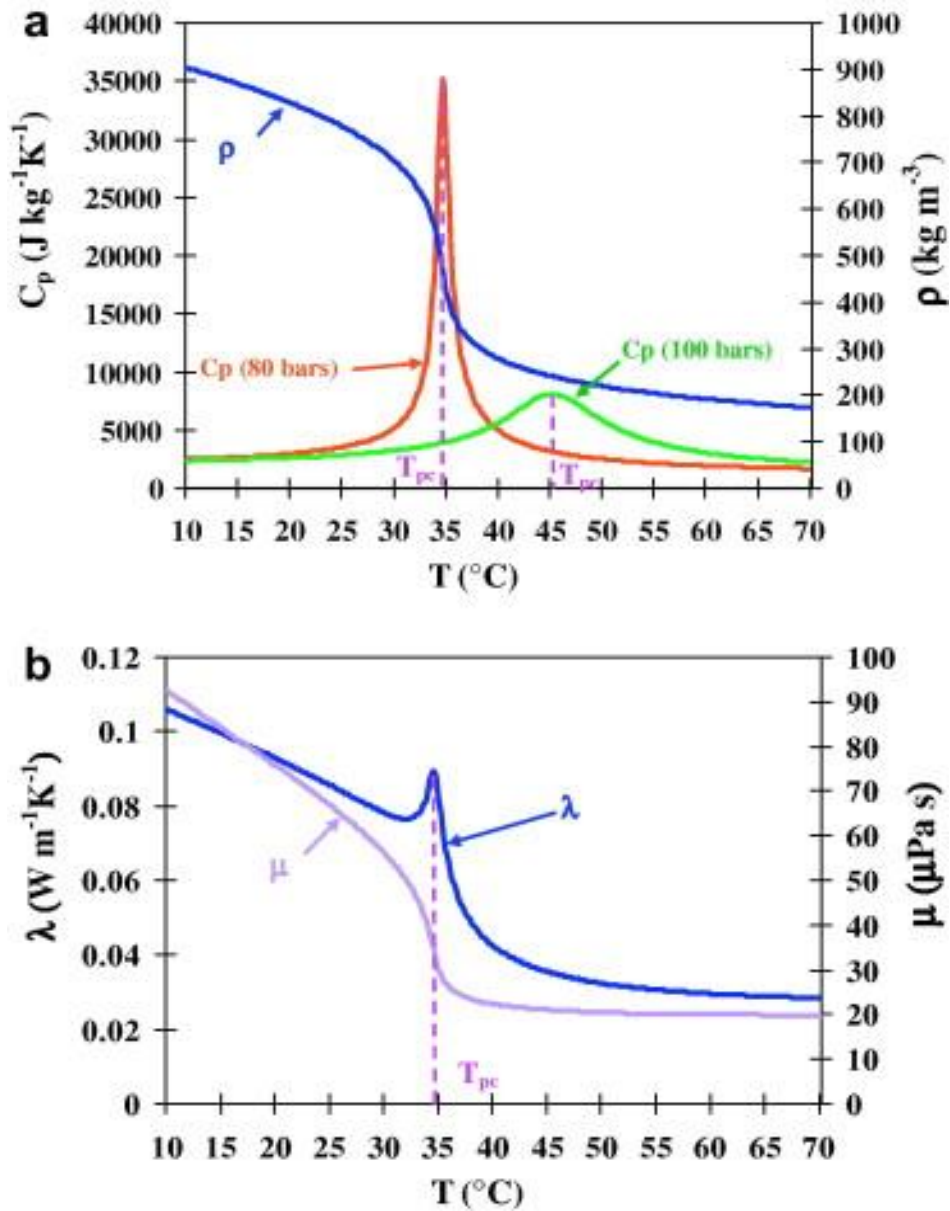
Figure 4-5Thermal capacity (C_p), density (ρ), thermal conductivity (λ) and viscosity (μ) of carbon dioxide

5 THE TOWER RECEIVER

Even though the solar receiver does not have a huge impact on overall capital investment of a tower-type CSP plant (it is estimated to cover about 14% of investment costs [12]), it can definitely be considered the most critical subsystem in terms of performance and reliability. In many designs the solar receiver is a single unit that centralizes all the energy collected by the large heliostat field and that requires two main characteristics: availability and durability. Typical operating temperatures at receiver/absorber are in the range from 500°C to 1200°C depending on the materials considered (from steels to super-alloys and finally to ceramics), and incident fluxes cover a wide range between 300 and over $1000[kW/m^2]$[12].Different receivers characterized by different constructive solutions, absorber materials, working fluids and heat transfer mechanisms, have been designed and tested. Therefore, to comprehend better the technology, in the first part of this section the principal differences regarding different fluids adopted and different geometry designed will be shown, while the second part will cover more in detail the receiver modeled in this work.

5.1 Receiver fluids

A first classification of receivers can be done looking at the different candidate working fluids that have been studied in the last years. The most promising power tower receiver technologies are:
1. Molten salts technology
2. Open or closed loop volumetric air technologies
3. Water/steam technology
4. Supercritical carbon dioxide (sCO_2), especially in the recent years

Roughly speaking, it can be said that researchers at the United States have initially bet on molten salts as the most interesting technology, as showed by the Solar Two plant that was tested up to 1999; on the contrary, the use of volumetric receivers (see description in the following) either with closed air loops, for efficient integration into gas turbine cycles, or open air, for intermediate storage and/or hybridization

solutions, have been promoted in Europe and Israel with projects like SOLGATE, PS10 (first version) and Colonsolar. More conservative approaches (SOLGAS initiative, as well as PS10 and PS20) pushed on saturated steam receivers, while the case of Supercritical carbon dioxide (sCO_2) is nowadays mainly subject of theoretical works, especially by the NREL[13].

5.1.1 Molten salts technology

Molten nitrate salts are, typically, a mixture of $NaNO_3$ and KNO_3 of variable composition even if the most commonly used is a mixture of, respectively, 60% and 40% that presents the following advantages:
- Low cost
- Excellent heat transfer properties: 0.52 W/m K thermal conductivity and 1.6 kJ/kg K heat capacity.
- Chemical stability at maximum operating temperatures.
- Excellent high temperature energy storage fluid.
- Environmentally friendly fluid.

Depending on its particular composition the mixture liquefies at a temperature between 120°C and 240°C and can be used in conjunction with metal tubes for temperatures up to 600°C without bringing about severe corrosion problems. Regarding mechanical integrity issues, studies[14-15]have shown that affordable values of heat flux on the receiver can be up to 800 kW/m, giving place to mixture temperatures around 600°C and maximum surface temperatures in the range from 650°C to 700°C. Molten salts technology has been developed in the U.S thanks to the operation of the 10 MW "Solar Two" plant in Barstow, California. Among other interesting features, this technology allows making solar collection and electricity generation more independent than water/steam systems and allows, even, the incorporation of a cost-effective energy storage system[16].

Solar Two

The *Solar Two* receiver, which was the first molten-salt receiver, was tested between 1996 and 1999 and is still the technical reference for molten salt tubular technology. It was rated to absorb 42 MW of thermal energy at an average solar energy flux of 430 $kW/m^2$and 800 kW/m^2 of peak, generating steam at 535°C and 100 bar by a 35 MW steam generator system. The receiver consisted of 24 panels that formed a cylindrical shell around internal piping, instrumentation and salt vessels. The external surfaces of the tubes were coated with a black Pyromark paint that was robust, resistant to high temperatures and absorbed 95% of the incident sunlight. All pipes, valves, and vessels for hot salt were constructed from stainless steel because of its corrosion resistance against molten-salt at 565°C, while lower cost carbon steel was used for cold-salt pipe work because of the lower corrosiveness of the salt at

290°C. The *Solar Two* receiver showed that, at full power (34 MW absorbed), the receiver efficiency was 88% although different problems were detected[17]:

- First, a heat-trace inadequacy in a receiver drain line resulted in salt solidification between two interconnected panels. If the center of the panels were heated while the ends remained cool could oblige constrained melting that could severely damage the receiver tubes.
- Second, a tube ruptured occurred when the receiver was on sun. Salts flow to the tube was obstructed causing a lack of cooling which resulted in a pressure failure as the extreme temperature weakened the stainless steel. The flow block was caused by debris that was accumulated in the receiver. The debris was originated in the cold salt carbon-steel piping in areas where localized overheating, due to inadequacies in the heat-tracking system, accelerated the corrosion process.

-
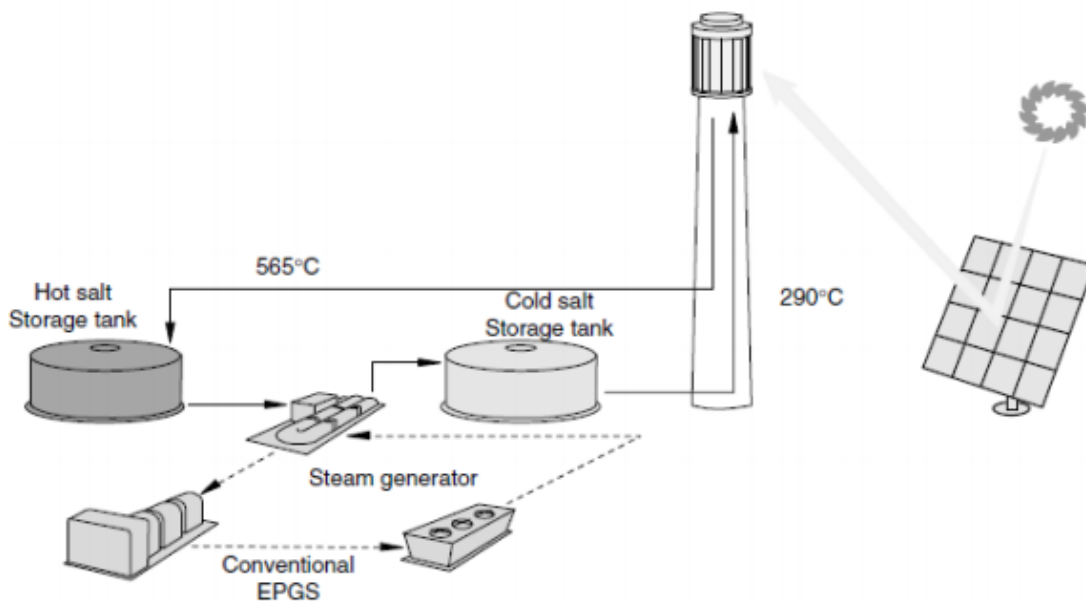
Figure 5-1 Molten salt central receiver scheme

Another characteristic problem of molten-salts technology is the high solidification temperature (120°C-240°C, depending on salt composition). When the mixture goes from solid to liquid state its specific volume increases (approximately 4.6%) and mechanical failures can take place.

Consequently it is necessary to maintain the mixture in liquid state with fusion or pre-heating systems during start-ups, or systems that guarantee a continuous circulation during the night. For example, at the Solar Two plant, before filling the

boiler with salt each morning, the receiver was heated to approximately 290°C to reduce thermal stresses and to insure that solidification of salts did not take place inside the tubes. This pre-heating was achieved by focusing a selected subset of the heliostat field onto the receiver to achieve a uniform temperature distribution both vertically and circumferentially. The problem was that the algorithm selecting and focusing heliostats on the receiver was unable to achieve the desired temperature distribution on the windward side of the receiver due to convective losses. For this reason a feedback control system was incorporated. Differently from the receiver, both pumps and thermal storage tanks functioned as expected with heat losses rates very close to prediction. The Solar Two work brought a few recommendations for future molten-salt receivers:

- All the pipe work of the salt loop must be made of stainless steel, while the use of mid steel for cold salt conductions must be avoided. Stainless steel pipes are much more resistant to corrosion and thus, it is safer in terms of control and installation problems related to the heat trace.
- The use of thin-walled piping must be avoided even if it more economical and allows a faster heating, since it often arrives bent or dented and has a lower corrosion tolerance.

5.1.2 Volumetric air technology

Using air as working fluid offers different benefits:
- It is free and fully available at the site.
- No risk of freezing.
- Higher temperatures can be reached with respect to molten salts and therefore the integration of solar thermal energy into more efficient thermodynamic cycles looks achievable.
- No phase change.
- Fast response to transients or changes in incident flux.
- No special safety requirements.
- No environmental impact.

The main problem of this technology is that air is a poor heat transfer medium, due to its low density and low heat conductivity, creating difficulties in the operation of tubular receivers, as already found in the GST project where two tubular receivers, one metal and one ceramic, were tested at PSA (Plataforma Solar de Almeria) in Spain.
For this reason air receivers use a different approach to gas heating based on wire, foam or appropriately shaped materials within a volume, labeled "*volumetric receivers*".
In these receivers, highly porous structures, operating as convective heat exchangers, absorb the concentrated solar radiation inside a "volume". Therefore gas is driven through the porous material where it is heated convectively.

Volumetric absorbers are usually made of thin heat-resistant wires (in knitted or layered grids) or either metal or ceramic open-cell matrix structures. Good volumetric absorbers are very porous, allowing the radiation to penetrate deeply into the structure. A very high specific surface combined with very small structures lead to a very efficient heat transfer with the gas, allowing to achieve very high heat fluxes (0.5 MW/m^2 to 2.5 MW/m^2)[18].
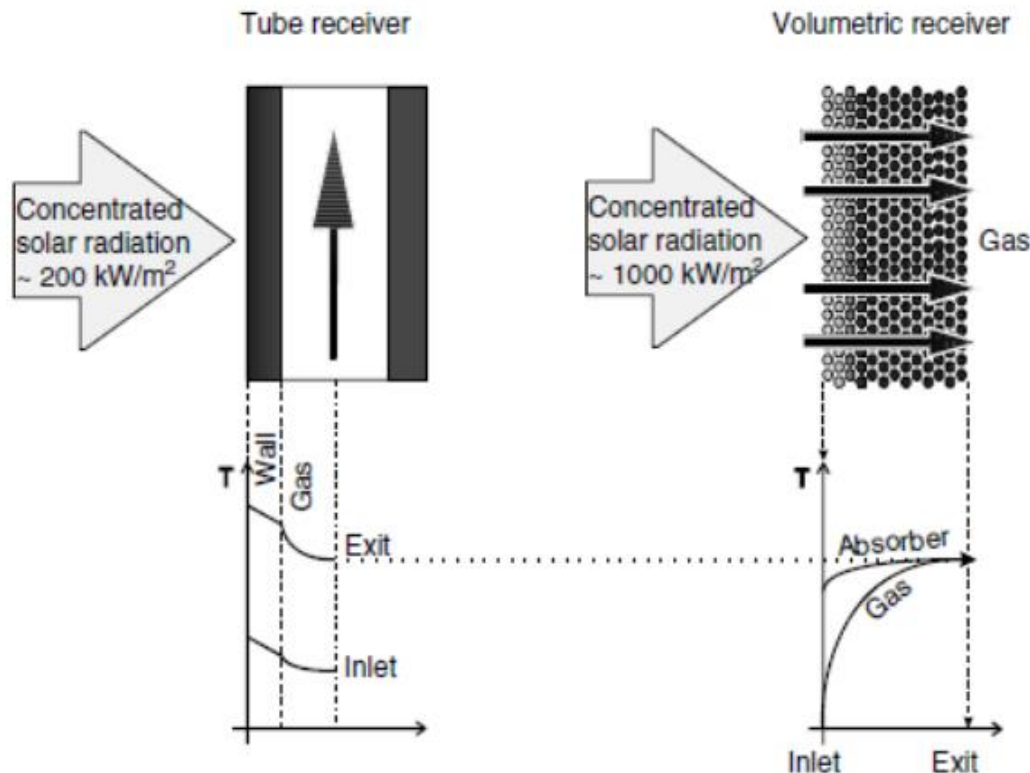
Figure 5-2 Heat transfer principles in tubular and volumetric receiver

In a pressurized version, the porous structure is placed into a pressure cavity vessel closed with a quartz glass window. Using this technology at pressures of up to 15 bar and temperatures up to 1100°C, the receiver could be employed to drive a gas-turbine or combined cycle system. Different studies conducted about the problems of these receivers have concluded that, in highly porous absorber materials, the airflow through the absorber structure is unstable under high solar flux, leading to the mechanical failure (cracks or melting) of the absorber due to local overheating.

TSA (Technology Program Solar Air Receiver) – PHOEBUS scheme – first PS10 design

This experimental open volumetric receiver was a $2.5MW_t$ air-cooled receiver tested on the PSA CESA-1 tower in late 1991. Atmospheric air was heated up through a wire mesh receiver to temperatures of about 700°C to produce steam at 480-540°C and 35-140 bar, with an average flux $300kW/m^2$ and a peak flux of 800 kW/m^2 [19].

The air went through a heat recovery steam generator with separate super-heater, re-heater, evaporator, and economizer feeding a steam turbine-generator.
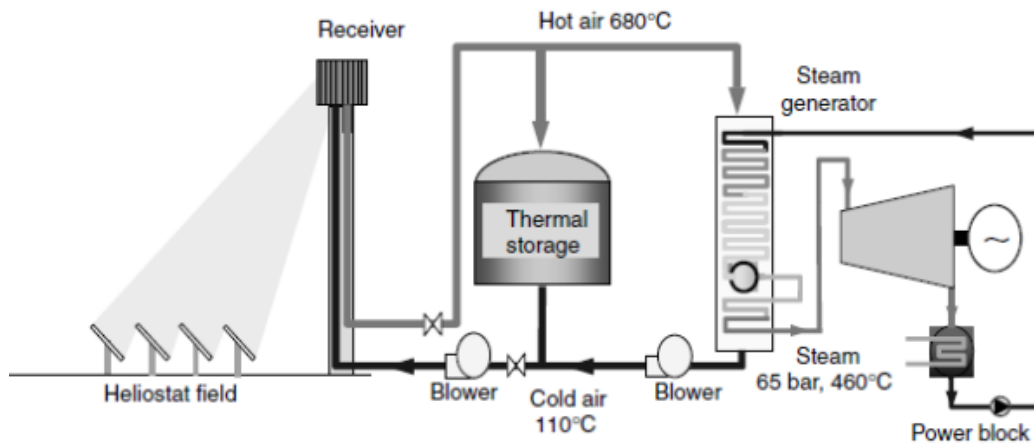
Figure 5-3 Example of solar tower power plant with air receiver

The TSA-PHOEBUS receiver was successfully operated for almost 400 h between April and December 1993, demonstrating that a receiver outlet temperature of 700°C could easily be achieved within 20 minutes of plant startup and achieving receiver thermal efficiencies of up to 75%.

This concept, after test evaluations, was taken into consideration for the PS10 project in Spain. The plant design considered a receiver inlet temperature of 110°C and an outlet of 680°C that should have been used to produce steam at 460°C and 65 bar for an electric output of $11MW_e$. Eventually, in the real plant, it was substituted with a more reliable water/steam receiver.
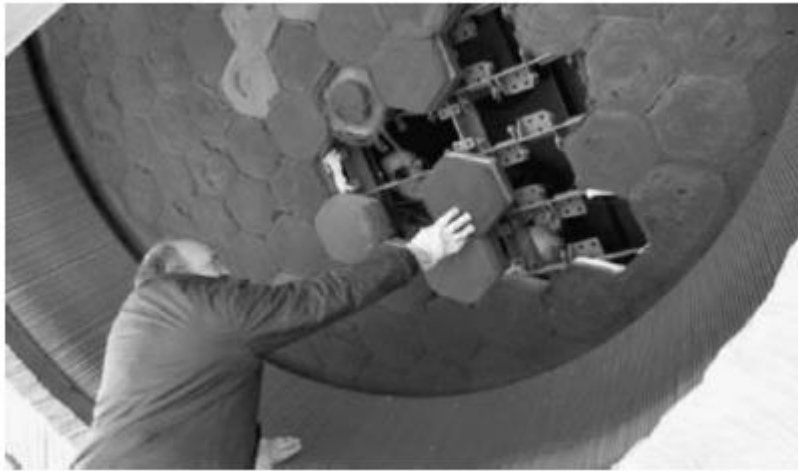
Figure 5-4 Front view of the TSA volumetric receiver

This technology is composed by a stainless steel support structure on the back of a set of ceramic absorber modules that form the base of the receiver. Clearly, the absorber modules are separated from the back in order to allow for axial and radial thermal expansion during start-up or shut-down.

The core element of this technology is the SiSiC absorber module which consists of an extruded parallel channel structure inserted into a cup. The inner surface of this structure is about 50 times larger than the aperture providing the maximum heat exchange surface to the air flow.

The support structure is a double sheet membrane that may be cooled by either ambient or re-circulated air. Cooling air flows between the two sheets and, as it leaves through the sides of the segments, also cools the supporting structure. Air reaches the absorber aperture through the free spaces between segments and is mixed with ambient air. The mixture then penetrates the absorber structure and is heated up by convection. On the back of the structure, an orifice previously sized according to solar flux simulations adjusts the air mass flow rate to provide homogeneous air temperature at the outlet from the module.
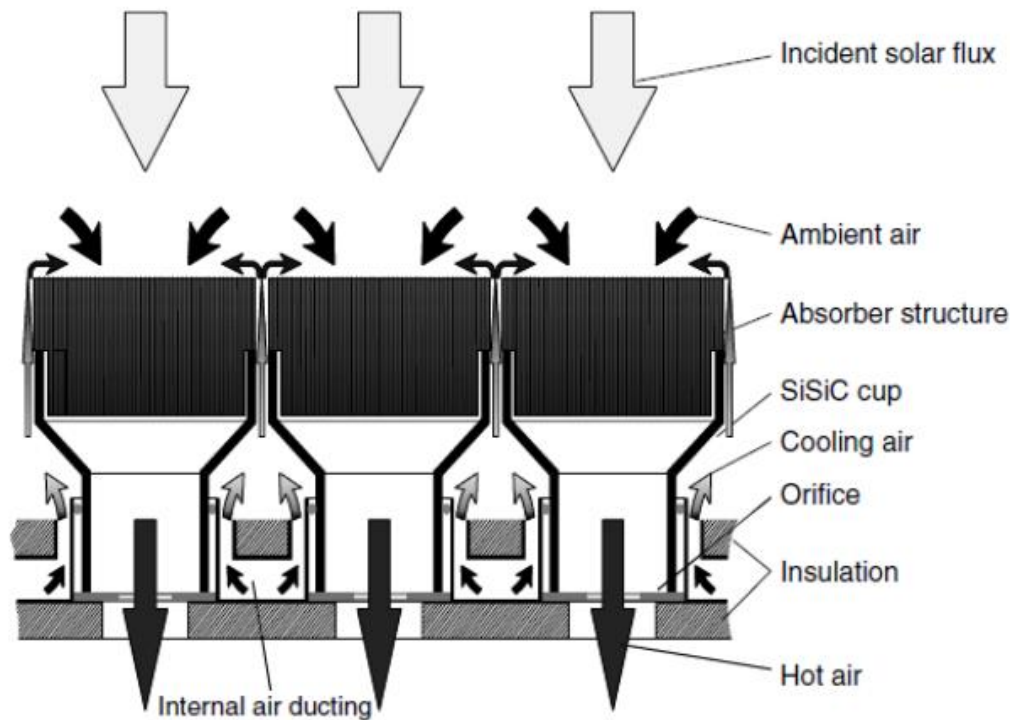
Figure 5-5 Principle in HiTRec and Solair receiver

During the tests conducted in 2003 and 2004, the Solair-3000 receiver produced air at 700-750°C with an average flux of 0.5 MW/m^2 and an efficiency of 72±9%.

These two projects (HiTRec and Solair) developed the same receiver concept and, after some prototype testing, gave way to a real plant that is the Solar Power Tower Jülich in Germany.
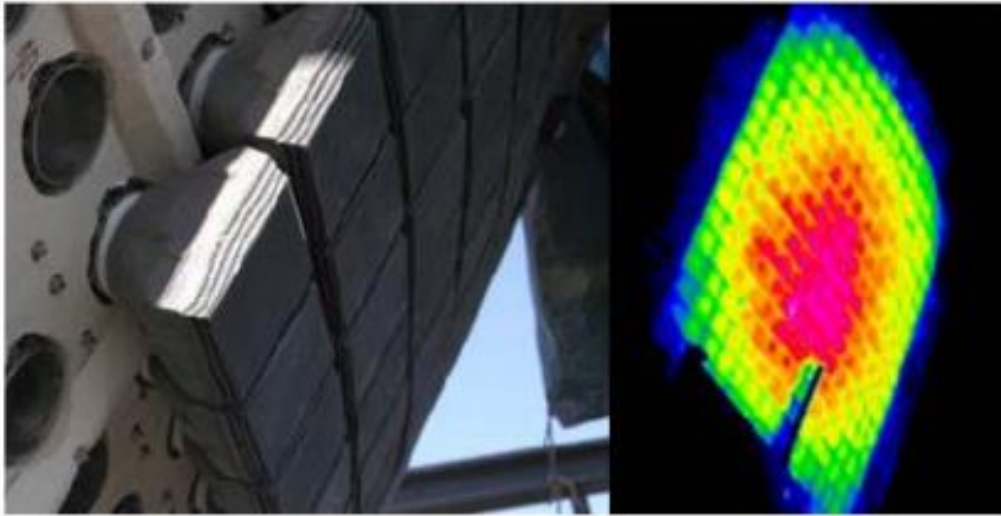
Figure 5-6 Prototype working

The Solar Tower Jülich (1.5 MW), developed with a major contribution from the German Aerospace Centre (DLR), is located in the city of Jülich in the north west of Germany and was completed at the end of 2008. The receiver of this plant is mounted on a 60 m height tower and consists of more than 1000 ceramic absorber modules incorporated in the receiver structure. Air is heated up to 700°C and then used to generate steam in a heating tube boiler that delivers live steam at 485°C and 27 bar[20].

Figure 5-7The Jülich plant tower

Air receiver for solar gas turbine – REFOS project

Another option for using air as working fluid is the windowed volumetric receivers that could be employed as a preheating chamber of a gas turbine combustor.

The combination of heat addition with high solar shares and high conversion efficiencies is one of the major advantages of solar gas turbine systems compared to other solar-fossil hybrid power plants. Solar gas turbine systems use concentrated solar power to heat pressurized air in a gas turbine before entering the combustion chamber. Therefore the combustion chamber only works to overcome the temperature gap between receiver outlet (800-1000°C) and turbine inlet (950-1300°C), thus providing constant turbine inlet conditions despite fluctuating solar input. Using this concept, concentrated solar energy feeding the Brayton cycle of a combined cycle plant can be converted into electricity with a solar to electric efficiency of up to 30%.
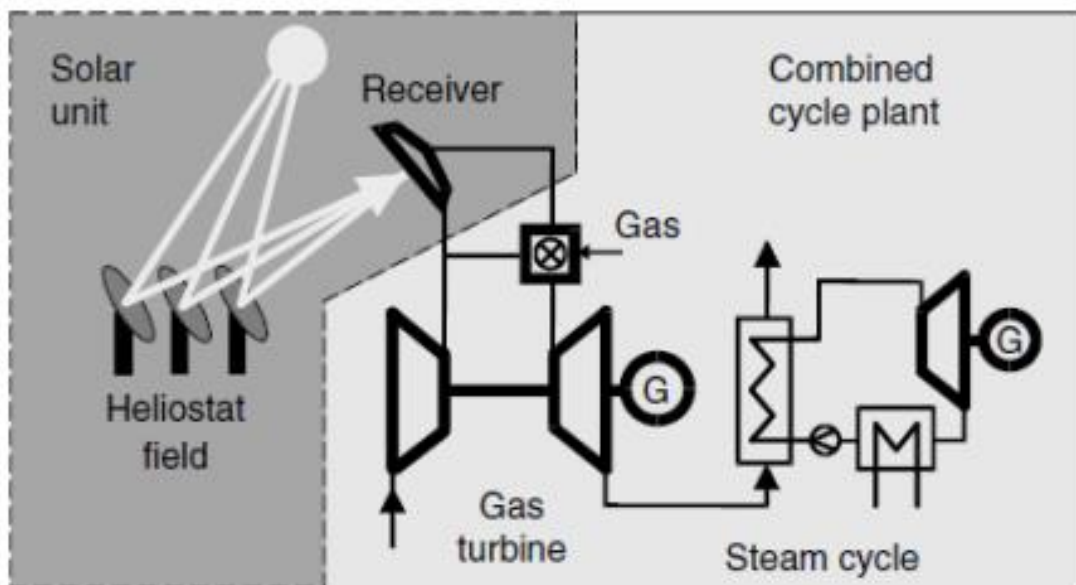
Figure 5-8 Solar air preheating system for gas turbine

For this reason, the German Aerospace Center (DLR) initiated a specific development program called REFOS, aimed at designing a windowed module able to work up to 1000°C and with pressures up to 15 bar. The REFOS receiver consists of a cylindrical vessel containing a curved knitted absorber, a quartz dome to pressurize the air cycle and a hexagonal secondary concentrator with a 1.2 m inner diameter to increment the flux density and protect the window flange.
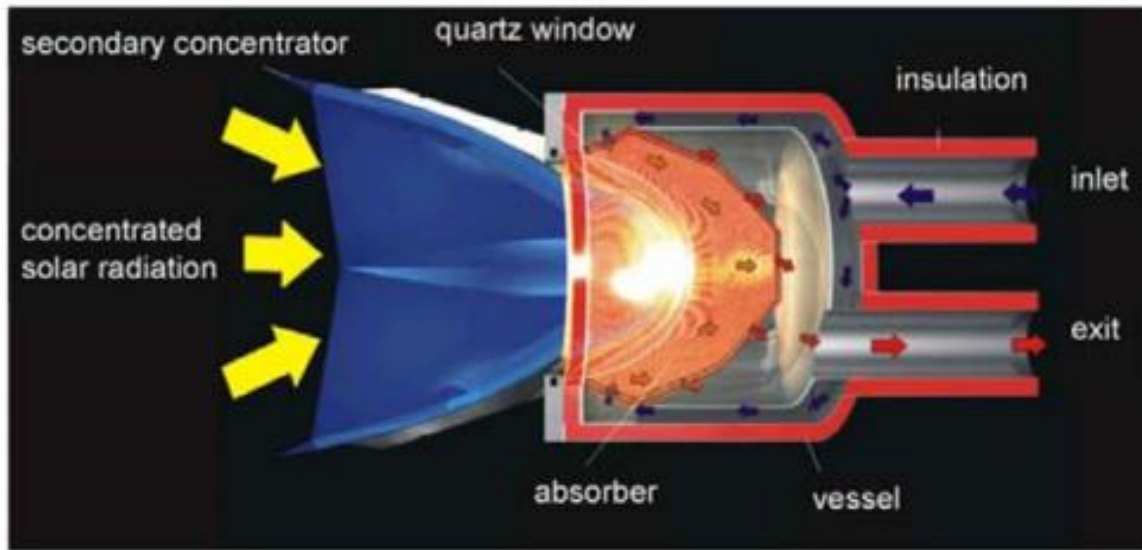
Figure 5-9 A REFOS receiver module

The development of this technology was followed by the SOLGATE project where a receiver formed by 3 modules was designed and erected in the CESA-1 solar tower test facility at the Plataforma Solar de Almeria (PSA) in Spain. The three receivers, connected in series, heated up air from 290°C to 1000°C to feed a modified helicopter gas turbine with a power output of $230 kW_e$.
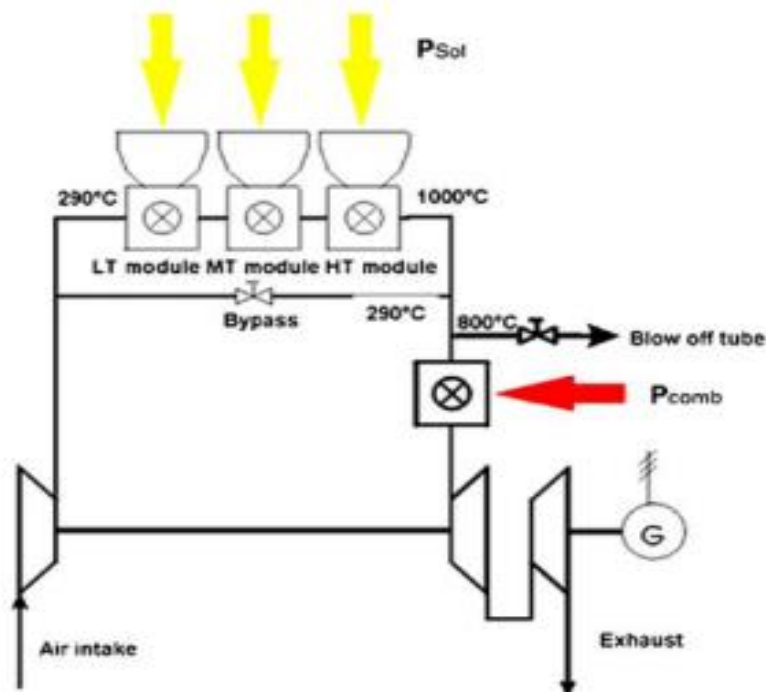
Figure 5-10Scheme of SOLGATE concept

5.1.3 Water steam technology

A water/steam receiver offers some thermal, logistic and economic benefits:

- The receiver fluid can be directly used in a steam-turbine cycle without further heat exchange.
- From a thermal point of view the evaporation of water offers excellent heat transfer characteristics so that this receiver can be made of less costly materials or it can be applied under high solar concentration.

At the same time, a few challenges have to be dealt with:
- Non-homogeneity of heat input onto a highly pressurized absorber tube when it is irradiated only from one side and their influences on material stability.
- Difficulty to handle the start-up and transient operation of the system.
- There is no simple solution to store large amounts of high temperature/high pressure steam, in order to operate the plant during night hours.

The water/steam receiver could be classified in two classes, according to the thermodynamic state of the steam used in the power block:

1) Saturated steam: the receiver is composed only by an evaporator.
2) Superheated steam: the receiver is composed by evaporator, super-heater and, eventually, a re-heater.

Solar One

The first solar power tower put into operation was the "Solar One" plant ($10 MW_e$) in the Mojave desert in California, USA. The Solar One receiver was a once-through superheated water-steam boiler with cylindrical shape that operated from 1984 to 1988.
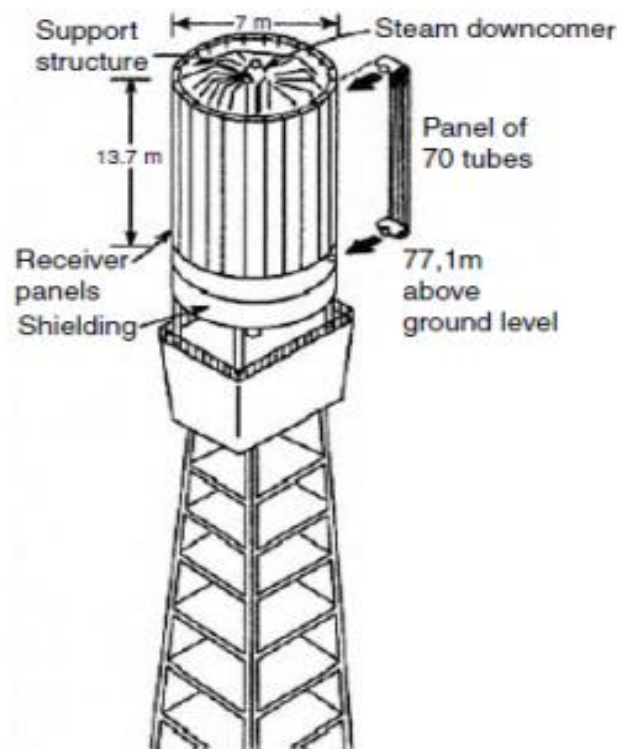
Figure 5-11scheme of Solar One receiver

The receiver was made by 24 rectangular panels. The six panels on the south side (lower radiation) were used to preheat feed-water after which the water was transferred to once-through boilers and super heaters on the north side. The design specifications of live steam were 516°C and 100 bar for a thermal capacity of 42 MW_t.

One of the main problems found during testing, which is typical of super-heaters, was overheating and deformation in the superheating section because of solar transients and poor heat transfer. After 18 months in operation, cracking and leaking problems were encountered at the top of the boiler, due to the fact that, during start-ups and shutdowns, the temperature gradient between the edges and the center of the tubes could be as high as 111°C, coupled with fast temperature changes during the daily sun irradiation cycle.

Weizmann Institute solar tower

This receiver was designed, fabricated, assembled and tested at the solar central receiver facility of the Weizmann Institute, Israel. With a 2 MW_{th} heat input capacity and a maximum flux on the evaporating panels of $300 kW/m^2$, the receiver was designed to generate steam at 15 atm. This solar steam receiver is a hexagonal shaped cavity with an 2.5×2.5m opening. Opposite the opening there are three

active absorbing panels made by vertical tubes where water is forcedly circulated at a ratio of 1:25 by a pair of high capacity low-differential pressure centrifugal pumps[21]. There are not welded connections among the tubes to create a so-called "water wall" panel, in order to reduce problems originated from temperature gradients and thermal stresses. This receiver, in nominal condition, produced 2500 kg/h of saturated steam at 15 atm and 200°C.

Figure 5-12 Weizmann Institute solar tower

Production of superheated steam has brought different problems in solar receivers, as demonstrated by several plants such as Solar One and CESA-1. On the contrary, better results regarding absorber panel lifetime and controllability have been reported for saturated steam receivers, as in the Weizmann receiver. With this kind of receiver, thanks to its better thermal behavior, a very high efficiency of the boiler can be reached, about 20% more than an air-volumetric receiver as shown by table 5-1[12].

Table 5-1Comparison of thermal losses and efficiency in Air Volumetric and Saturated Steam Receivers

Losses	Air[%]	Steam[%]
Reflection	7.9	2
Radiation	8.6	0.8
Convection	0	2.6
Spillage	5	2.1
Air return	3.7	0
Total efficiency	74.8	92.4

The PS10 project

The PS10 is a tower plant of 11 MW_e located in the town of Sanlucar la Mayor, 15 km far from Seville. Thanks to 624 heliostats, the cavity receiver, composed by four tubular panels (5.36 × 12 m), produces saturated steam at 40 bar and 250°C. It is, with its sister plant PS20 ($20MW_e$), the first commercial solar power tower in the world and, for this reason, one of the reference points for this technology. Hence, this plant has been taken as reference system in this work and will be described more in detail in the following sections.

5.1.4 Water /Steam receiver problems

Different problems must be faced when adopting a water/steam central receiver. These problems are linked to two aspects:

1) Mechanical problems
2) Dynamic operative requirements

Mechanical problems: thermal stresses

One of the main problems is the temperature distribution of metallic pipes receiving radiation on a single side. This phenomenon originates, during the thermal expansion, stresses in the pipes: compression near the inner wall and extension near the outer wall. With the aim of reducing these stresses (called *bowing*), it is useful to pre-stress the pipes in the opposite way and use highly reflective surfaces in the internal side in order to make the temperature profile as homogenous as possible. Another important aspect to deal with is allowing for pipe expansion under thermal load. For this reason the pipes are suspended in the tower structure permitting their vertical elongation in the downward direction. Regarding dynamic aspects, it is clear that the receiver will be subjected to daily start/stop. This leads to cycle fatigue that can cause creeping of the hotter part of the boiler (SH and RH). In order to reduce this effect several measures should be taken:

- The drum diameter should be reduced, limiting its function to accumulate water instead of phase separation and using four external separators one for each side of the tower.
- The pipe-collector connections of SH/RH should be provided with forged pieces that connect more gradually different thickness, therefore reducing thermal stresses.
- The drum should be kept warm during the night by an electric heater.
- The panels should be pre-heated with auxiliary steam before letting the general steam to flow through.

Dynamic operative requirements

Starting

This phase occurs every day and usually concludes 30 min after sunrise. Starts are divided in three phases:

1. Solar radiation is applied to the evaporator pipes producing steam that is used to preheat the SH/RH section. SH and RH panels are not radiated already.
2. SH and RH panels are radiated and start producing superheated steam. Until that moment, steam is re-circulated by-passing the turbine.
3. The turbine by-pass is closed gradually and the turbine is started.

Low radiation

In these conditions, the heat input is lower than the minimum requested by the turbine to work regularly (e.g. clouds passage) and, since it is absolutely necessary to keep the boiler and the rest of the plant in a state from which it can be rapidly re-started, the boiler is kept working using the remaining radiation but the turbine is by-passed. If the radiation were too low the drum would be kept at high pressure/temperature by an external electrical heater while an auxiliary gas boiler would provide steam to the.

Night stop

As the sun is setting, the solar steam generator continues to feed the turbine, which is working in "sliding pressure" mode, with decreasing pressure until a minimum drum pressure is achieved. When this condition is hit, the system is stopped and the interception valves are closed in order to maintain the drum at high pressure/temperature.
At night, the evaporators are kept hot by an electric heater with the aim of reducing thermal stresses and reducing start time.

Emergency shut-down

Should an alarm go off (high metal temperature, high wind speed, low level of drum water…), the mirrors would be brought to their stow position. At this time the procedure is the same as for night shut down and so the interception valves are closed to maintain the drum pressure.

5.2 Receiver type

From a geometrical point of view, there are two general receiver configurations:
  – *Cavity receiver*
  – *External receiver*
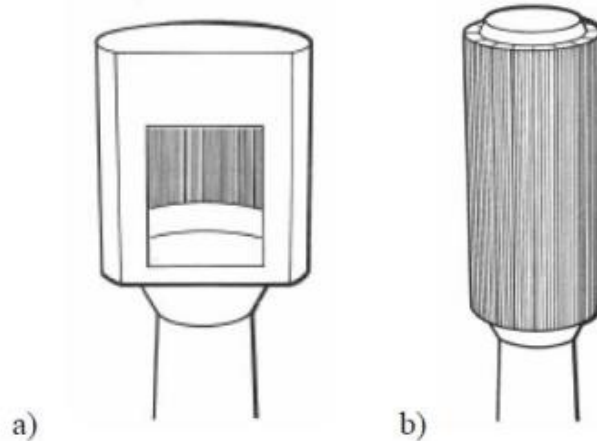
Figure 5-13Two different types of superficial receivers: a) cavity internal receiver and b) external superficial receiver

External receivers have heat absorbing surfaces that are either flat or convex toward the heliostat field. For a large plant, an external receiver could be a multi-panel polyhedron that approximates a cylinder, with a surrounding heliostat field. Instead, smaller plants typically use a north field configuration with a partial cylinder receiver, omitting most of the south-facing panels.

In a cavity receiver, the radiation reflected from the heliostats passes through an aperture into a box-like structure before impinging on the heat transfer surfaces; this box and aperture define the cavity. Even if a receiver may be composed of more than one cavity (each facing a different sector of the heliostat field), studies have demonstrated that the preferred configuration is a single cavity facing a north (in the northern hemisphere), heliostat field.
Other internal areas of the cavity such as the roof and the floor, do not normally serve as active heat absorbing surfaces. These areas must be effectively closed and insulated to minimize heat loss and to protect structure, headers, and interconnecting piping from incident flux. Although they are not exposed to high levels of direct flux, the inactive internal areas are exposed to radiation from the hot absorber panels and therefore must be protected to prevent the achievement of high temperatures.

Several factors distinguish external and cavity receivers[22]:

- *Radiative losses*: are generally larger for external receivers since the hot receiver panels are more exposed and have larger view factors to colder ambient environment. Instead cavity receiver panels are more protected and have low view factor due to the small aperture.
- *Spillage losses*: are generally larger for cavity receiver because the heliostat radiation must fit through the relative small aperture, and thermal and convection losses may be larger because of the large heated surface area of the cavity.
- The receivers mass and number of components are larger and generally more costly for a cavity than for an external receiver. The mass provides some thermal inertia which enables buffering of transient weather conditions and the presence of a door, in a cavity receiver, which may be closed during times of low insulation, helps to reduce thermal losses and to simplify start up procedures.
- Receiver tubes in a cavity are more protected from the effects of weather than the external receiver ones. This means less degradation of high absorptivity coatings during service.

5.3 Tower

The tower provides support for the solar receiver at the required height above the heliostat field and also provides support for the beam characterization system target, piping, and associated mechanical and electrical equipment that are located outside the tower, just below the receiver.

Primary access within the tower is by means of an elevator for transporting plant personnel and portable maintenance equipment.

Towers are constructed of steel or reinforced concrete. Steel towers are similar to guy-wire supported television transmission towers. Instead concrete towers are similar to tall chimneys of conventional fossil power plants.

*Figure 5-14 Left one: **steel tower**   Right one: **Reinforced concrete tower***

The choice of tower construction depends primarily on the required height of the tower. Steel towers are most likely to be cost effective when the height is less than 120 m while reinforced concrete towers have been shown to be more cost effective for towers taller than 120 m [22].

5.4 Thermal behaviour of a central receiver

The radiation coming from the heliostat field is reduced due to several dispersion effects as loss caused by lack of focalization and loss due to the diffusion, which cut the flux reaching the tower.

When a certain amount of flux has reached the tower it is important to understand the fraction that is effectively absorbed by the fluid inside the pipes. In the usual design process the best performance is looked for by a variety of design tradeoffs among several loss mechanisms.
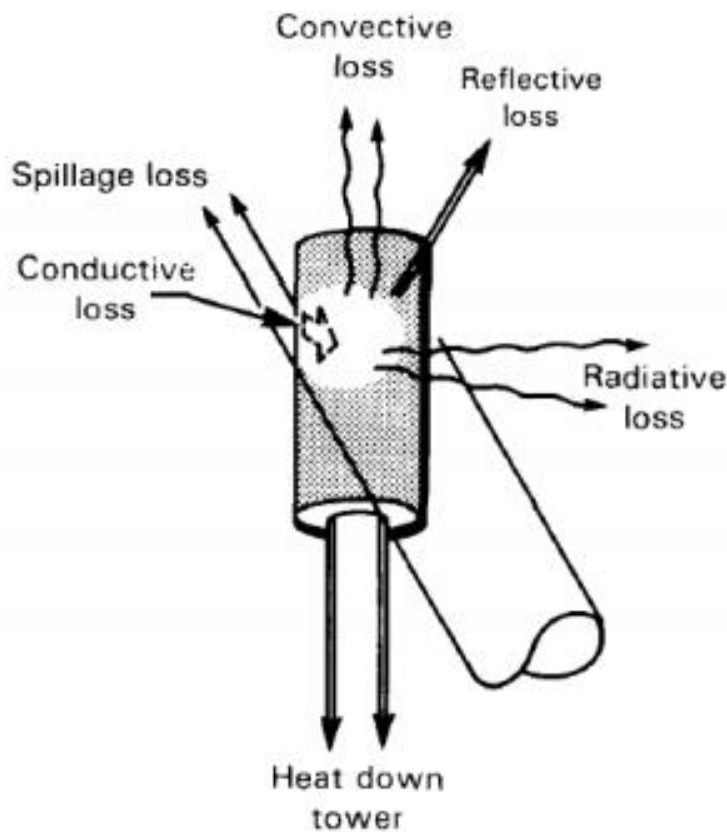
Figure 5-15Receiver losses processes

These losses, shown in Figure 5-15, include:

Spillage losses: is a loss due to the fact that part of the energy reflected by the heliostat field, after accounting for atmospheric absorption between heliostat and receiver, is not intercepted by an absorber surface containing the receiver internal fluid, or re-reflected or radiated from an intermediate surface to that absorber surface.

This component is very high for SH/RH pipes that have no membrane. Due to the cyclic work the pipes tend to be bended and to create empty spaces between two next tubes.

A reasonable estimation of this loss is about 0.3-0.5% of the total incident radiation[23].

− *Reflection losses*: is a loss due to the light energy from the heliostat field that is scattered from the receiver surface and then escapes from it. For this reason high absorptivity paint is used on the absorber surfaces to minimize this loss. Reflection loss is generally 2-3% or less with a freshly-painted absorber

surface, but may increases during service as a result of degradation of the coating.

- *Convection losses*: is the thermal energy lost in heating the air adjacent to the receiver. It is, obviously, a combination of free (thermally driven) and forced (wind driven) convection, with the free convection component usually larger.

- *Radiation losses*: is the thermal energy lost by infrared and visible light emission due to the high temperature of the receiver. Both the radiative and convective losses are a function of the temperature of the receiver and its configuration (cavity or external).   Typical combined radiation and convection losses are in the range of 5 to 15% [22]of the peak incident energy on the receiver.

- *Conduction losses*: is the thermal energy lost through the insulating surfaces and structural parts. This loss is less than 1% for a well-insulated receiver and for this reason they have not be taken into consideration in the thermal model but they are present in the overall efficiency used in the plant model.

- *Radiation losses towards the tower interior*: the non-radiated part of the pipes panels is covered by further panels of nonconductive material and they are coated (in the pipes side) by a continuous steel sheet with a high reflective coefficient. In this way two important effects can be obtained:

  o Thermal effect: without any protection, the heat radiated from pipes to the cold side would be dissipated and it would not contribute to the heat transfer. Instead, in this way, a large part of the radiation is redirected towards the pipes and the working fluid.

  o Mechanical effect: a pipe exposed to radiation on a single side tends to buckle. By a good reflection of the back non-conductive panel this effect is minimized reducing the mechanical stress on the pipes.

  The insulating panel after the reflective sheet is designed in order to assure a temperature of the cold side of the panel of 70-80°C. An average value of this loss is about 0.5-1%[23].

Cavity receivers have, in general, better thermal efficiency than external receivers. This is largely due to the reduction in radiative losses when a cavity enclosure is employed.

5.5 Modelled receiver description

The receiver considered for the creation of the model is practically inspired by the PS10 receiver, considering modification in materials and sizes since this boiler was designed to work with water.

This receiver was designed and built by *Technical-Tecnicas Reunidas*, a Spanish Engineering Company for the ABENGOA 11MW_e plant PS10. It is a cavity receiver with only one aperture toward north because it has been thought for a north heliostat field (as already said, considered the best configuration in the North hemisphere).

Figure 5-16 the cavity receiver of PS10 plant under construction

In the case of PS10 and PS20, the receiver consists only in an evaporator section without the presence of economizer, or super-heater, or re-heater, because it is the most economical solution thanks to the use of relatively cheap material. It is important to point out that having only boiling water in the pipes increases enormously the internal heat transfer coefficient, letting the water to cool in a very efficient way the pipes. Another important aspect of this kind of solution is that it is possible to reduce the presence of too many collectors or junctions among different pipes, which are the most critical components because of the great thermal stress suffered.

A map of the radiation hitting the receiver in a typical day is shown in fig. 5.17 together with a sketch of the hydraulic circuit circulating boiling water along the receiver[24].
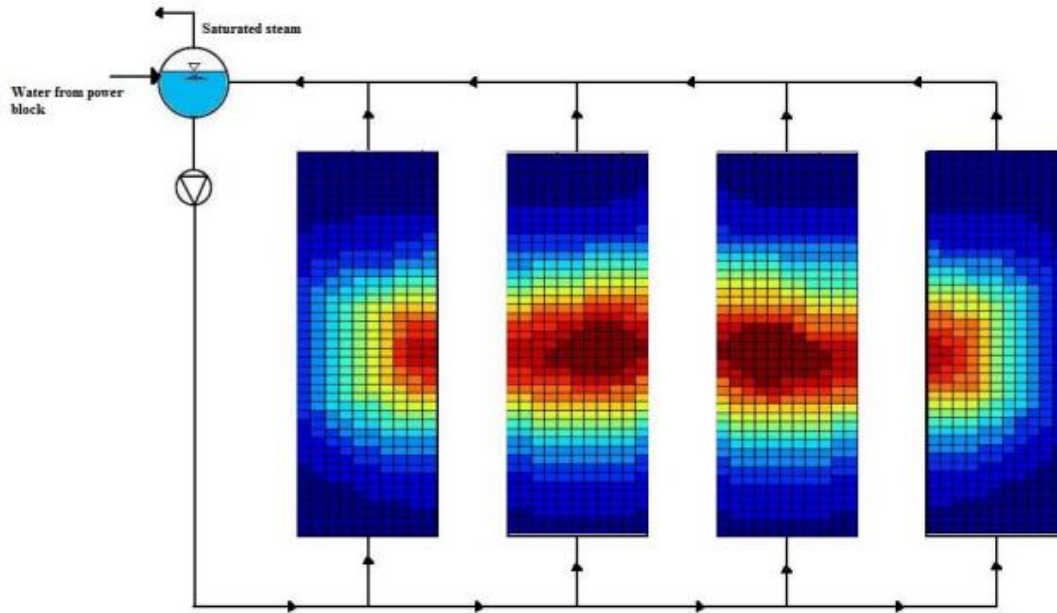
Figure 5-17the receiver radiation map of PS10 on 21^{st}March 2007 at 12:00

But taking into account that we are applying supercritical CO_2 as the working fluid both in boiler and power cycle in this study, it is easy to figure out that there should be a substantial modification in boiler design and materials due to two important aspects:

1. The very high pressure in the pipes needs to be controlled by applying a high strength material and proper pipe thickness.
2. Due to the fact that CO_2 is in the gas phase while heating up in the boiler, it causes a lower internal heat transfer coefficient compared to steam, so the highest material temperature resistance will become a critical issue and should be taken care of.

For the mentioned reasons, a possible choice to be applied in the boiler pipes is AISI316 stainless steel(SS316 or X5CrNiMo17-12-2), which has been widely considered in projects of advanced nuclear power plants for the same purpose, where they use supercritical CO_2 as working fluid as well[25].

The properties of 316 stainless steel can be found in the tables below.

Table 5-2 Basic components of 316 stainless steel

Element	Carbon	Manganese	Silicon	Chromium	Nickel	Molybdenum	Phosphorus	Sulfur	Nitrogen	Iron
Percentage by weight	0.08	2.00	0.75	16.00	10.00	2.00	0.045	0.03	0.01	Bal.

Table 5-3 Physical properties of 316 stainless steel

Physical property	Value
Melting Range	1390-1440°C
Density	8.027 g/cm^3
Modulus of Elasticity in Tension	200,000 Mpa
Modulus of Shear	82,000Mpa

Radiation map

The radiation map is the key input of the model. These maps have been taken as real data from the PS10 operation and consist of matrixes with a fixed number of cells containing an average flux value (radiation map resolution), expressed in kW/m^2.
Maps have been taken by a previous work developed at Politecnico di Milano together with the University of Seville[24, 26].
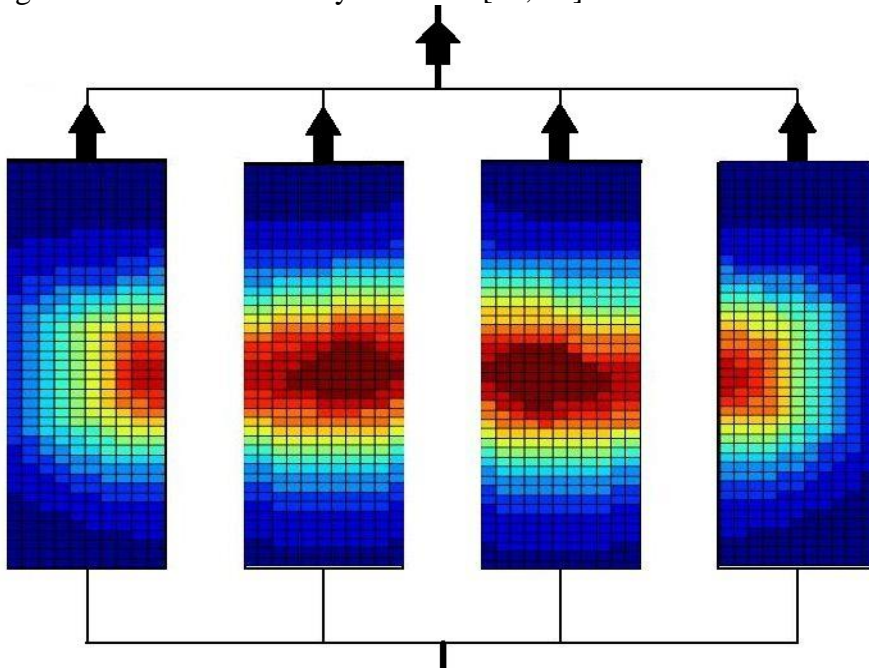
Figure 5-18Overal radiation map of PS10 used for sCO$_2$ case

As it can be seen on the figure 5-18 the radiation map consists of four tables, each one of them composed by 44x11 cells containing the average value of the solar flux in that area.

Due to the fact that these data were directly available from ABENGOA SOLAR and are, obviously, very representative of the real operation, it has been decided to maintain this layout (number of panels and cells for each panel) even for other radiation maps, for example in off-design conditions.

Number and layout of absorbing panels

As for the *radiation maps* the main geometry of the panels and their layout is fixed following the internal configuration of the PS10 plant. In this plant, as in the model, there are four panels that are placed inside the cavity of the receiver.
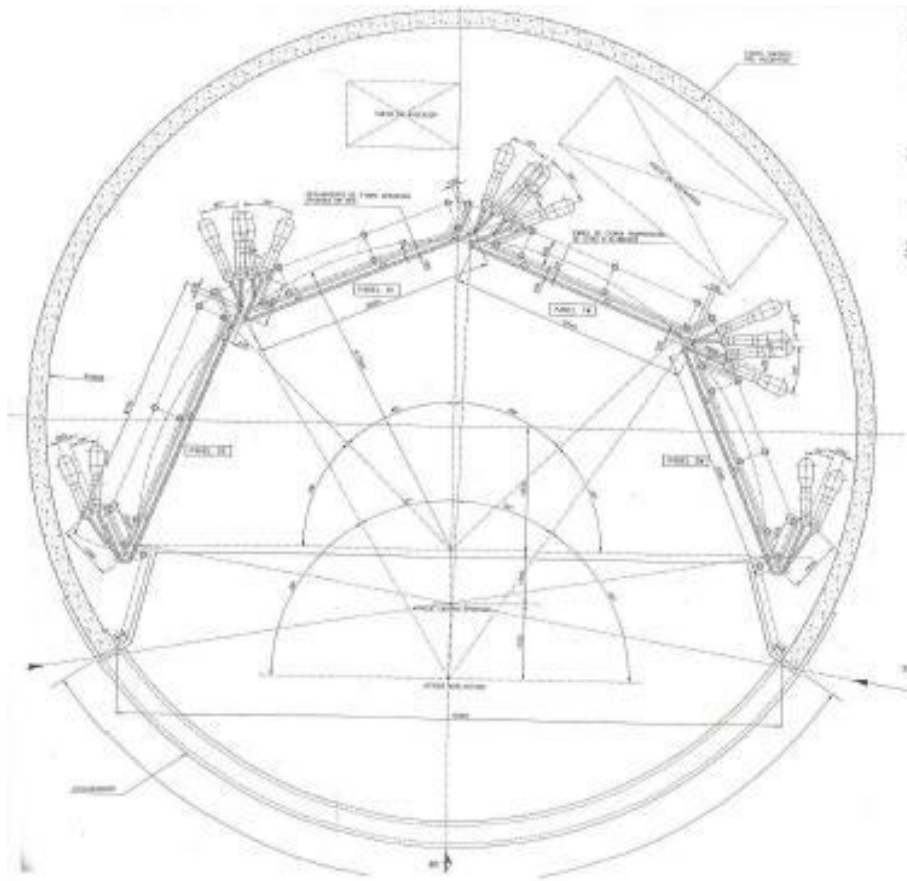
Figure 5-19 technical design of the PS10 panels[27].

In the PS10 this configuration has been chosen to perform below flux limits ($650\ kW/m^2$) minimizing spillage losses that are about 1% of the incident radiation. Geometrical parameters regarding the panel disposition have not been considered because this information is already present in the radiation map. Another important aspect that is fixed is the rate between height and width of each panel that is equal to 2.2388 according to the PS10 design[27].

In the model considered in this work, for simplicity, a simple layout has been chosen. In particular, all the pipes are vertical and do not have any bend. The preheated supercriticalCO_2enters from the bottom and the high temperature CO_2exits from the top, going to the turbine. In this way, the computational time needed to solve the model is reduced because it is possible to associate each pipe of the panels to a single column of the radiation map and, for this reason it is possible to reduce the number of pipes studied significantly.

The real size of each column in the radiation map depends on boiler size but normally it includes more than a single pipe. In our case, the height of the boiler has been fixed as it was in PS10 case (12.96 m), since the ratio between height and width is constant and equal to 2.2388, the width of each of four modules will be 5.79 m. Since the module is consisting of 11 columns, the width of each module can be calculated as 0.5263 m and each cell height (based on the cell height in the radiation map) will be$12.96/44 = 0.294\ m$. As explained before, for the case of on-design model, with pipes outer diameter equal to 0.0145m, the number of pipes per cell that receives the same radiation power input can be find out as bellow:

$$\frac{cell\ width}{d_{ext}} = \frac{0.5263}{0.0145} = 36.29 \cong 36$$

In this way instead of studying the behavior of 36 pipes it is possible to study only 1 pipe and in general, 44 pipes instead of 1584 pipes. In summary, it can be said that the resolution of the computational domain (i.e. number of pipes) is determined by the resolution of the available radiation map. With this simplification, the computational time is therefore uncoupled from the boiler size.
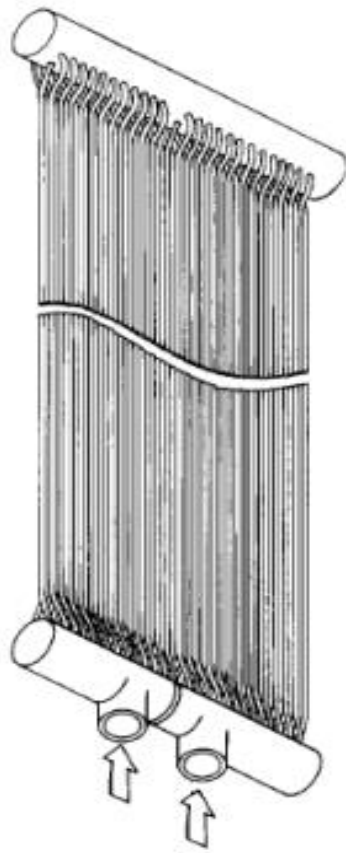
Figure 5-20 Vertical pipes layout in a solar boiler

6 MODEL DESCRIPTION

Generally there are different configurations of supercritical CO_2 that can be used for CSP plants in which the supercritical CO_2 is both the heat transfer fluid of the receiver and working fluid of the power block at the same time.

Concentrating solar thermal power (CSP) plants have been given great impetus in the last years, especially in countries like Spain, with plants in different construction stages[28]. The development of these power plants has been associated to the adaptation of proven steam power generation technologies combined with particular concentrating solar power components. Among others, the latter components include heliostats or solar receivers for central receiver solar power plants (CRS) [26, 29-30] and linear collectors, oil pumps and oil to water/steam heat exchangers for parabolic trough power plants. For the first type of plants, the high solar flux hitting the receiver (averaging between 300 and 1000kW/m^2) enables operating at rather high temperatures and values up to1000℃ are considered feasible[31], even if the maximum receiver temperature is limited to around 700℃ at the current stage of development[29]. Higher temperatures have nonetheless been obtained in experimental or demonstration plants like the Directly Irradiated Annular Pressurized (DIAP) facility[32] of the Weizmann Institute (Israel), with temperature exceeding 1300 °C when pressurized air at 10-30 bar and multistage receivers are used [33], with air temperature in the range of800 − 1000℃. In this sense, an analysis by Segal and Epstein [34] concluded that the optimum power plant performance would correspond to a receiver temperature close to 1600 K, what would allow using conventional gas turbine and combined cycle technologies.

Alternative power cycles, or cycles that make use of nonconventional fluids, are a different option to achieve higher efficiencies without reaching such high temperatures in the receiver.

Among them, the supercritical and trans-critical closed Brayton cycles working with carbon dioxide are deemed interesting. This cycle has been studied for the last 40 years, since firstly proposed by Feher and Angelino[34-35], for nuclear power production in gas reactors, though its applicability to solar power plants has also been explored [36-38].Thermodynamically, the main advantage of the Brayton

carbon dioxide cycle relies on its high useful to expansion work ratio (i.e. much lower compression work than expansion work) which is in the range 0.7-0.85 when compressor inlet is in supercritical conditions. At cycle level, different layouts were studied by Carstens et al.[39] and Dostal et al.[40] in order to increase cycle efficiency. From the point of view of major equipment, the necessary features of turbo machinery were analyzed by Vilimet al. [41] and Gong et al. [42] and heat transfer and heat exchanger layouts were analyzed by Utamura[43].

In the same category of alternative cycles, Organic Rankine Cycles (ORC) yield higher efficiencies than conventional steam cycles when heat delivery is at temperatures below370°C[44]and when a low power output does not allow exploiting the highest efficiency of more complex steam turbine designs (reheat or feed-water heating among others). Combined cycles with topping recuperative gas turbines and bottoming ORCs have been reported as an alternative to conventional combined cycles by Chacartegui et al. [45]and to low temperature solar thermal electric generation by Gang et al.[46].

This thesis is focused on the analysis of the receiver for sCO_2 (TIT below 1100 K, which allows working with local hot-spot temperatures in the receiver below approximately 1250 K) in order to improve the performance of the power plant. In all cases, carbon dioxide cycles have been considered, ether in stand-alone or combined cycle layouts with ORC bottoming cycles. The results show the interest of these cycles, which are envisaged as promising technologies for solar tower facilities.

Figure 6-1 shows the most basic and common cycle which can be designed for this purpose, a closed recuperated cycle which consists of 5 main components and operates over the critical point ($T_{cr} = 304.1282$[K]and $P_{cr} = 73.73[bar]$).
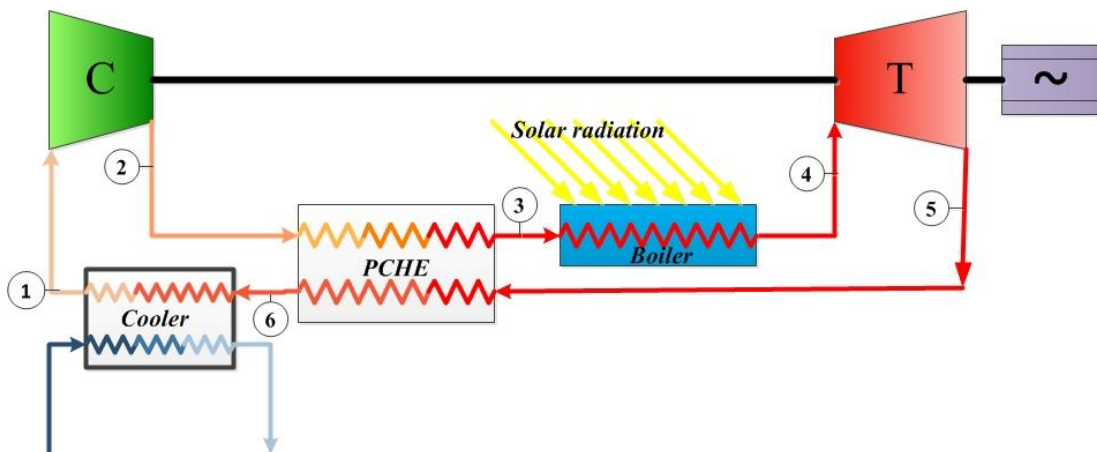
Figure 6-1Schematic of the simple recuperative carbon dioxide cycle
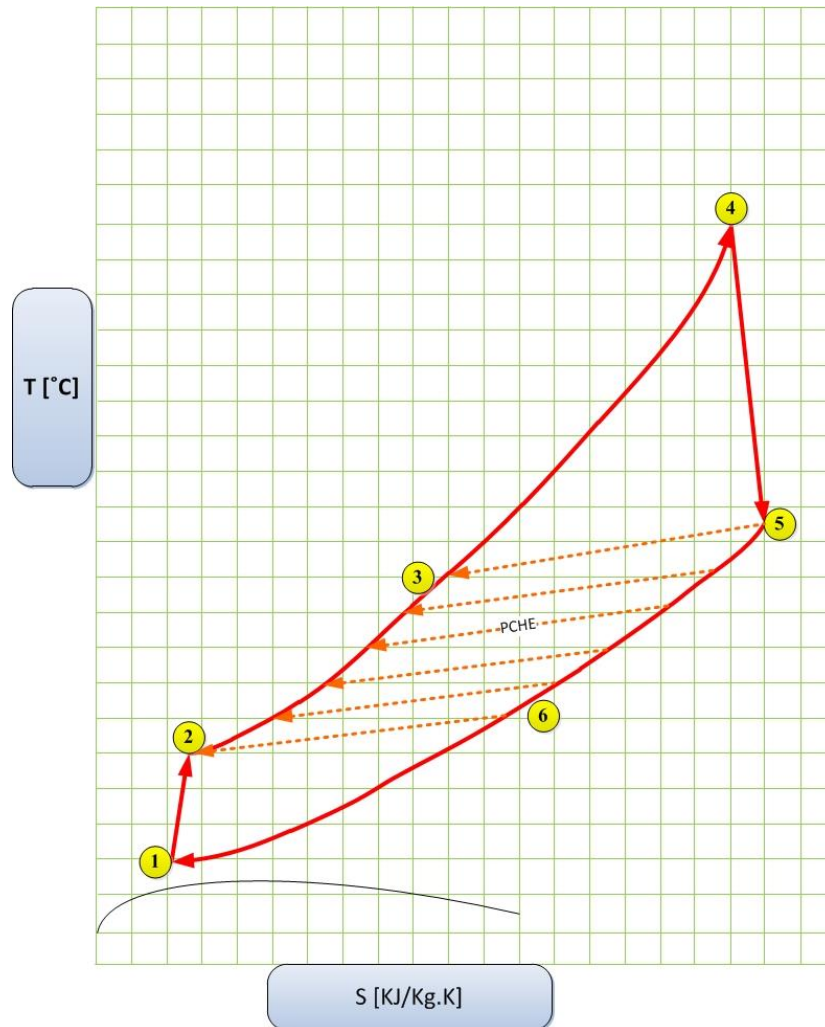
Figure 6-2 T-S diagram of simple recuperative carbon dioxide cycle

Figure 6-2 also shows the T-S diagram of the plant in Figure 6-1.
As it can be seen, the working fluid will be firstly compressed from point 1 which is slightly over the critical point, up to point 2 with a higher pressure and temperature. Afterward, the fluid will go through a heat exchanger (we have considered the Printed Circuit Heat Exchanger type, labeled PCHE, which will be better described in the following) and will preheat there up to point 3, thanks to hot gas exiting the turbine.
Later the preheated CO_2 will be heated up to maximum temperature of the cycle (point 4) in the receiver. The cooled fluid coming out of PCHE at point 6 will be cooled down in a cooler by means of water. This heat exchanger is also considered to be PCHE type since it`s still dealing with quit high pressure. The cooling water can

be finally cooled to reject heat to the environment, either using a cooling tower or a dry air cooler. Since normally the CSP plants are located in hot and dry areas, it`s preferable to apply a compact air cooled heat exchanger in order to prevent the consumption of water due to the cooling tower.

Two carbon dioxide cycles have been compared in order to select a configuration for the plant analysis.

First, a stand-alone closed recuperative Brayton cycle with a recompression is considered, as it can be seen in Figure 6-3, and then a combined cycles composed by a topping carbon dioxide cycle and a bottoming ORC cycle is presented. The latter is based on the layout presented in Figure 6-1, yielding the combined cycle shown in Figure 6-4.
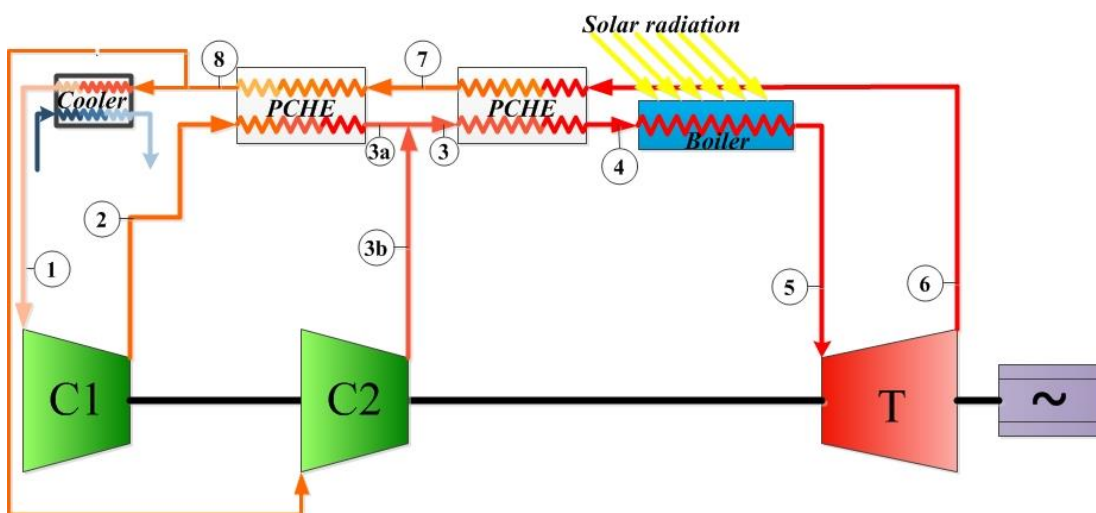
Figure 6-3 schematic of supercritical carbon dioxide cycle with recompression
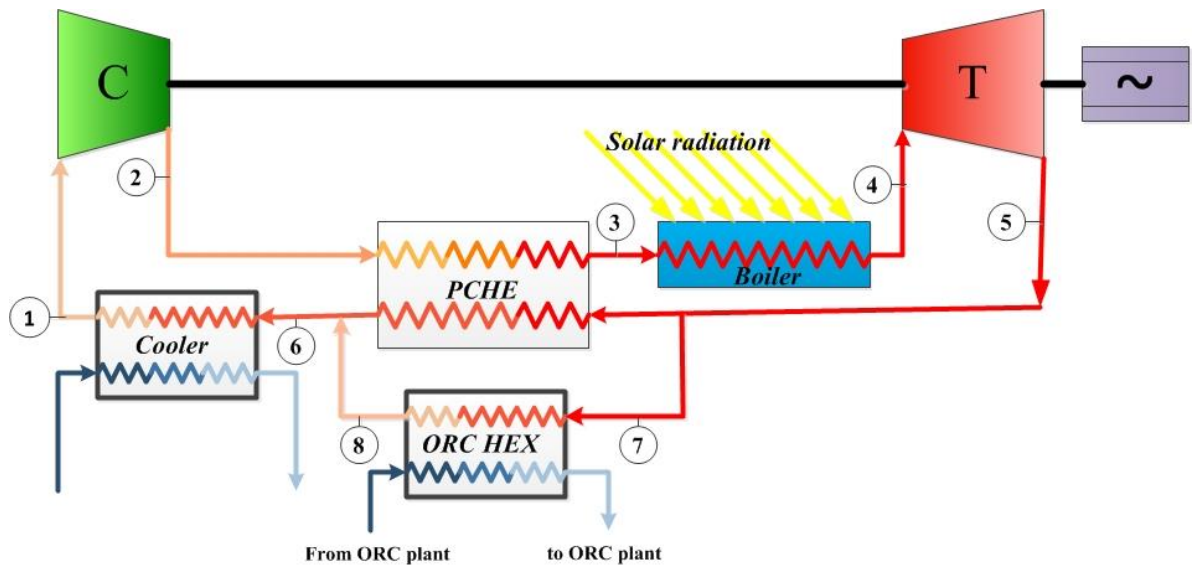
Figure 6-4schematic of combined cycle composed by a topping carbon dioxide cycle and a bottoming ORC cycle, driven by the ORC heat exchanger shown in the lower part of the figure.

The two cycles based on different thermodynamic design parameters will show different behavior in sense of cycle efficiency, but for our interested and possible (due to material constraint) range of design parameters (maximum allowable pipes temperature and pressure), both cases of Figure 6-3 and Figure 6-4 will result to the same range of cycle thermal efficiency(combined with ORC cycle slightly more), but for the sake of simplicity in coding, just the layout of Figure 6-4 has been chosen and detailed finite element analysis on the receiver has been applied to this second scheme in order to have a parametric study which will be explained in detail in the following sections.

The comparison between the two cycles for a specific operating point (on-design situation) has been shown in Table 6-1:

Table 6-1 design parameter of the two plants

Design Parameter	Layout in Figure 6-3	Layout in Figure 6-4
Compressor inlet temperature [K]	320	320
Compressor inlet pressure [bar]	75	75
CO_2 mass flow rate [kg/s]	70.22	70.22
Compressor pressure ratio(β)	5	5
Receiver inlet temperature [K]	650	650
Receiver outlet temperature [K]	950	950

Table 6-2 results of the comparison between the two plants

Results	Layout of Figure 6-3	Layout of Figure 6-4
T_1[K]	320	320
T_2[K]	472	472
T_3[K]	515	650
T_4[K]	650	950
T_5[K]	950	692.3
T_6[K]	692.9	359.1
T_7[K]	528.5	692.3
T_8[K]	476.43	359.1
Receiver input power [kW]	2.365×10^4	2.369×10^4
Net electric output power [kW]	1.146×10^4	1.199×10^4
Cycle efficiency [%]	48.46	50.6

The requisite code was developed in MATLAB, with a subdivision in routines that follows the combination of compressors, turbines and heat exchangers typical of the Brayton cycle. Heat exchangers can be divided into three categories:

- Recuperators (sometimes called regenerators, where the working fluid is on both sides, but does not necessarily have the same mass flow rate) are used to preheat the working fluid before it enters the component in which the heat is added to the cycle (the solar receiver).
- Coolers (i.e. working fluid on one side and cooling medium, water, on the other), which are used to exchange heat from the cycle to water.
- Dry cooler (i.e. the cooling water on one side and ambient air on the other side) which are used to reject heat to the environment.

The general outline of the code is based on a combination of subroutines.
Subroutine MASSOFF has been modeled in such a way that it iteratively evaluates the required carbon dioxide mass flow rate in order to meet the desired power output, considering the pressure drops of piping and all components of the system.

Turbo machinery components, i.e. turbine and compressor, are modeled in subroutines COMPRESS and TURB for compressors and turbines respectively. Both COMPRESS and TURB subroutines are written in such a way that they contain the whole compression or expansion process.

Subroutine CSP is in charge of loading the radiation map and having the inlet temperature and pressure as an input, calculate the temperature and pressure distribution along the vertical pipes of the boiler.

Then there are three main heat exchanger subroutines that govern the heat exchanger calculations. Subroutine RECUPERATOR evaluates recuperators, subroutine

COOLER models the cooler and subroutine COND models heat rejection in the dry cooler. The user can specify the operating conditions and the basic geometry characteristics and let the code evaluate the length of tubes or stream passages and the pressure drops (subroutine PCHElen).

6.1 Subroutines for turbo machinery (COMPRESS and TURB)

Compressors and turbines are modeled in the code by the subroutines COMPRESS for compressors and TURB for turbines. Since both subroutines are very similar they will be described together in this section.

The main input parameters for both routines are the inlet temperature, the inlet pressure, the isentropic efficiency of the turbo machine, the mass flow rate and the total pressure ratio across all compressor or turbine components. As an output, this subroutine will give back the output temperature, the inlet and outlet enthalpy value, and the required or produced power.
The approach is very simplified and there is no attempt to investigate the machine geometry, number of stages and poly-tropic compression/expansion effects.

The evaluation of the compression or expansion process starts from the machine inlet conditions that were specified in the input. The subroutine calculates the outlet conditions based on the total pressure ratio, machine efficiency and the inlet fluid conditions. The calculation procedure is the following:

$$P_{cout} = P_{cin} r_c \tag{6-1}$$

$$P_{tout} = \frac{P_{tin}}{r_c} \tag{6-2}$$

$$S_{cout\_id} = S_{cin}(P_{cin}, T_{cin}) \tag{6-3}$$

$$S_{tout\_id} = S_{tin}(P_{tin}, T_{tin}) \tag{6-4}$$

$$W_c = \frac{h_{cout\,id}(P_{cout}, T_{cout\,id}) - h_{cin}(P_{cin}, T_{cin})}{\eta_c} \tag{6-5}$$

$$W_c = \eta_t[h_{tout\,id}(P_{tout}\,,T_{tout\,id}) - h_{tin}(P_{tin}\,,T_{tin})]$$ (6-6)

Where p stands for pressure, s for entropy, w for work (kJ/kg), h for enthalpy T for temperature, r_c for pressure ratio and η for total to total efficiency. Suffix c denotes a compressor and suffix t denotes a turbine. Suffixes in and out denote the inlet or outlet conditions respectively. The suffix id denotes the ideal state, i.e. if the turbine or compressor were ideal components and the compression or expansion process was isentropic.

6.2 Subroutines for ORC

This part of the code is in charge of thermal analysis of ORC plant and calculating the added power to gas cycle power output. The detail analysis of the ORC cycle has been avoided and it had been considered just as a bottoming cycle which will take the power supplied by the ORC HEX as the input and report the possible net electric power to be produced as the output. This subroutine will also calculate the efficiency of the combined gas-ORC cycle. The considered efficiency for the ORC cycle has been considered to be 21% which was reported in literatures[47].

6.3 Subroutines for heatexchangers

To perform the design of heat exchangers it is first necessary to establish the heat exchanger geometry, heat transfer model and the pressure drop model. Once those are established then the iteration schemes for different design approaches need to be developed.

6.3.1 Heat transfer model

There are at most three different types of heat exchangers in any gas cycle: the recuperator, which operates with the working fluid, CO_2 in our case, on both sides; the cooler that cools the working fluid with a stream of cooling water; and the compact air cooled heat exchanger, which transfers the heat from the primary coolant to the environment. Therefore, it is necessary to develop a heat transfer model for supercriticalCO_2 , water and air.

The PCHE channels are semicircular channels that can be either straight or wavy. Straight channels were used in this work, because of better understanding of this geometry and lack of literature correlations for the heat exchange process in wavy channels. Thus the obtained results are conservative, as wavy channels are generally recognized to improve the heat transfer performance significantly. Hesselegraves[48] recommends using the Gnielinski correlation for the straight semicircular channels for the turbulent flow regime (Re > 2300), which is expressed as follows:

$$Nu = \frac{\frac{f_c}{8}(Re - 1000)Pr}{1 + 12.7(Pr^{\frac{2}{3}} - 1)\sqrt{\frac{f_c}{8}}} \tag{6-7}$$

Where Nu is the Nusselt number, Re is the Reynolds number; Pr is the Prandtl number and f_c is the Moody friction factor defined as:

$$f_c = \left(\frac{1}{1.8 \log Re - 1.5}\right)^2 \tag{6-8}$$

These equations are valid up to Reynolds numbers of 5×10^6 and Prandtl numbers ranging from 0.5 to 2000. This range of Prandtl numbers is applicable for CO_2.

Reynolds number is defined as:

$$Re = \frac{V d_{eq}}{\nu} \tag{6-9}$$

Where v is the fluid velocity, d_{eq} is the hydraulic diameter and ν is the fluid kinematic viscosity.

The hydraulic diameter for the semi-circular channel can be evaluated from:

$$d_{eq} = \frac{4\pi d_c{}^2}{8\left(\pi \frac{d_c}{2} + d_c\right)} \tag{6-10}$$

Where d_c is the semi-circular channel diameter.

Prandlt number is defined as:

$$Pr = \frac{\mu C_p}{k} \tag{6-11}$$

Where μ is dynamic viscosity in (Pa.s); C_p is the specific heat in (J/kg-K) and k is the fluid thermal conductivity in (W/m.K).

For laminar flow Hesselgraves[48]recommends use of Nu = 4.089. Since the value of the Nusselt number from the Gnielinski correlation at 2300 is not 4.089, there would be a discontinuity in the evaluation of the Nusselt number. That could introduce convergence difficulties in the code, therefore the range of Reynolds number between 2300 and 5000 is considered as a transitional region, where the Nusselt number is evaluated by linear interpolation, i.e.:

$$Nu = 4.089 + \frac{Nu_{G(Re=5000)} - 4.089}{5000 - 2300}(Re - 2300) \tag{6-12}$$

Where $Nu_{G(Re=5000)}$ is the Nusselt number from the Gnielinski correlation evaluated at Reynolds number of 5000.

Once the Nusselt number is known the heat transfer coefficient h (W/m^2.K) can be calculated from:

$$h = \frac{Nu.k}{d_{eq}} \tag{6-13}$$

The heat transfer model for straight channels is well established and the Gnielinski correlation is one of the most accurate. It was recommended by Olsen[49] for use with supercritical CO_2, with further possible corrections to take into account also the property gradients between the core fluid and the wall, by applying a density ratio and specific heat ratio. However, since the simple Gnielinski correlation gives more conservative results and the property gradients vanish at temperatures far from the critical point (both recuperators and part of the cooler) the simple Gnielinski correlation was used.

6.3.2 Pressure drop model

The pressure drop model consists of two major parts: one for form losses and the other for friction losses. It does not reflect gravitational or acceleration losses since these will be recovered in other parts of the cycles. Only the friction and form losses relate to energy dissipation.

The types of pressure losses for straight channels are two, the entrance and the exit loss. Both can be evaluated from:

$$\Delta p = C\rho \frac{V^2}{2} \tag{6-14}$$

where C is the form loss coefficient that was taken to be 0.5 for the entrance loss and 1.0 for the exit loss [50], ρ is the local fluid density (kg/m^3) and v is the local fluid velocity (m/s).

The friction losses can be estimated from:

$$\Delta p = f \frac{L}{d_{eq}} \rho \frac{V^2}{2}$$
(6-15)

Where L is the length and d_{eq} is the equivalent hydraulic diameter for the semi-circular channel.

For friction factor for the sake of simplicity the pipes have been considered to have a fully developed regime and turbulent situation, so that for this regime the Colebrook-White correlation can be used:

$$f = \frac{1}{\left[2 log_{10} \left(\frac{2.51}{Re\sqrt{f}} + \frac{\Delta}{3.7}\right)\right]^2}$$
(6-16)

6.3.3 Heat exchanger modeling

Heat exchangers are the largest components in the cycle their careful design is an important issue. In order to reduce the total volume of heat exchangers compact heat exchanger must be used. Printed circuit heat exchangers (PCHE) are considered the best suited for this type of application. This heat exchanger consists of plates into which the channels are chemically etched or 'printed'. The plates are built in sequence and later they are diffusion bonded into a monolithic block; due to that this type of heat exchanger is also called diffusion-bonded heat exchanger. The arrangement of the flow can be of different types, the case considered here is counter-current and the channels are semi-circular in cross-section. A real section and a conceptual sketch of this heat exchanger are shown in Figure 6-5 and Figure 6-6, respectively.

There are several unique characteristics that contribute to the superior performance of PCHE. The most distinctive ones are the high allowable pressure and temperature limits. Specifically, the manufacturing company claims that they are able to operate at pressures up to 500 bar and temperatures not exceeding 1173 K which in our case are both in a safe mode (P_{inlet_cold}= 398.29 bar and T_{inlet_hot} = 796.5 K). To allow operation under such extreme conditions, the materials commonly employed in PCHE include austenitic stainless steel, titanium and nickel (pure/alloys), all which are corrosion resistant. Carbon steel is typically not used for two reasons. First, because of the small channel diameter, the heat exchangers are designed for

essentially zero corrosion allowance in order to avoid channel blockage. Second, carbon steel is unsuitable for diffusion bonding[51].
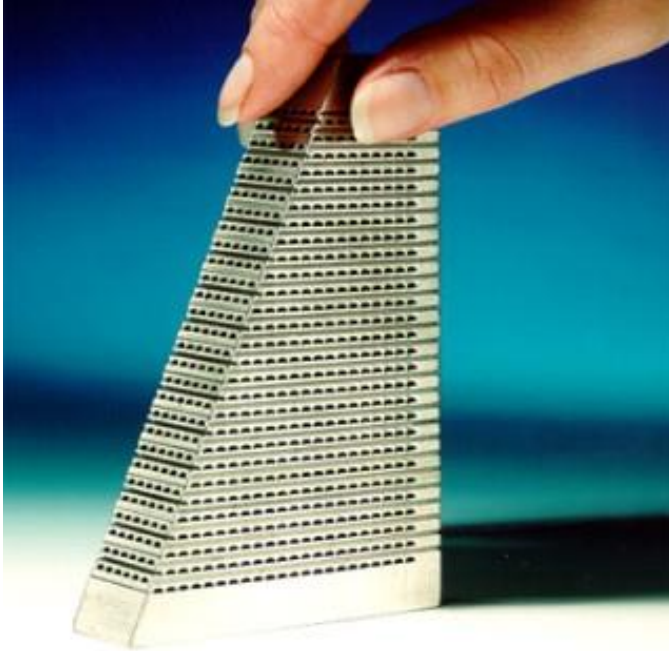
Figure 6-5 PCHE (real section)
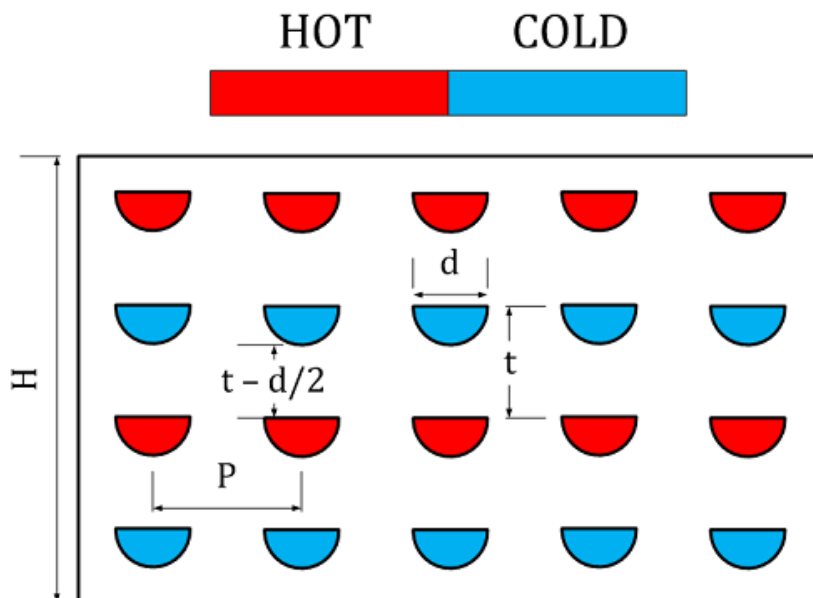
Figure 6-6 PCHE cross-section (conceptual sketch)

The correlations presented in paragraph6.2.1 and 6.2.2 have been used to evaluate the heat exchange coefficient of the carbon dioxide in both cold and hot side of the recuperator(blue and red in Fig. 6-5) and the pressure drop of both sides. Once the overall heat transfer coefficient, U, is found, the necessary heat exchange area and corresponding heat exchanger length would be find out, since one can write:

$$Q = U \times A \times \Delta T_{lm} \tag{6-17}$$

Where,

$$U = \cfrac{1}{\cfrac{1}{h_h} + \cfrac{k}{t} + \cfrac{1}{h_c}} \tag{6-18}$$

where h_h and h_c are the heat transfer coefficients on hot and cold sides respectively and k is the thermal conductivity of the heat exchanger material and t is the plate thickness.

The geometry of the PCHE is evaluated based on the following basic dimensions for both hot and cold sides which has been suggested by Floyd et.al [52] in a study for nuclear applications, featuring the same class of pressures considered in this work:

- Chanel diameter (d) = 2.3 [mm]
- Plate thickness (t) = 2.2 [mm]
- Channel pitch (p) = 4.6 [mm]

When the basic dimensions like d, t, p, the module height (H) and width (W) have been decided, the subroutine RECUPERATOR and COOLER will find the necessary length (L) in order to have the required heat transfer surface to fulfill the needed heat exchange.
In this subroutine the length and the pressure drops of the PCHE are estimated based on the heat exchanger face dimensions and operating conditions. The operating conditions are all known with the exception of pressures on the hot and cold side outlets, which depend on pressure drops.
The related heat transfer area and fluid passage area can be finding by the following formulas:

$$N_{channel,row} = floor(\frac{H - 0.02}{p}) \tag{6-19}$$

$$N_{channel,column} = floor\left(\frac{W - 0.02}{t}\right) \tag{6-20}$$

$$N_{channel,row,Hot} = floor(\frac{N_{channel,row}}{2}) \qquad (6\text{-}21)$$

$$N_{channel,row,Cold} = N_{channel,row} - N_{channel,row,Hot} \qquad (6\text{-}22)$$

$$\dot{m}_{channel,Hot} = \frac{\dot{m}_{Hot}}{(N_{channel,row,Hot} \times N_{channel,column})} \qquad (6\text{-}23)$$

$$\dot{m}_{channel,Cold} = \frac{\dot{m}_{Cold}}{(N_{channel,row,Cold} \times N_{channel,column})} \qquad (6\text{-}24)$$

$$A_{cross,channel} = \frac{\pi \times d^2}{8} \qquad (6\text{-}25)$$

$$d_{hydraulic} = \frac{4 \times \pi \times d^2}{(8 \times (\pi \times \frac{d}{2} + d))} \qquad (6\text{-}26)$$

6.4 Subroutine for the receiver (CSP)

This section is dedicated to the modeling of the solar receiver. Two important aspects will be discussed in this section:
    1) Calculations for thermal balances
    2) Calculations for pressure losses
We remind here that the solar receiver is divided into elementary cells, according to the geometry and the resolution of the solar radiance map available for the PS20 solar plant already discussed at paragraph 5.5.

6.4.1 Thermal model

In each cell, a thermal balance between incident radiation and carbon dioxide flow in the pipe is done. This balance, which yields the stream temperature that enters into the following cell, is based on an overall energy balance on each cell of the pipes.
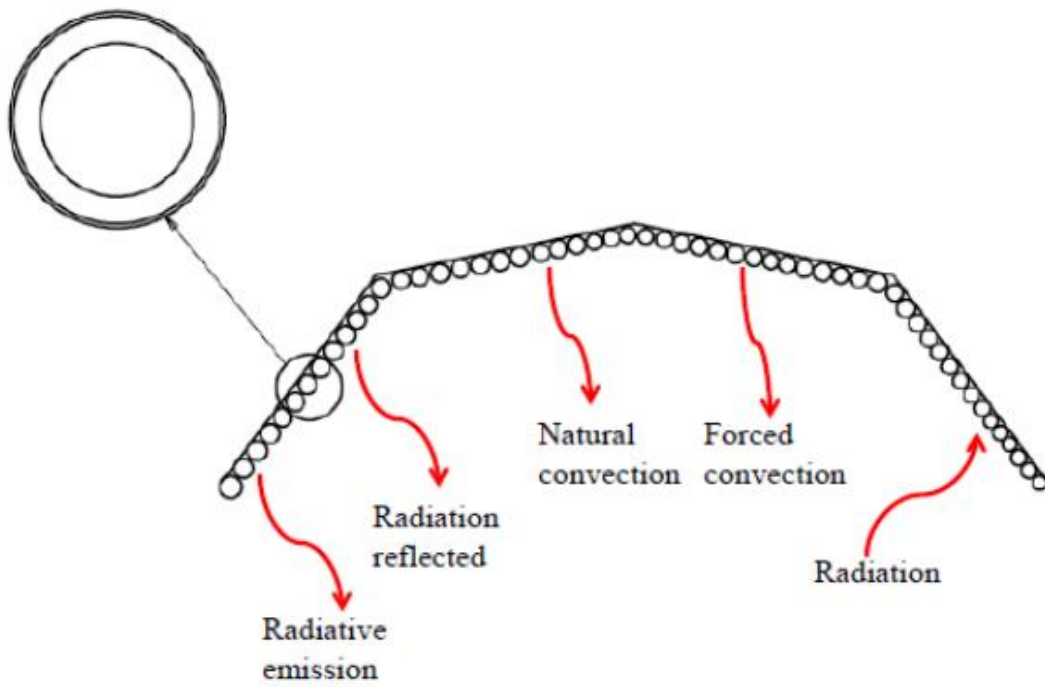
Figure 6-7 Heat transfer component in a cavity receiver
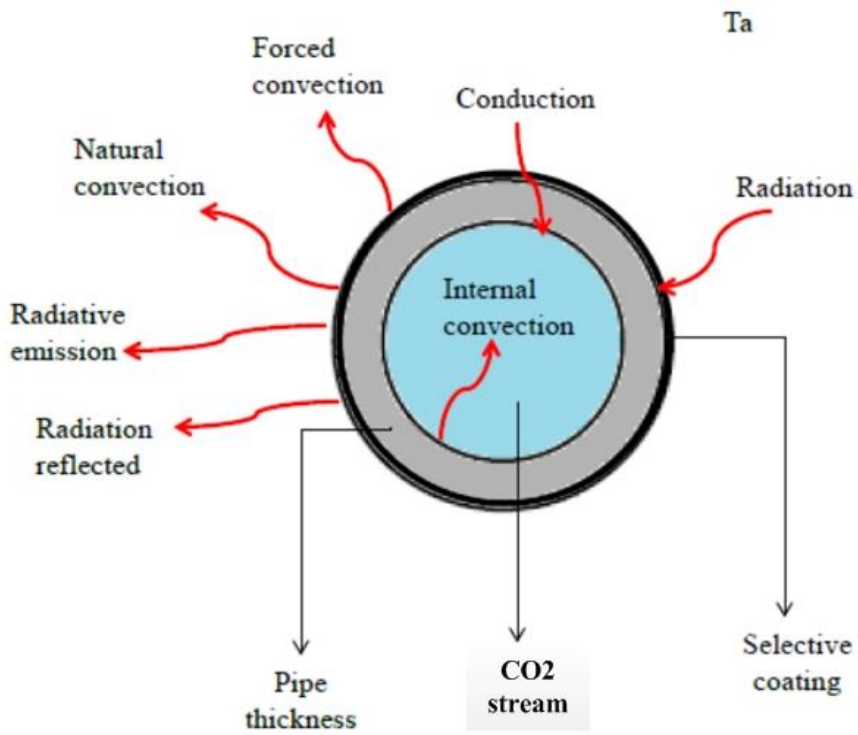
Figure 6-8 Heat transfer balance for a single pipe

The *solar radiation (q_sol)* is concentrated by the heliostat field on the cavity receiver and then absorbed by the selective coating that, for a new and clean pipe, has an *absorptivity* of about 98% [27] or rather a reflectivity value of the selective coating at the solar radiation wavelengths of 2% *(q_sol_refl)*.

Part of the radiation absorbed by the coating is transferred by *conduction (q_cond)* across the metallic wall of the pipe and then transferred to the internal fluid by *internal convection (q_conv_int)*. The higher temperature of the external wall of the pipes with respect to the environment is responsible for three types of thermal losses:

–*Natural convection (q_air_ext_nat)*
–*Forced convection (q_air_ext_forc)*
–*Radiative emission (q_rad_abs_sky)*
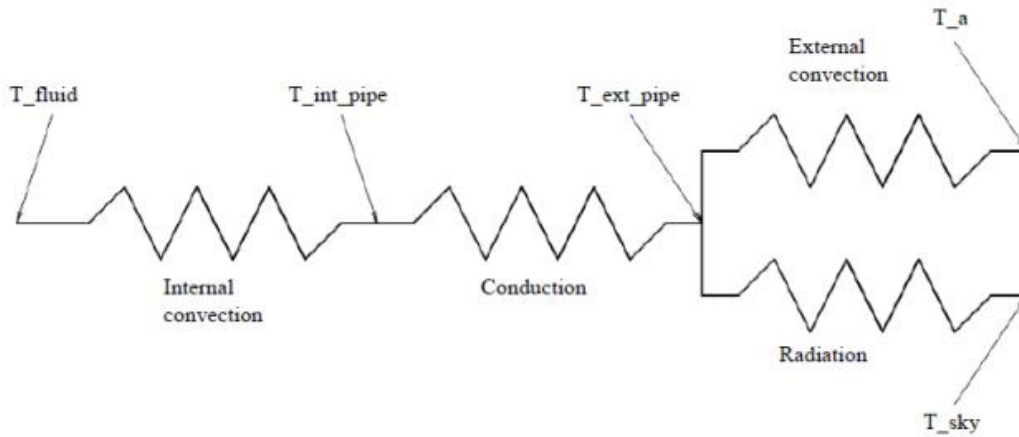
Figure 6-9 Equivalent electric circuit for each element of the pipe

So the energy balance for each element can be written as:

$$q_{conv,int} = q_{cond} \tag{6-27}$$

$$q_{cond} = q_{sol} - q_{conv,ext,nat} - q_{conv,ext,forc} - q_{rad,sky} \\ - q_{reflection} \tag{6-28}$$

According to Fourier's law, convection between working fluid and inner walls of the pipe obeys the following relation:

$$q_{conv,int} = h_{HTF} \times \pi \times d_{int}(T_{fluid} - T_{int,pipe}) \tag{6-29}$$

with:

$$h_{HTF} = \frac{Nu_{d,int}\,k_{fluid}}{d_{int}} \tag{6-30}$$

Where:

- h_{HTF} : convection heat transfer coefficient $[\frac{W}{m^2.K}]$
- d_{int} : Pipe internal diameter [m]
- T_{fluid} : Temperature of working fluid [K]
- $T_{int,pipe}$: Temperature of internal wall of the pipe [K]
- $Nu_{d,int}$: Nusselt number for the internal diameter
- k_{fluid} : Thermal conductivity of the fluid $[\frac{W}{m.K}]$

Starting from the governing equations for quasi-steady axi-symmetric incompressible turbulent flow, Petukhov and Popov (1963) developed analytical expressions for temperature and velocity profiles given the wall temperature and heat flux distribution data. They proposed a systemic approach to evaluating heat transfer coefficient h for circular pipe flow of the fluid with temperature dependent physical properties.

Simplifying the above results with constant physical properties assumption, they came up with the following heat transfer correlation for the Nusselt number, N_u, obtained for Reynolds number Re between 10×10^4 and 5×10^6 and Prandtl number Pr between 0.5 and 2000[53] :

$$Nu = \frac{\left(\frac{\gamma}{8}\right) \times Re \times Pr}{K_1(\gamma) + K_2(Pr) \times \left(\frac{\gamma}{8}\right)^{1/2} \times (Pr^{2/3} - 1)} \tag{6-31}$$

With:

$$\gamma = (1.82 \log(Re) - 1.64)^{-2} \tag{6-32}$$

$$K_1(\gamma) = 1 + 3.4\,\gamma \tag{6-33}$$

$$K_2(Pr) = 11.7 + 1.8\,Pr^{-1/3} \tag{6-34}$$

Where γ is the friction factor.

The correlation used to calculate the heat exchange coefficients for supercritical CO_2 in a vertical pipe upward flow that had been used in this section is the one suggested by Hyung and Kune[25], which considers the effect of fluid properties change due to temperature on Nu_0 which is the one obtained from Petukhov correlation :

$$Nu = Nu_0 \left(\frac{\rho_w}{\rho_b}\right)^{m_1} \left(\frac{\bar{C}_p}{C_{p_b}}\right)^{m_2} \left(\frac{\mu_w}{\mu_b}\right)^{m_3} \left(1 - \frac{10^4 \overline{Gr}_b}{Re_b^{2.7} \overline{Pr}_b^{0.5}}\right)^{m_4} \tag{6-35}$$

Where:

$$m_1 = 4.04 - 3.63 \times 10^{-2} \left(\frac{\dot{q}_{av}}{G}\right) + 1.26 \times 10^{-4} \left(\frac{\dot{q}_{av}}{G}\right)^2 - 1.33 \tag{6-36}$$
$$\times 10^{-7} \left(\frac{\dot{q}_{av}}{G}\right)^3$$

m_2 (6-37)

$$= \begin{cases} for\ \dfrac{T_b}{T_{pc}} < \dfrac{T_w}{T_{pc}} \le 1\ \ or\ \ 1.2 \le \dfrac{T_b}{T_{pc}} \le \dfrac{T_w}{T_{pc}} & : \\[2ex] for\ \dfrac{T_b}{T_{pc}} \le 1 < \dfrac{T_w}{T_{pc}} & : \qquad 0.4 + 0.2 \left(\dfrac{T_w}{T_{pc}}\right. \\[2ex] for\ 1 < \dfrac{T_b}{T_{pc}} < 1.2\ and\ \dfrac{T_b}{T_{pc}} < \dfrac{T_w}{T_{pc}} : 0.4 + 0.2 \left(\dfrac{T_w}{T_{pc}} - 1\right)\left[1 - 5\left(\dfrac{T_b}{T_{pc}} - \right.\right. \end{cases}$$

$$m_3 = 0.62 - 9.02 \times 10^{-2} \left(\frac{\dot{q}_{av}}{G}\right) + 9.51 \times 10^{-4} \left(\frac{\dot{q}_{av}}{G}\right)^2 - 3.22 \tag{6-38}$$
$$\times 10^{-6} \left(\frac{\dot{q}_{av}}{G}\right)^3 + 3.53 \times 10^{-9} \left(\frac{\dot{q}_{av}}{G}\right)^3$$

$$m_4 = -2.44 - 1.54 \times 10^{-2} \left(\frac{\dot{q}_{av}}{G}\right) - 1.11 \times 10^{-4} \left(\frac{\dot{q}_{av}}{G}\right)^2 \tag{6-39}$$
$$for\ 46.57 \le \frac{\dot{q}_{av}}{G} < 151.82$$

$$m_4 = -13.4 - 1.03 \times 10^{-1} \left(\frac{\dot{q}_{av}}{G}\right) - 2.08 \times 10^{-4} \left(\frac{\dot{q}_{av}}{G}\right)^2 \tag{6-40}$$
$$for\ 151.82 \le \frac{\dot{q}_{av}}{G} < 212.4$$

$$m_4 = -13.41 - 1.06 \times 10^{-1} \left(\frac{\dot{q}_{av}}{G}\right) - 1.8 \times 10^{-4} \left(\frac{\dot{q}_{av}}{G}\right)^2 \tag{6-41}$$

$$for\ 212.4 \leq \frac{\dot{q}_{av}}{G} < 334.88$$

Where $\dot{q}_{av}$ is the axially average pipes wall heat flux $[W/m^2]$, G is the mass velocicty of CO_2 inside the pipe$[kg/s.m^2]$,

It is worth to note that since the heat flux considered in Hyung and Kune correlations is different than our case, in some hot spot of the receiver the Nu number evaluated from equation 5-35 will be an order of magnitude higher than Nu_0, so that the correlations is evidently out of range or too much extrapolated. Therefore we have considered as a 'safety' numerical rule that whenever the Hyung and Kune equation result rises more than 30% the Nu_0, the code will consider Nu_0, as the corresponding Nu for that special element. The choice is conservative, since we do not consider too high heat exchange coefficients and we consequently avoid under-estimating the hot spot temperatures in the pipes.

The output of the routine is the temperature map along all pipes in the receiver, as well as the pressure drop along the receiver. An example of this temperature map is given in Figure 7-6 and Table 7-7.

6.4.2 Pressure drop model

For carbon dioxide pressure drop in a vertical pipe moving upward, considering the effect of change in density, the correlation suggested by Todreas and Kazimi has been used[50], resulting in the following expression:

$$P_{out} = P_{in} - \left(\frac{\dot{m}}{A}\right)^2 \left(\frac{1}{\rho_{out}} - \frac{1}{\rho_{in}}\right) - \frac{f}{2d_e\rho_{avg}}\left(\frac{\dot{m}}{A}\right)^2 \Delta z - \rho_{avg}\ g\ \Delta z \qquad (6\text{-}42)$$

Where ρ_{avg} is the density evaluated in average temperature between inlet and outlet temperature of each element and d_{eq} is the equivalent hydraulic diameter.
There should be also taken into account the entrance and the exit loss, which both can be evaluated from:

$$\Delta p = C\rho \frac{V^2}{2} \qquad (6\text{-}43)$$

where C is the form loss coefficient that was taken to be 0.5 for the entrance loss and 1.0 for the exit loss [50], $\rho$is the local fluid density (kg/m^3) and v is the local fluid velocity (m/s).

6.5 Subroutine for mass flow rate (MASSOFF)

Subroutine MASSOFF is in charge of finding the proper CO_2 mass flow rate in order to meet the desire net power output. This function will take as input, the desired power, compressor inlet pressure and temperature, compressor pressure ratio and isentropic efficiency, turbine inlet temperature, turbine isentropic efficiency and pressure drop of all the piping system and all the components of the system; based on that it will give as the output the necessary mass flow rate of CO_2.

The logic of this subroutine is based on iteratively calling subroutines COMPRESS and TURB, feeding them with proper data as it will described in the following in order to have the net power equal to the one requested by the user.

MASSOFF will call COMPRESS with the following input:
–   Compressor inlet temperature (T_1)
–   Compressor inlet pressure (P_1)
–   Compressor outlet pressure which is equal to $\beta \times P_1 + \Delta P_{cycle}$
–   Compressor isentropic efficiency

And will calculate the needed compressor power $W_{compressor}$ (J/kg).
Later the routine will call TURB with following input data:
–   Turbine inlet temperature (T_4)
–   Turbine inlet pressure which is equal to $\beta \times P_1 + \Delta P_{PCHE,cold} + \Delta P_{CSP} + \Delta P_{pipinguptoTurbine}$
–   Turbine outlet pressure which is equal to $P_1 + \Delta P_{PCHE,hot} + \Delta P_{cooler} + \Delta P_{fromTurbinetocompressorinlet}$
–   Turbine isentropic efficiency

In order to find out the available power that can be produced $W_{turbine}$ (J/kg). At the end it will calculate the necessary mass flow rate of the plant based on the following equation:

$$\dot{m}_{CO_2} = \frac{P_{net,requested}}{W_{turbine} - W_{compressor}} \tag{6-44}$$

6.6 Solving procedure

The loop will start with estimation of the total mass flow rate of CO_2 based on a guess on turbine inlet temperature and also the pressure drop of all the component of the cycle and the pressure drop among all the connecting pipes. The subroutine

MASSOFF will estimate the needed mass flow rate in order to have the desired net power output as explained before.

Then the calculation will start from node 1 and based on inlet pressure, inlet temperature, isentropic efficiency and needed pressure drop, the subroutine COMPRES will calculate the temperature and pressure of node 2. At this moment since the user had already decided the temperature of node 3 as an input data, the program will jump to the receiver and delay the analysis of PCHE till the moment that it finishes the analysis of turbine, so that it can know about the hot flow temperature entering PCHE.

Long story short, the program will call the subroutine CSP in order to find out the effect of solar power input on CO_2 stream. The function will give back the pressure and temperature of sCO_2 exiting the boiler and going toward the turbine.

The procedure will go on based on the real turbine inlet temperature calculated by the CSP function and also the real pressure since in each subroutine, the pressure drop will also be calculated and updated upon the primary pressure drop assumptions. Running the subroutine TURB will result in finding the temperature and pressure of node 5.

At this moment the cold stream input and output temperature of PCHE, the hot stream input and also the inlet pressure of both sides will be known, So the subroutine PCHE can be called by the main program and it will calculate the pressure drop of both cold and hot stream, the outlet temperature of the hot stream and also the needed heat exchanger length in order to have the desired cold flow outlet temperature which was one of the input data.

Here the last component of the cycle named COOLER will be called in order to close the chain and find the appropriate heat exchanger length in order to come up with known compressor inlet pressure and temperature.

In the main code, all these components are placed in two conditional loops by means of "while" command in MATLAB and inner loop will have correction on desired power output and the outer one will correct the total pressure drop of the cycle and after completing each loop, the subroutine MASSOFF will be feed by new pressure drops of pipes and components and also the corrected turbine inlet temperature in order to calculate the new mass flow rate of CO_2.

Whenever the difference between the loop number (K) and loop number (K+1) are less than a defined tolerance, the calculation will end and the software will give back all nodes temperature and pressure and the thermal efficiency of the system as output result.

The described procedure can be seen in logic flowchart of the program presented in Figure 6-9.
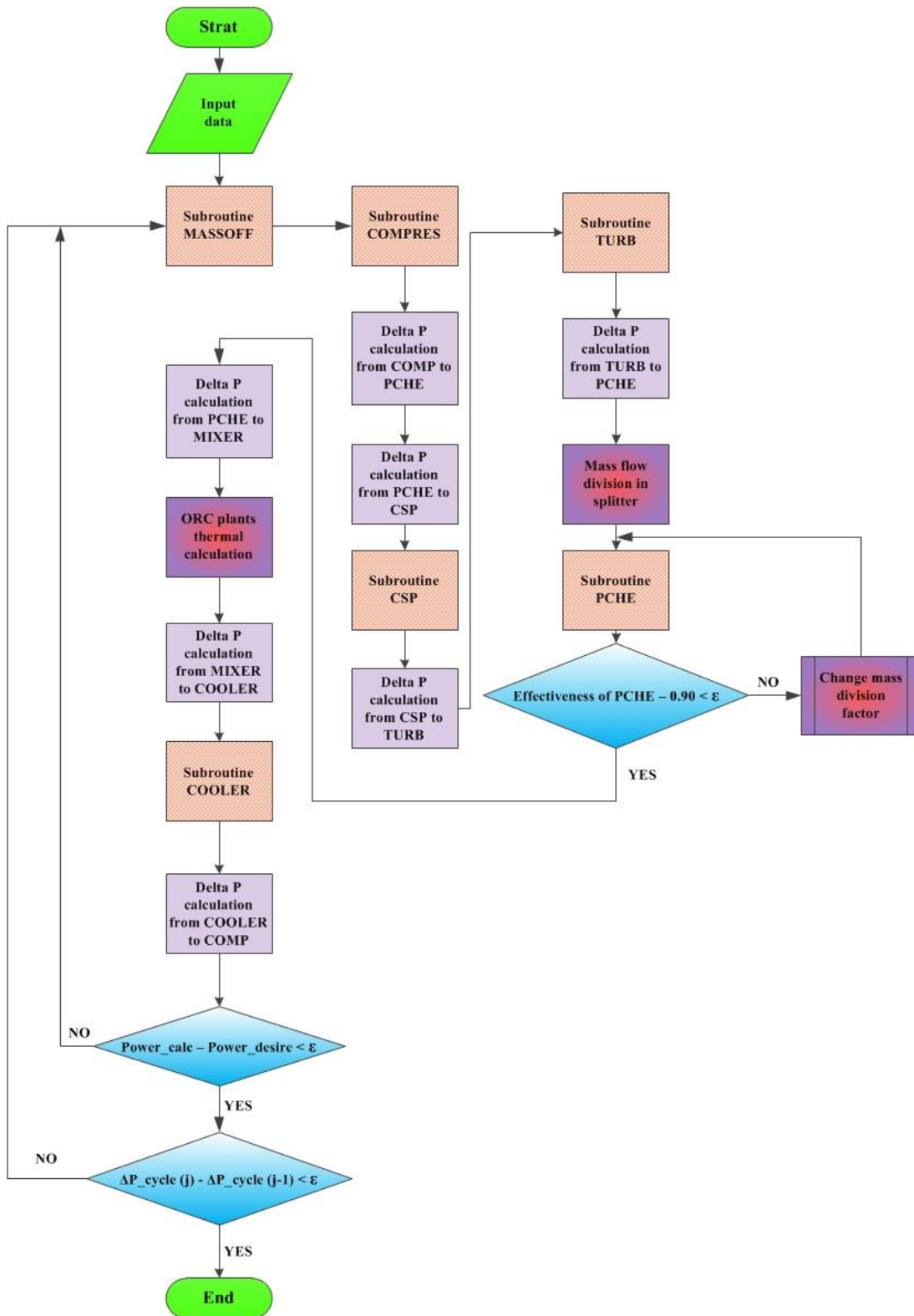
Figure6-10 Logic of solving procedure in the main code in on-design simulation.

In the off-design model, as it will be well explained in section 7-3, the solving procedure will be based on the fact that some of the results of the on-design program, like mass flow rate of the carbon dioxide, size of the heat exchangers, and the mass division factor in splitter will be considered as the input, since these parameters are not changeable anymore once the plant is built and the components are bought and installed. So the model will consider the mentioned parameters as constant values and will find out the effect of environmental changes like change in radiation map (different hours of the year), the air temperature, wind velocity etc.

7RESULTS AND DISCUSSION

7.1 On-design model

Before starting the program, the user must define several input data. These data and their default values are listed in the Tables 7-1 to 7-6.

Table7-1Environmental inputs

	Default value
Sky temperature [K]	285
Environment temperature [K]	300
Wind velocity [m/s]	2
Environmental pressure [bar]	1

One of the most critical nodes in the plant is the input temperature and pressure of the compressor, since it should stay always above the critical temperature, therefore this point pressure and temperature, P1 and T_1respectively, has been considered as an input parameter as it can be seen in Table 7-2.

Table7-2Powerblock thermodynamic inputs

	Default value
Desired power output [kW]	14000
Compressor inlet pressure(P_1) [bar]	75
Compressor pressure ratio [-]	5
Compressor inlet temperature(T_1) [K]	320
Degree of preheating(T_3) [K]	650
Compressor isentropic efficiency [-]	0.91
Turbine isentropic efficiency [-]	0.93
ORC thermal efficiency [-]	0.21
Cooling water inlet temperature [K]	310

Cooling water inlet pressure [bar]	6

The length and the size of the pipes used in the plants has been found and calculated based on the work of Floyd et al.[52] and available data in[27] as it can be seen in the next table:

Table 7-3 Piping sizing and properties input (stainless steel 316L)[52].

From – To	Length [m]	Internal diameter [m]	Absolute roughness [m]
Compressor – PCHE	25	0.15	5.47×10^{-5}
PCHE – Boiler	135	0.15	5.47×10^{-5}
Boiler – Turbine	110	0.15	5.47×10^{-5}
Turbine – Splitter	25	0.15	5.47×10^{-5}
Splitter – PCHE	3	0.1	5.47×10^{-5}
PCHE – Mixer	3	0.1	5.47×10^{-5}
Splitter – Mixer	40	0.1	5.47×10^{-5}
Mixer – Cooler	3	0.15	5.47×10^{-5}
Cooler – Compressor	25	0.15	5.47×10^{-5}

And for the two heat exchangers we defined:

Table7-4Subrotuine PCHE input data

	Definedvalue
No. of units	1
Unit width [m]	0.6
Unit height [m]	0.6
Hot channeldiameter(d) [m]	0.023
Coldchanneldiameter(d) [m]	0.023
Channel pitch(p) [m]	0.046
Platethickness(t) [m]	0.022

Table7-5SubrotuineCOOLERs input data

	Definedvalue
No. of units	1
Unit width(W) [m]	0.9
Unit height(H) [m]	0.9
Hot channeldiameter(d) [m]	0.027
Coldchanneldiameter(d) [m]	0.027

Channel pitch(p) [m]	0.054
Platethickness(t) [m]	0.025

And finally for the receiver modules and pipes, the geometry, as already said, follows the PS10 boiler design.

Therefore, the height of the boiler and the number of the modules have been considered to be equal to the one from PS10, but due to very high pressure application, the pipes size and material should be modified as mentioned in section 5.5. The input data for the subroutine CSP are listed in Table 7-6.

Table7-6Receiver input data[27, 44].

	Defined value
Pipes internal diameter [m]	0.0081
Pipes external diameter [m]	0.0145
Pipes roughness [m]	5.47×10^{-5}
Pipes absorptivity [-]	0.98
Pipes conductivity [$W/m.K$]	3.46
Number of modules [-]	4
Modules height [-]	12.963155
Module height to width ratio [-]	2.2388
Module columns [-]	11
Module rows [-]	44

For high pressure cycles such as the sCO_2 cycle, manufacturing and material considerations place an upper limit on pipe diameters. The required thickness,t_{min}, for a pipe at pressure P, with external diameter d_{ext}, can be obtained from the next equation according to section RB3632.12 of the[54] :

$$t_{min} = \frac{P \times d_{ext}}{2(S_m - 0.4P)} \qquad (7\text{-}1)$$

The material admissible stress, S_m , is dependent on temperature and so the 'worst-case' pipe in the sCO_2 cycle, in terms manufacturing, would be those located in the center of the receiver which are at both the high temperature (1250 K) and pressure (approximately 40 MPa). High temperature sCO_2may require stainless steels to be used and, for 316 stainless steel, the RCC-MR code lists the admissible stress at 1250K to be 105MPa, which corresponds to a thickness of minimum 0.0018m for this worst-case pipe. This thickness with the considered internal diameter for the pipes wills results to a minimum required external diameter of 0.0118m which for the sake of safety had been considered to be 0.0145m.

But as it was said in paragraph 5.5 the radiation map is one of the key components of the model as it contains all the information about the heliostat field that has not been developed in this work. Therefore an appropriate radiation map is necessary to obtain realistic results of the plant. The map used here is a simple matrix of 44×44 cells (11 columns × 4 panels) that contains the average value of heat flux on the absorbing surface. In order to have realistic results, real radiation maps have been used thanks to data from ABENGOA SOLAR[27]. These maps have been created in EXCEL first, having a graphical vision of the surface, and then exported to MATLAB.

The on-design map used was obtained on the 21st March 2007 at 12:00 when the nominal conditions of the PS10 boiler were reached:

- Irradiance: $981 \ W/m^2$.
- Atmospheric transmittance: 95%.
- Solar azimuth position: $00.0°$.
- Sun elevation: $52.2°$.
- Net power onto absorber panels: 51953.86 kW.
- Peak irradiance on receiver surface: $644 W/m^2$.
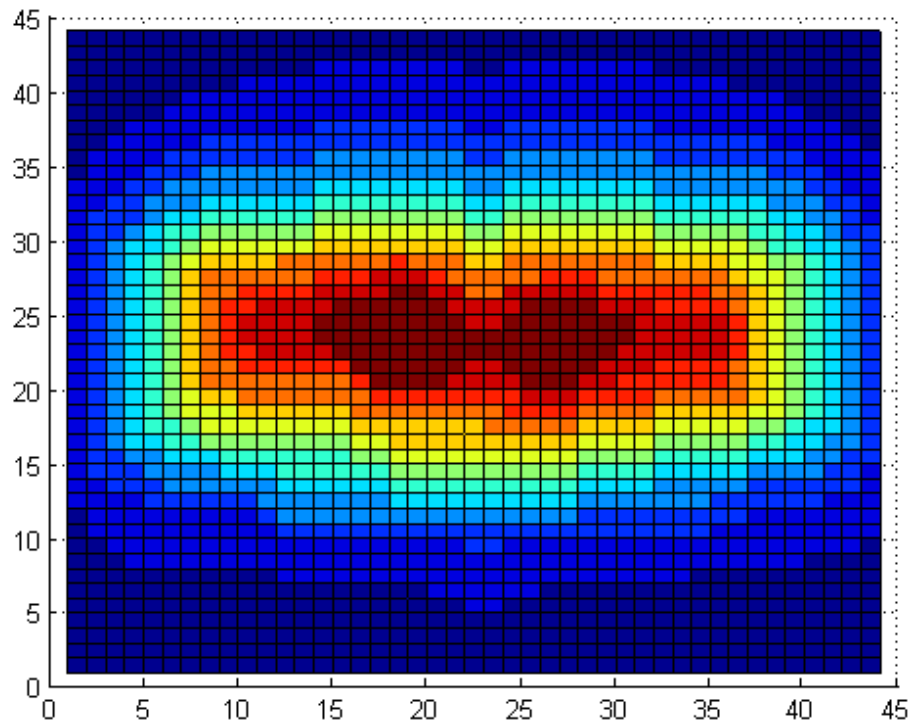
Figure 7-1 On-design radiation map

The developed code has the ability to load other maps for different days or hours, provided that they consists of a 44×44 cells and solar flux values are expressed inkW/m^2.

7.2 On-design results

7.2.1 Sensitivity analysis on degree of preheating for receiver

As it can be seen in Figure 7-2, for a fixed turbine inlet temperature, the thermal efficiency of the cycle will rise as we preheat more the CO_2 before entering the receiver. For the case of $T_{in\_receiver} = 650k$ the maximum efficiency will occur in compressor pressure ratio near 13.
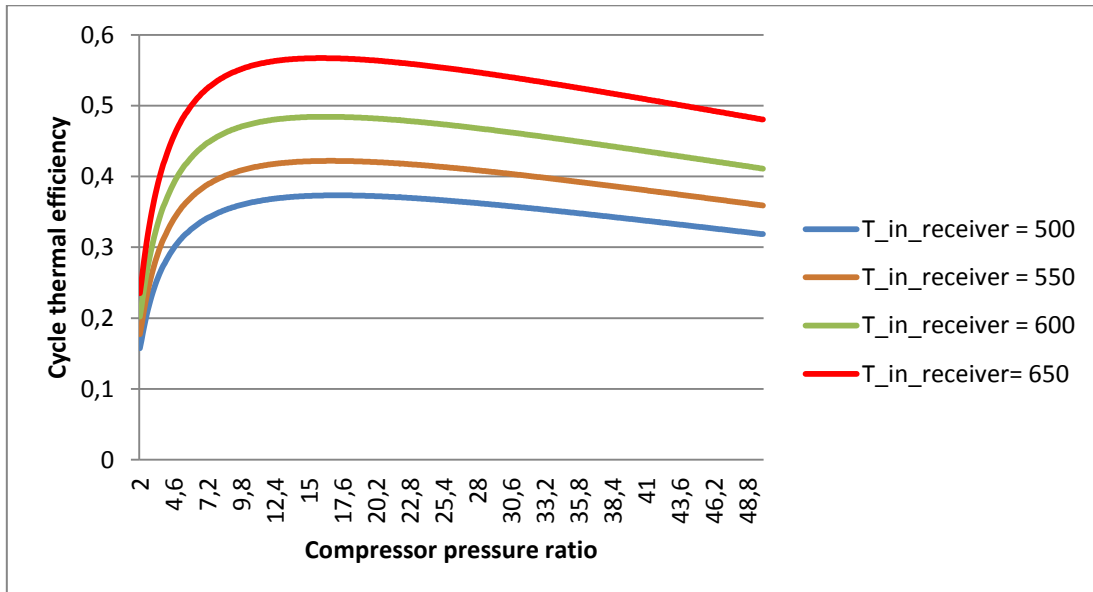
Figure 7-2 η-β diagram with different $T_{inlet\_receiver}[K]$ ($T_{inlet\_turbine} = 950K$)

7.2.2 Sensitivity analysis on Turbine inlet temperature

Figure 7-3 demonstrates the thermal efficiency of the cycle for different pressure ratio and different values of turbine inlet temperature (TIT) while receiver inlet temperature is fixed at $650\ K$. It can be seen that for smaller TIT, the efficiency will show a higher peak in lower compression ratios. But for very high pressure ratios the efficiency of the plant with higher TIT will be higher than for the plants with lower TIT. Of course this happened due to the fixed $T_{inlet\_receiver}$ that had been considered for this case. For smaller pressure ratios, since the gain in terms of efficiency due to

the increase in turbine power output (by increasing TIT) is less than the loss due to introducing more solar power input (bigger receiver), the efficiency will decrease by increasing TIT, but it is worth to note that for very high pressure ratios, since the lines of the constant pressure in T-S diagram will get more open, the share of increase in efficiency due to increase of turbine output power will rise and so that the efficiency line corresponding to higher TIT will go higher than the ones with less TIT.
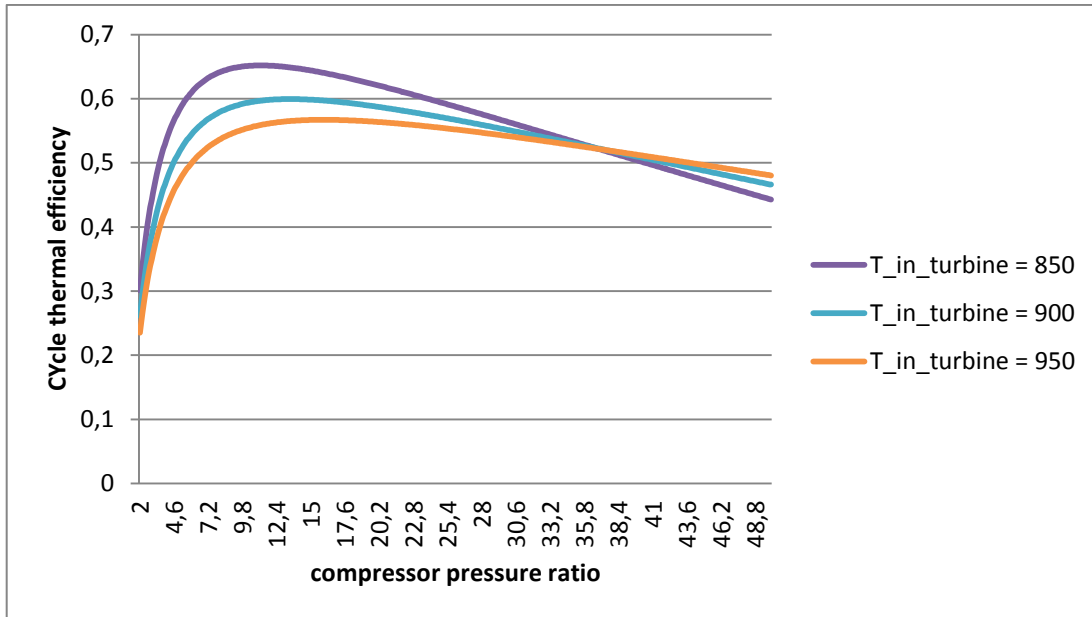
Figure 7-3η-β diagram with different $T_{inlet\_turbine}[K]$ ($T_{inlet\_receiver} = 650K$)

Figure 7-2 shows that ideally, for a fixed TIT, the best choice would be to preheat the CO_2 as much as possible (smaller receiver), but one should keep in mind the constraint due to the turbine outlet temperature since it should remain more than receiver inlet temperature with a proper ΔT in order to make the preheating possible and prevent the need of a very large heat transfer area.

In this study, as shown in Table 7-1, the $T_{inlet\_receiver}$ had been assumed to 650 K and since the geometry of the receiver is fixed as the one from PS10, the design required power output had been considered equal to 14 MW in order to respect the material constraint for the maximum allowed pipe temperature occurring in receiver which is equal to 1250 K in this case.
Since the turbine inlet pressure is equal to 75 bar, the compressor pressure ratio had been chosen equal to 5 in order to limit the very high pressures in the receiver pipes (75×x5 already gives 375 bar) and the need to use special materials with too high thickness.

7.2.3 Sensitivity analysis on compressor inlet pressure

Figure 7-4 demonstrates the thermal efficiency of the cycle with respect to compressor pressure ratio (β) for three different compressor inlet pressure (P_1) while the receiver inlet and outlet temperature kept constant. As it can be seen, for a specificβ, the efficiency rises as P_1 goes higher. The reason for this behaviour can be explained by looking into Figure 7-5. It is visible from the graph that for a constant β increasing P_1 will lead to higher turbine work production and lower compressor work consumption. Although the required solar input power will also rise, which will causes a decrease in efficiency, the gain in net power of the cycle will be slightly more than the increase in required solar input power.
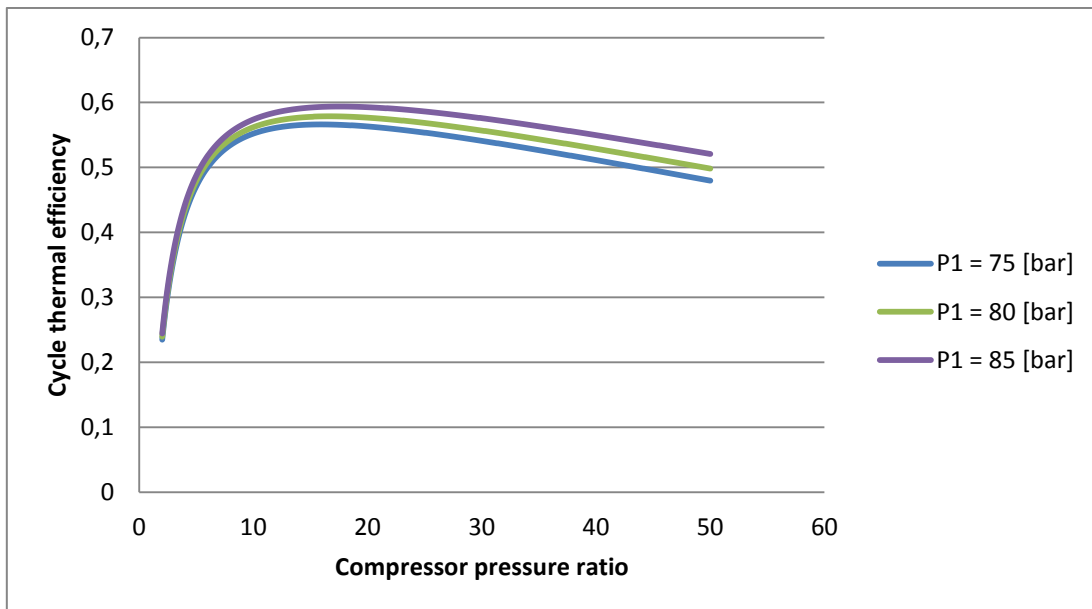
Figure 7-4η-β diagram with different $p_{inlet\_compressor}$ ($T_{inlet\_receiver} = 650K$ and $T_{inlet\_turbine} = 950K$)
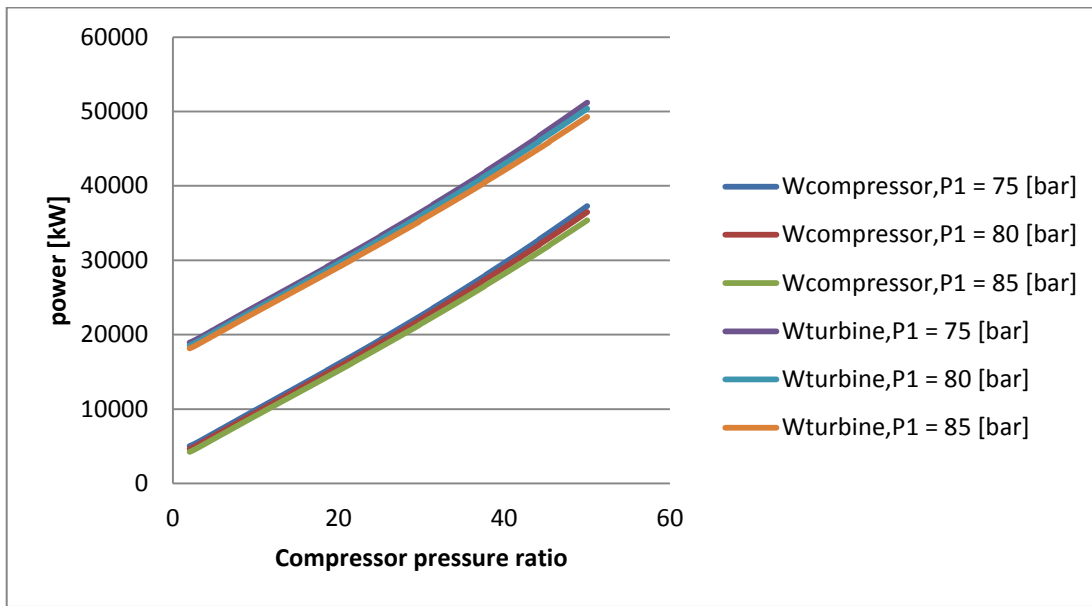
Figure 7-5 Net power ($W_{compressor}$, $W_{turbine}$)-β diagram with different $p_{inlet\_compressor}$ ($T_{inlet\_receiver} = 650K$ and $T_{inlet\_turbine} = 950K$)

7.2.4 Receiver analysis

As it can be seen in Figure 7-1, the radiation coming from heliostat field is concentrated in the middle section of the middle pipes of the receiver. Taking into account the losses explained in section 6.3.1 and the equation 6-28, the result of finite element analysis on boiler has shown that the upper cells of the middle pipes will lose more power than they receive from the sun. The most responsible phenomena for this high loss is radiation since in the upper part of the receiver the temperature is very high and the income power from sun is relatively low. The receiver total temperature distribution is demonstrated in Figure 7-6.
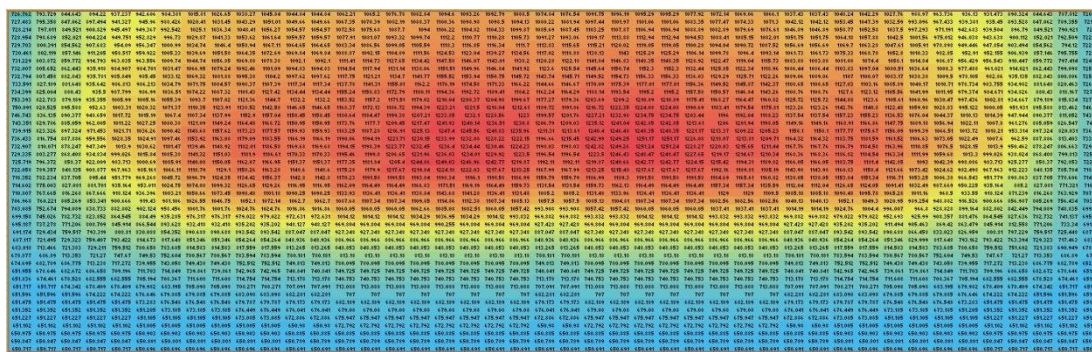
Figure 7-6Reciever temperature distribution.

For the sake of better understanding the temperature distribution of module number 2 is also shown individually in Table 7-7. The numbers are Kelvin.
As it can be seen for example the cell group in column 4 of module 2, column 15 of receiver, will be first heated up from 650.69 [K] to 1199.902[K] and then when the radiation losses effect becomes more powerful than income radiation, the pipe will cool down to1065.198[K] .

For the mentioned column, Table 7-8 shows the power income and losses in each cell and also the power transferred to/from the carbon dioxide.

Table 7-7 Temperature distribution of module number 2 [K]

|										
1044.843	1044.843	1062.212	1065.198	1076.783	1082.844	1094.604	1093.257	1092.788	1088.498	1074.844
1049.663	1049.663	1067.349	1070.39	1082.191	1088.369	1100.356	1098.983	1098.505	1094.131	1080.217
1054.57	1054.57	1072.581	1075.679	1087.703	1094	1106.222	1104.821	1104.333	1099.874	1085.689
1059.566	1059.566	1077.911	1081.068	1093.321	1099.741	1112.203	1110.774	1110.277	1105.73	1091.269
1064.654	1064.654	1083.34	1086.557	1099.049	1105.594	1118.303	1116.846	1116.339	1111.701	1113.834
1069.836	1069.836	1088.874	1092.153	1104.888	1111.562	1124.527	1123.04	1139.269	1134.563	1117.022
1092.1	1092.1	1111.406	1114.731	1127.65	1134.422	1147.581	1146.071	1143.011	1138.2	1120.279
1094.833	1094.833	1114.542	1117.938	1131.136	1138.057	1151.508	1149.964	1146.836	1141.918	1123.605
1097.621	1097.621	1117.745	1121.214	1134.698	1141.771	1155.523	1153.945	1150.746	1145.719	1143.736
1117.339	1117.339	1137.782	1141.307	1155.011	1162.203	1176.188	1174.583	1171.329	1166.217	1144.657
1124.442	1124.442	1155.244	1148.832	1162.786	1170.111	1194.358	1192.723	1189.408	1184.199	1162.243
1132.202	1132.202	1153.521	1157.199	1171.51	1179.024	1210.036	1208.366	1204.982	1199.667	1177.268
1146.645	1146.645	1168.374	1172.125	1186.72	1194.386	1223.208	1221.501	1218.042	1212.608	1189.72
1158.452	1148.452	1170.636	1174.467	1199.377	1207.211	1233.853	1232.105	1228.562	1222.998	1199.572
1150.949	1150.949	1173.758	1177.699	1209.454	1217.472	1241.934	1240.14	1236.506	1230.8	1206.786
1159.927	1159.927	1183.245	1187.275	1216.914	1225.134	1245.401	1245.559	1241.826	1235.965	1211.311
1166.187	1166.187	1190.06	1194.188	1221.707	1230.147	1246.989	1232.082	1228.219	1222.154	1196.659
1169.676	1169.676	1194.152	1198.386	1223.768	1232.446	1247.397	1234.436	1230.464	1224.229	1198.031
1170.329	1170.329	1195.456	1199.805	1226.645	1241.957	1248.025	1234.006	1229.916	1223.497	1196.543
1151.372	1151.372	1177.346	1199.844	1225.403	1244.863	1249.032	1246.963	1242.771	1219.871	1192.108
1148.603	1148.603	1175.28	1199.902	1217.668	1219.843	1224.18	1222.028	1217.668	1213.25	1167.993
1142.804	1142.804	1170.227	1191.576	1191.576	1193.836	1198.342	1196.105	1191.576	1186.986	1159.794
1116.954	1116.954	1162.094	1164.489	1164.489	1166.833	1171.509	1169.188	1164.489	1159.728	1131.544
1090.247	1090.247	1133.927	1136.407	1136.407	1138.836	1143.681	1141.276	1136.407	1131.476	1085.197
1062.7	1062.7	1087.675	1107.34	1107.34	1109.852	1114.864	1112.376	1107.34	1085.126	1057.495
1016.86	1016.86	1060.049	1060.049	1060.049	1062.657	1085.078	1082.508	1060.049	1057.422	993.9079
972.6309	972.6309	1014.117	1014.117	1014.117	1034.291	1036.954	1034.291	1014.117	993.8318	969.882
948.127	948.127	969.8043	969.8043	969.8043	969.8043	990.2549	969.8043	969.8043	969.8043	927.4275
887.0474	887.0474	927.3477	927.3477	927.3477	927.3477	927.3477	927.3477	927.3477	927.3477	887.0474
848.9363	848.9363	886.9657	886.9657	886.9657	886.9657	886.9657	886.9657	886.9657	886.9657	848.9363
813.265	813.265	848.8528	848.8528	848.8528	848.8528	848.8528	848.8528	848.8528	848.8528	813.265
780.1813	780.1813	813.1799	813.1799	813.1799	813.1799	813.1799	813.1799	813.1799	813.1799	780.1813
749.8125	749.8125	780.0947	780.0947	780.0947	780.0947	780.0947	780.0947	780.0947	780.0947	749.8125
740.8413	740.8413	749.7246	749.7246	749.7246	749.7246	749.7246	749.7246	749.7246	749.7246	740.8413
713.1783	713.1783	740.7526	740.7526	740.7526	740.7526	740.7526	740.7526	740.7526	740.7526	713.1783
707.0906	707.0906	713.0884	713.0884	713.0884	713.0884	713.0884	713.0884	713.0884	713.0884	707.0906
682.2811	682.2811	706.9999	706.9999	706.9999	706.9999	706.9999	706.9999	706.9999	706.9999	682.2811
679.1725	679.1725	682.1893	682.1893	682.1893	682.1893	682.1893	682.1893	682.1893	682.1893	679.1725
676.0406	676.0406	679.08	679.08	679.08	679.08	679.08	679.08	679.08	679.08	676.0406
672.8855	672.8855	675.9474	675.9474	675.9474	675.9474	675.9474	675.9474	675.9474	675.9474	672.8855
650.9799	650.9799	672.7917	672.7917	672.7917	672.7917	672.7917	672.7917	672.7917	672.7917	650.9799
650.8848	650.8848	650.8848	650.8848	650.8848	650.8848	650.8848	650.8848	650.8848	650.8848	650.8848
650.789	650.789	650.789	650.789	650.789	650.789	650.789	650.789	650.789	650.789	650.789
650.6909	650.6909	650.6909	650.6909	650.6909	650.6909	650.6909	650.6909	650.6909	650.6909	650.6909

As it can be seen in Table 7-8, in the final cells on the top of the pipes of the boiler for this specific column the power transferred to CO_2 is negative. As already has

been explained, the negative sign means that the heat has been rejected from CO_2 and has been transferred to the environment.

But it should be kept in mind that this happens for this specific radiation map on the 21st March 2007 at 12:00, and the same group of pipes in this column may heat up the CO_2 completely till it passes the last cell when another map should be applied, as it happens for the column 1 in this simulation.

Table 7-8 Energy balance for a column in the receiver [kW]

Cell number	q_{sol}	$q_{rad,sky}$	$q_{reflection}$	$q_{conv,ext,nat}$	$q_{conv,ext,forc}$	$q_{conv,int}$
44	0.107696	0.253357	9.28E-06	0.127255	0.026566	-0.29949
43	0.107696	0.257514	9.28E-06	0.1283	0.026718	-0.30485
42	0.107696	0.26179	9.28E-06	0.129366	0.026874	-0.31034
41	0.107696	0.266192	9.28E-06	0.130452	0.027032	-0.31599
40	0.107696	0.270723	9.28E-06	0.131559	0.027192	-0.32179
39	0.107696	0.275389	9.28E-06	0.132687	0.027356	-0.32775
38	0.323087	0.298845	2.78E-05	0.138192	0.028147	-0.14213
37	0.323087	0.30104	2.78E-05	0.138694	0.028219	-0.14489
36	0.323087	0.303288	2.78E-05	0.139206	0.028291	-0.14773
35	0.538478	0.325363	4.64E-05	0.144114	0.028987	0.039968
34	0.75387	0.345308	6.50E-05	0.148379	0.029586	0.230531
33	0.75387	0.341412	6.50E-05	0.147558	0.029471	0.235364
32	0.969261	0.358596	8.35E-05	0.151139	0.029971	0.429472
31	1.184652	0.372884	0.000102	0.154039	0.030373	0.627254
30	1.184652	0.361781	0.000102	0.151792	0.030062	0.640916
29	1.400044	0.372364	0.000121	0.153935	0.030359	0.843266
28	1.615435	0.379477	0.000139	0.155355	0.030555	1.049909
27	1.830827	0.382898	0.000158	0.156032	0.030648	1.26109
26	2.046218	0.382469	0.000176	0.155948	0.030637	1.476988
25	2.046218	0.35612	0.000176	0.15063	0.0299	1.509391
24	2.261609	0.35137	0.000195	0.149646	0.029763	1.730635
23	2.692392	0.364367	0.000232	0.152319	0.030135	2.145339
22	2.692392	0.327632	0.000232	0.144607	0.029057	2.190864
21	2.692392	0.292745	0.000232	0.136786	0.027946	2.234683
20	2.692392	0.259851	0.000232	0.128884	0.026804	2.276622
19	2.477001	0.213338	0.000213	0.116618	0.024988	2.121843
18	2.261609	0.174577	0.000195	0.105122	0.023234	1.958481
17	2.046218	0.142549	0.000176	0.094429	0.02155	1.787513
16	1.830827	0.116287	0.000158	0.084562	0.019945	1.609875
15	1.615435	0.094897	0.000139	0.075526	0.018426	1.426447
14	1.400044	0.077578	0.000121	0.067316	0.016997	1.238031
13	1.184652	0.063625	0.000102	0.059915	0.015664	1.045346
12	0.969261	0.052431	8.35E-05	0.053298	0.01443	0.849019
11	0.75387	0.043485	6.50E-05	0.047432	0.013297	0.649591
10	0.75387	0.041029	6.50E-05	0.04571	0.012957	0.654109
9	0.538478	0.034194	4.64E-05	0.040608	0.011925	0.451706
8	0.538478	0.032759	4.64E-05	0.039471	0.01169	0.454512
7	0.323087	0.027511	2.78E-05	0.035078	0.010761	0.249708
6	0.323087	0.026831	2.78E-05	0.034478	0.010632	0.251118
5	0.323087	0.02616	2.78E-05	0.03388	0.010502	0.252517
4	0.323087	0.0255	2.78E-05	0.033283	0.010372	0.253904
3	0.107696	0.021584	9.28E-06	0.029574	0.009547	0.046982
2	0.107696	0.021476	9.28E-06	0.029467	0.009523	0.04722
1	0.107696	0.021368	9.28E-06	0.02936	0.009499	0.04746

7.2.5 Outputs of the on-design program

Considering the inputs represented in section 7-1, the result of the on-design program will be as follow:

Table7-9Plant's pressure and temperature report ($\dot{m}_{CO_2} = 70.6\ kg/s$)

Node	Pressure [bar]	Temperature [K]
Compressor inlet	75.00	320.0
Compressor outlet	398.29	461.1
PCHE cold side inlet	397.91	461.1
Receiver inlet	393.03	650.0
Turbine inlet	386.95	1039.9
Turbine outlet	86.66	796.5
PCHE hot side inlet	83.16	796.5
Cooler inlet	77.15	494.7

As it can be seen in the table, the temperature of compressor outlet and PCHE cold side inlet are the same, as it is also for the turbine outlet and PCHE hot side inlet. This is due to the fact that it had been assumed that they're going to be no temperature decrease along the piping of the system and all the pipes had been perfectly isolated.

Table 7-10 Pressure drop of different parts of the plant

	Pressure drop [bar]
Cold side of PCHE	1.35
Hot side of PCHE	4.39
Receiver	1.24
Hot side of cooler	1.16
From compressor to PCHE	0.38
From PCHE to receiver	3.49
From receiver to turbine	4.84
From turbine to splitter	3.50
From PCHE to mixer	1.35
From mixer to cooler	0.27
Cooler to compressor	0.96

Table7-11Plant energy balances

Parameter	value
Turbine power production [MW]	20.7
Compressor power consumption [MW]	6.7
Receiver power input [MW]	35.6
Total CO_2CO2 mass flow rate [kg/s]	70.6
ORC cycle HEX CO_2CO2 mass flow rate[kg/s]	16.6
Cycle thermal efficiency[-]	39.4
Combined cycle thermal efficiency[-]	42.8
Receiver thermal efficiency[-]	57.8
PCHE needed length[m]	0.6
PCHE effectiveness[-]	90.2
Cooler needed length[m]	0.9
Cooler effectiveness[-]	87.3

7.3 Off-design model

The off-design program will be feed by all the data in Table 7-1, 7-2, 7-3, 7-4, 7-5 and 7-6, but not the "desired power output" and "Degree of preheating (T_3)" in Table 7-2.
 Beside, from the result of on-design program, the data listed in Table 7-12 will also be loaded as input for off-design program.

Table 7-12 Input of off-design program from results of on-design program

Parameter	value
The PCHE length [m]	0.6
The Cooler length [m]	0.9
The total CO_2CO2 mass flow rate [kg/s]	70.6
The ORC cycle`s CO_2CO2 mass flow rate [kg/s]	16.6

The main parameter that can be given as input in the off-design simulation is the new radiation map, according to the particular condition that the user wants to analyze. The availability of a high number of radiation maps on the receiver would allow the calculation of the plant part-load operation in the most representative conditions,

allowing also for an annual approximate simulation. Regrettably, the public availability of radiation maps is extremely scarce and, hence, only three maps, representatives of three different times of the day and of the year, are currently available in the model. One has already been used in the on-design analysis; the other two are the following:

    – June21st, 16:00. Seville latitude and PS10 heliostat field[27].

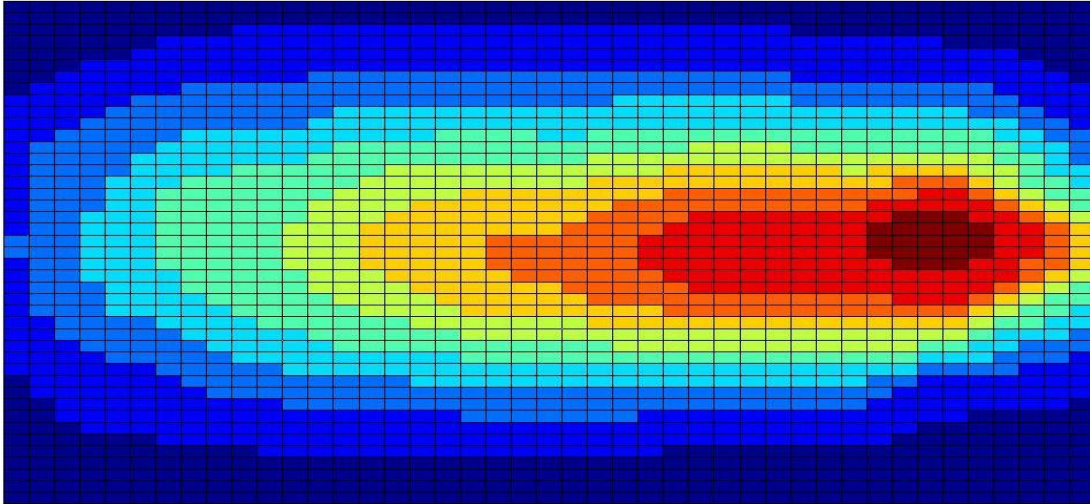*Figure 7-7June 21st16:00.*

    – June21st, 10:00. Seville latitude and PS10 heliostat field. This map has actually been created as a mirror of the previous one, but it can be considered to represent the real map with a good approximation.
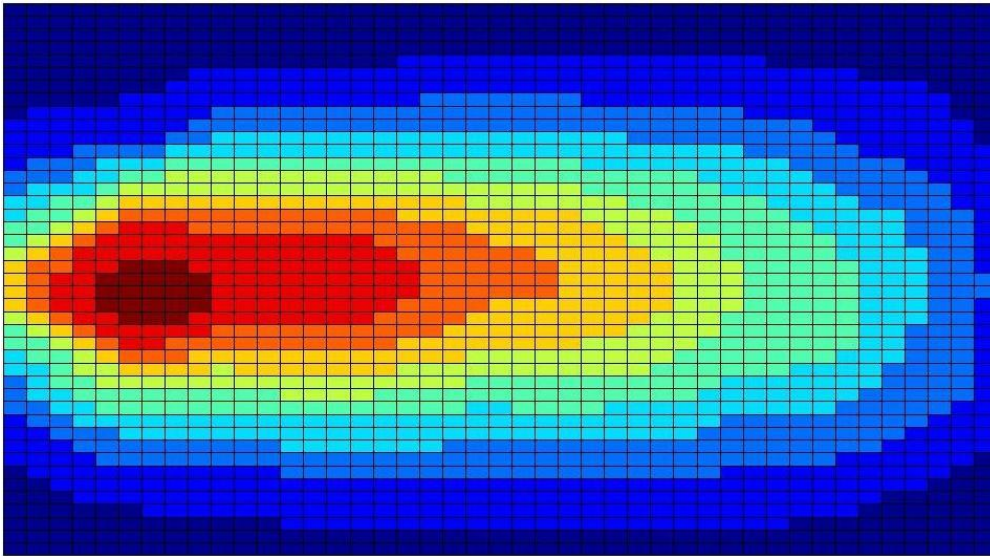
Figure 7-8June 21st*, 10:00.*

The logical procedure of off-design plant is based on correction of two parameters.
- − The pressure drop of the cycle
- − The inlet temperature of receiver

The procedure will starts with an initial guess on receiver inlet temperature, the pressure drop of all the component of the cycle and also the pressure drop among all the connecting pipes.

Then the calculation will start from node 1 and based on inlet pressure, inlet temperature, isentropic efficiency and needed pressure drop, the subroutine COMPRES will calculate the temperature and pressure of node 2. At this moment since the temperature of node 3 has already been guessed, the program will jump to boiler and delay the analysis of PCHE till the moment that it finishes the analysis of turbine, so that it can know about the hot flow temperature entering PCHE.
Therefore the program will call the subroutine CSP in order to find out the effect of solar power input on CO_2 stream. The function will give back the pressure and temperature of sCO_2 exiting the boiler and going toward the turbine.

The procedure will go on based on the turbine inlet temperature calculated by the CSP function and also the real pressure since in each subroutine, the pressure drop will also be calculated and updated upon the primary pressure drop assumptions.
Running the subroutine TURB will result in finding the temperature and pressure of node 5.
At this moment the cold and hot stream input temperature of PCHE, and also the inlet pressure of both sides will be known, so the subroutine PCHE can be called by the main program and it will calculate the pressure drop of both cold and hot stream

and also the outlet temperature of both cold and hot stream since the heat exchanger surface is already known. At this part of the program, the new cold stream outlet temperature will be compared to the initial guess, if the difference be less than the decided tolerance, the program will move forward and if not, it will go back to inlet of receiver and uses the new temperature as the input of subroutine CSP. This loop will keep going on till the difference become less than tolerance.

If so, the last component of the cycle named COOLER will be called in order to find the cooling water`s outlet temperature.

At this level, the total pressure drop of the cycle will be calculated and compared with the initial guess. If the difference be less than the decided tolerance the program will turn back the results to user, if not, the whole procedure will be repeated again based on the new pressure drops till it converges to a unique pressure for each point.

The logic of this part of the program can be seen in the next Figure.
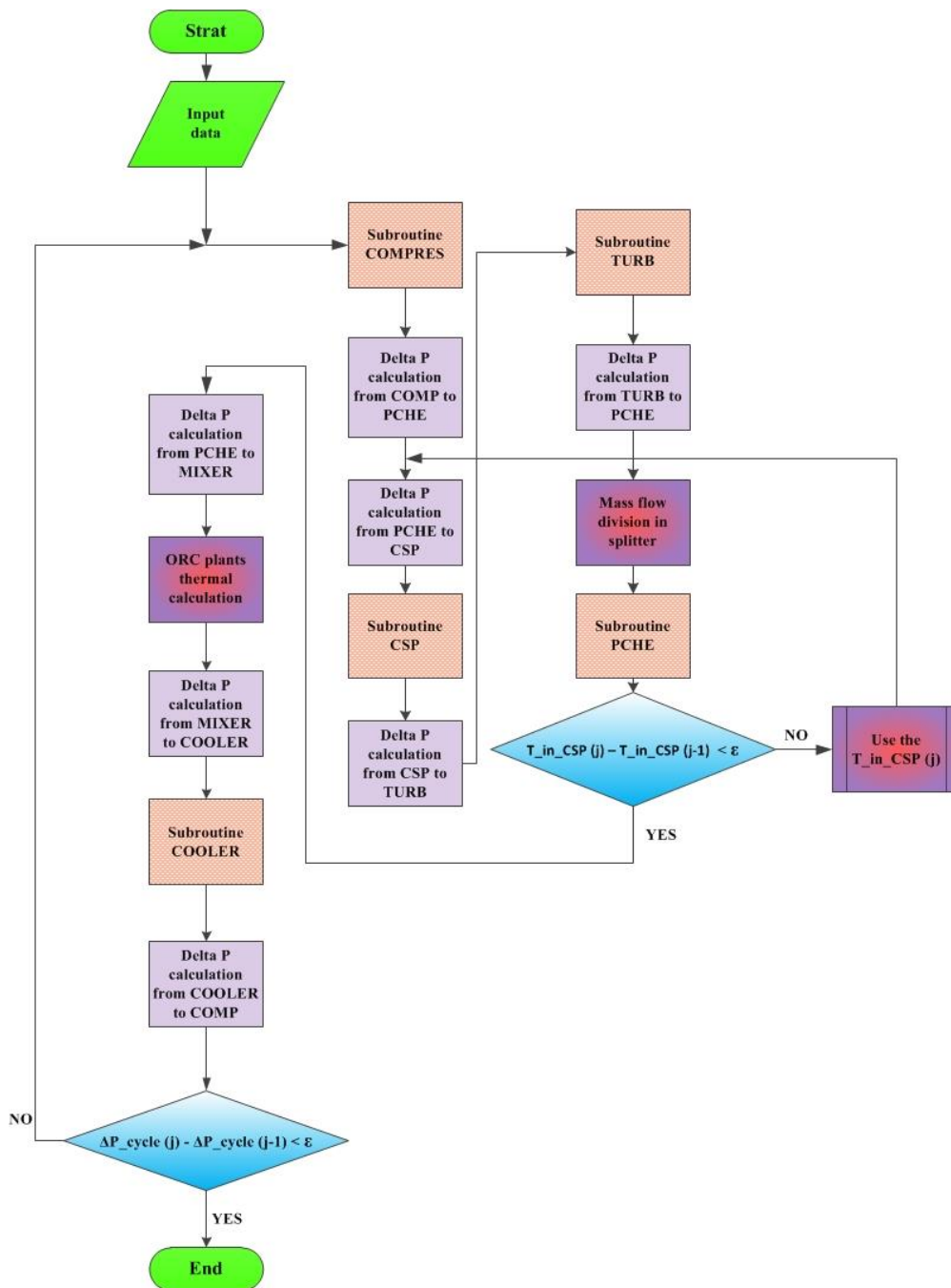
Figure 7-9 Logic of solving procedure in the main code of Off-design

7.4 Off-design results

Considering the input data mentioned in section 7-3, the results of off-design program for the June21st, 16:00map is as follow:

Table7-13Plant's pressure and temperature report

Node	Pressure [bar]	Temperature [K]
Compressor inlet	75.00	320
Compressor outlet	394.95	460
PCHE cold side inlet	394.58	460
Receiver inlet	390.43	597
Turbine inlet	385.08	943
Turbine outlet	85.14	714
PCHE hot side inlet	82.10	714
Cooler inlet	76.95	485

Table 7-14 Pressure drop of different parts of the plant

	Pressure drop [bar]
Cold side of PCHE	1.1428
Hot side of PCHE	3.6496
Receiver	1.1357
Hot side of cooler	1.0590
From compressor to PCHE	0.3706
From PCHE to receiver	3.0086
From receiver to turbine	4.2215
From turbine to splitter	3.0402
From PCHE to mixer	1.2438
From mixer to cooler	0.2564
Cooler to compressor	0.9209

Table7-15Plant`s enegy balances

Parameter	Value
The turbine power production [MW]	18.3
The compressor power consumption [MW]	6.5
The boiler power input [MW]	31.1
The cycle thermal efficiency[-]	38.2
The combined cycle thermal efficiency[-]	41.1
Net electric produced power [MW]	11.8
ORC plant`s produced power [MW]	0.9716
The PCHE effectiveness[-]	90.4
The Cooler effectiveness[-]	86.8

8CONCLUSIONS

Solar tower technology and the use of sCO_2 as working fluidwithin a closed-loop gas cycle have gained increasing interest in the power generation field. Due to the lack of easy and reliable specific models to simulate the behavior of this kind of plant, a MATLAB based code has been developed in order to clarify the particular characteristics of the plant with a selected cycle configuration at either on or off-design operating conditions.

In particular, the developed model allows for the description of both on and off design behavior of the plant. Considering that this technology could be a competitor of the one using steam as working fluid, the model has been developed in such a way that results can be compared with each other by means of their performances.

The goal is to find out that what would happen if there was a solar-sCO_2 plant instead of the solar-steam one. It is worth to note that this comparison takes place based on the fact that we apply the same size of receiver with the same heliostat field. Net power output, compressor pressure ratio and degree of preheating can be chosen in the model respectively in the range $4 - 20MW_e$, $2 - 5$ and $500 - 650$ K while the majority of the initial assumptions can be easily changed to adapt to several different cases.

The constraint on the choice for power output comes from the need to adjust the working fluid mass flow rate. Since the program is using the same amount of receiver surface area and radiation map as like as the already existing steam plant`s one, in order to respect the maximum temperature allowed by pipe material, the program will iteratively introduce more and more mass flow rate so that nowhere in the receiver the temperature exceeds the maximum allowed one. While doing that, the code also calculates the pressure drops in the receiver as well as in the other heat exchangers of the power cycle.

As an example, the comparison which has been done in this work was with PS10 plant in Seville in Spain height and heliostat field arrangement had been considered

to be the same as PS10 so that the radiation map on the receiver remains the same. The results which are demonstrated in table 8-1 shows that with the same receiver surface, higher net electric output power and efficiency could be achieved, at least within the advanced assumptions (in terms of maximum pressures and temperatures) for the gas cycle shown in the last chapters.

Table 8-1 Model and PS10 comparison

	Model results	PS10 results
$P_{el,net,cycle}$ [MW]	14.02	11.00
$P_{el,net,combined\ cycle}$ [MW]	15.23	-
$P_{input,solar}$ [MW]	35.60	35.80
$\eta_{el,net,cycle}$ [%]	39.4	30.7
$\eta_{el,net,combined\ cycle}$ [%]	42.8	-

In other words, the developed code will allow the user to know if it's possible to produce a specific amount of power with a specific existing receiver or not. For this case, it shows that with a receiver as the same size as boiler of PS10, the minimum power produced should be 14 MW instead of 11 MW, otherwise there will be failure in receive pipes due to very high temperatures.

The limits for increasing the pressure ratio and receiver inlet temperature are also coming from the material constraint. As it has been shown before, although more preheating would raise the efficiency of the plant but since the receiver size is fixed, very high temperatures would occur in some parts of the receiver.

As it can be seen in Table 8-1, the results show quite an interesting improvement in terms of power output and efficiency of the plant. The other advantages of applying sCO_2 instead of steam can be that, since the turbo machinery components and heat exchangers of sCO_2 plants are extremely compact, one can take in mind of installing all the components on the top of the tower and reduce the pressure losses of the piping of the plant notably.

As future developments on this work that can be mentioned is to have a detailed economic analysis in order to be able to compare the plant with existing plants not only from thermodynamic point of view, but also economic point of view.
This could be developed also to see if it makes sense to change an existing plant from steam to sCO_2 by the point of view of economic payback, replacing the components of steam plant with sCO_2 plant and instead gaining more efficiency and power output for the life time of the plant.
Moreover, further study should be done around the gas cycle, to better find optimized operating conditions and to further explore different thermodynamic cycle

design, as well as around the turbo machinery design and optimization, which is not addressed in this work.

Moreover, it could be developed software as mentioned before to have the study on the heliostat field and different possible configuration and arrangement for the power block of the plant in order to increase the efficiency of the plant more and more.

REFERENCES

[1]http://www.aalborgcsp.com/products-and-services/concentrated-solar-power/what-is-csp/history-of-csp.aspx.

[2] http://www.csp-world.com/resources/csp-facts-figures, in, 2012.

[3] E.S.T.E.A. (ESTELA), Solar power from the sun belt, in, June 2009.

[4] M. Romero, Produccion de hidrogeno con energia solar in: CIEMAT (Ed.), PP presentation

[5] G.e.d.f. rinnovabili, Enciclopedia degli idrocarburi, in.

[6] X. Wei, Z. Lu, W. Yu, Z. Wang, A new code for the design and analysis of the heliostat field layout for power tower system, Solar Energy, 84 (2010) 685-690.

[7] V. Ruiz Hernandez, M.A.S. Perez, La electricidad solar termica, tan lejos, tan cerca, gasNatural Fundaciòn, (2009).

[8] J.M.H.L. Levelt Sengers, Supercritical Fluids: Their Properties and Applications, Kluwer Academic Publishers, Netherlands, 2000.

[9] L.S. Pioro, I.L. Pioro, Industrial Two-Phase Thermosyphons, Begell House, New York, NY, USA, 1997.

[10] International Encyclopedia of Heat & Mass Transfer, in: G.F. Hewitt, G.L. Shires, Y.V. Polezhaev (Eds.) Supercritical heat transfer, Boca Raton, FL, USA, 1998, pp. 1112–1117.

[11] I.L. Pioro, R.B. Duffey, Heat Transfer and Hydraulic Resistance at Supercritical Pressures in Power Engineering Applications, in: ASME Press, , New York, NY, USA, 2007, pp. 328.

[12] F. Kreith, D.Y. Goswami, Handbook of Energy Efficiency and Renewable Energy, in.

[13] http://www.nrel.gov/csp/, in, 2013.

[14] H.Hasuike, Y. Yoshizawa, A. Suzuki, Y.Tamaura, Study on design molten salt solar receivers for beam-down solar concentrator, May 2006, (May 2006).

[15] M.Yang, X.Yang, X.Yang, J.Ding, Heat transfer enhancement and performance of the molten salt receiver of a solar power tower, (April 2009).

[16] J. Pacheco, R.Gilbert, Overview of recent results of the Solar Two test and evaluations program in, Sandia National Labs.

[17] J.M.Lata, M. Rodriguez, M.A.d. Lara, High flux central receivers of molten salts for the new generation of commercial stand-alone solar power plants, in: SolarPACES, 2006

[18] R. Pitz-Paal, High temperature solar concentrators.

[19] C.Tyner, G.Kolb, M.Prairie, Solar Power Tower Development: Recent Experiences, in.

[20] G.Koll, P. Schwarzbozl, K.Hennecke, T.Hartz, M.Schmitz, B. Hoffshmidt, The solar tower Jülich – A research and demonstration plant for central receiver systems, in.

[21] M.Epstein, D.Liebermann, M.Rosh, A.J.Shor, Solar testing of 2 MW water/steam receiver at the Weizmann Institute solar tower, Solar Energy Materials, (1991).

[22] P.K. Falcone, A Handbook for Solar Central Receiver Design, Sandia National Laboratories, Livermore, CA 1986.

[23] Ing. Mazzi, Corso su generatori di vapore ad ingegneria solare, in, Politecnico di Milano, June 2009.

[24] F. COLZI, S. PETRUCCI, Modeling On/Off – Design performance of solar tower plants in: Engenieria di energetica, politecnico di milano, Milan, 2009, pp. 337.

[25] H.M. Son, K.Y. Suh, Experimental heat transfer to supercritical carbon dioxide flowing upward vertical tube with highly conducting surroundings, Nuclear Engineering and Design, 250 (2012) 573-584.

[26] F. Colzi, S. Petrucci, G. Manzolini, R. Chacartegui, P. Silva, S. Campanari, D. Sánchez, Modeling on/off-design performance of solar tower plants using saturated

steam, in: International Conference on Energy Sustainability ES2010, ASME 2010 May 17e22, Phoenix, Arizona, USA., 2010.

[27] PS10: a 11.0 MW Solar Tower Power Plant with Saturated Steam Receiver, available at

http://www.upcomillas.es/catedras/crm/report05/Comunicaciones/Mesa%20IV/D%20Valerio%20Fern%C3%A1ndez%20-%20Solucar%202.pdf in, 2005.

[28] http://www.protermosolar.com, in.

[29] R. Buck, C. Barth, M. Eck, W.-D. Steinmann, Dual-receiver concept for solar towers, Solar Energy, 80 (2006) 1249-1254.

[30] S. Alexopoulos, B. Hoffschmidt, Solar tower power plant in Germany and future perspectives of the development of the technology in Greece and Cyprus, Renewable Energy, 35 (2010) 1352-1356.

[31] M. Romero, E. Zarza, Concentrating Solar Thermal Power, Handbook of Energy Efficiency and Renewable Energy, Taylor & Francis Group, 2007.

[32] A. Kribus, R. Zaibel, D. Carey, A. Segal, J. Karni, A solar-driven combined cycle power plant, Solar Energy, 62 (1998) 121-129.

[33] A. Kribus, P. Doron, R. Rubin, J. Karni, R. Reuven, S. Duchan, E. Taragan, A Multistage Solar Receiver:: The Route To High Temperature, Solar Energy, 67 (1999) 3-11.

[34] A. Segal, M. Epstein, Optimized working temperatures of a solar central receiver, Solar Energy, 75 (2003) 503-510.

[35] E.G. Feher, The supercritical thermodynamic power cycle, Energy Conversion, 8 (1968) 85-90.

[36] X.R. Zhang, H. Yamaguchi, An experimental study on evacuated tube solar collector using supercritical CO2, Applied Thermal Engineering, 28 (2008) 1225-1233.

[37] H. Yamaguchi, X.R. Zhang, K. Fujima, M. Enomoto, N. Sawada, Solar energy powered Rankine cycle using supercritical CO2, Applied Thermal Engineering, 26 (2006) 2345-2354.

[38] J. Wang, Z. Sun, Y. Dai, S. Ma, Parametric optimization design for supercritical CO2 power cycle using genetic algorithm and artificial neural network, Applied Energy, 87 (2010) 1317-1324.

[39] N.A. Carstens, P. Hejzlar, M.J. Driscoll, Control System Strategies and Dynamic Response for Supercritical CO

Power Conversion Cycles, in, MIT-GFR-038,, 2006.

[40] V. Dostal, M.J. Driscoll, P. Hejzlar, A Supercritical Carbon Dioxide Cycle for Next Generation Nuclear Reactors, in: MIT-ANP-TR-100, 2004.

[41] R.B.V.e. al., Dynamic System Analysis of a Supercritical CO2 Compression Loop, in: Anaheim (Ed.) Proceedings of ICAPP'08, CA USA,, June 8e12, 2008, pp. Paper 8343.

[42] Y. Gong, N.A. Carstens, M.J. Driscoll, I.A. Matthews, Analysis of Radial Compressor Options for Supercritical CO

Power Conversion Cycles, in: MIT-GFR-034, 2006.

[43] M. Utamura, Thermal-hydraulic characteristics of microchannel heat exchanger and its application to solar gas turbines, in: Power for Land, Sea, and Air Proceedings of ASME Turbo Expo 2007, Montreal, Canada, May 14e17,2007.

[44] T.C. Hung, T.Y. Shai, S.K. Wang, A review of organic rankine cycles (ORCs) for the recovery of low-grade waste heat, Energy, 22 (1997) 661-667.

[45] R. Chacartegui, D. Sánchez, J.M. Muñoz, T. Sánchez, Alternative ORC bottoming cycles FOR combined cycle power plants, Applied Energy, 86 (2009) 2162-2170.

[46] P. Gang, L. Jing, J. Jie, Analysis of low temperature solar thermal electric generation using regenerative organic Rankine Cycle, Applied Thermal Engineering, 30 (2010).

[47] T.C. Hung, S.K. Wang, C.H. Kuo, B.S. Pei, K.F. Tsai, A study of organic working fluids on system efficiency of an ORC using low-grade energy sources, Energy, 35 (2010) 1403-1411.

[48] J. hesselgreaves, E., Compact heat exchangers,selection, design and Optimization, 1st ed., Pergamon, 2001.

[49] D.A. Olsen, "Heat Transfer of Supercritical Carbon Dioxide Flowing in a Cooled Horizontal Tube", in: NISTIR 6496,, 2000.

[50] N.E. Todreas, K. E., M., S.,, Nuclear Systems 1, Taylor & Francis, New York, 2000.

[51] S.P. kar, CFD ANALYSIS OF PRINTED CIRCUIT HEAT EXCHANGER, in: Mechanical Engineering, National Institute of Technology Rourkela, Rourkela, 2007.

[52] J. Floyd, N. Alpy, A. Moisseytsev, D. Haubensack, G. Rodriguez, J. Sienicki, G. Avakian, A numerical investigation of the sCO2 recompression cycle off-design behaviour, coupled to a sodium cooled fast reactor, for seasonal variation in the heat sink temperature, Nuclear Engineering and Design, 260 (2013) 78-92.

[53] B.S. Petukhov, V.N. Popov, Theoretical calculation of heat exchange and frictional resistance in turbulent flow in tubes of an incompressible fluid with variable physical properties, Teplofiz. Vyosk, 1963.

[54] R.-M. Code., Design and construction rules for mechanical components of FBR nuclear islands, Tome I, Z. Paris,AFCEN. (2007).